THE EVOLUTION OF COASTAL LOWS ALONG THE SOUTH COAST OF SOUTH AFRICA

T. J. CARTER

Thesis submitted in fulfillment of the requirements for the Master of Science degree at the University of Zululand, KwaDlangezwa, South Africa.

2005

ABSTRACT

Coastal lows occur frequently along the South African coast. Coastal low passage along the coast of southernmost Africa is signaled by a marked change in both wind direction and speed. Occasionally, a dramatic and rapid increase in wind speed takes place, which may cause damage to property and is potentially hazardous to aviation and shipping. Current global scale numerical weather prediction models do not forecast the intensity of these mesoscale systems well. A study of the coastal low is made with the aim of improving knowledge about the coastal low in general, and of strong coastal lows in particular, in order to improve the ability to predict the strong to gale force southwesterly winds associated with the more intense coastal lows. An average climatic profile of the coastal low is established in order to study the basic nature and evolution of the coastal low. This profile is compared against a similar profile of strong cases in order to locate mesoscale and synoptic scale elements that distinguish between normal and strong coastal lows. Links between intense coastal lows, and higher than normal pre-coastal low temperatures at surface and in the lower levels of the atmosphere over the southern parts of the country, are examined. The upper level northwesterly winds, associated with the upper troughs that follow closely behind the coastal lows, are a contributing cause in the development of stronger coastal lows on the south coast.

PREFACE

Coastal lows are relatively small scale weather systems of limited vertical extent which belong to the larger family of orographically trapped disturbances that are found across the world within particular orographical and atmospheric conditions.

Coastal lows occur frequently along the South African coast. Due to their mesoscale properties, their intensity is more difficult to forecast than that of the larger synoptic scale systems. The general coastal low pattern of relatively hot and dry conditions, followed abruptly by cooler, moist and windy weather, is experienced regularly along the coast from Namibia in the west to the east coast of South Africa. In the case of an intense overland front following the coastal low, the warm offshore flow may dominate until the passage of the front itself. Occasionally the change in weather, as the coastal low passes by, may be hazardous as the typically light offshore flow changes rapidly into a very strong to gale force side-shore wind.

In this study, coastal lows along the south coast of Africa, and in the Port Elizabeth region in particular, are examined. Port Elizabeth lies on the southeastern edge of South Africa, at the tip of a peninsula facing eastwards onto Algoa Bay. The intention of the study is to create a general profile of the coastal low in this region, and then to investigate factors that differentiate strong coastal lows from the norm, in order to improve the forecasting of the intense coastal lows.

The relationship between both higher pre-coastal low temperatures and stronger offshore flow ahead of the coastal low in the lower atmosphere, and intense coastal lows, is examined.

Literature related to the study of coastal lows is reviewed in Chapter 1. Chapter 2 describes the data sources and the method used in the study, gives a synopsis of the basic background climatology of Southern Africa and includes a theoretical framework. A climatological profile of the coastal low based on station data is presented in Chapter 3 while Chapter 4 consists of a more detailed seasonal study of the coastal low during the SON (September, October and November) season through the use of composite analysis. In Chapter 5 correlations are provided, a conceptual model is presented and a case study of a strong case coastal low is analyzed using a mesoscale model, to test previous findings and to show the improvement in forecasting ability using mesoscale models for mesoscale systems. A basic mathematical framework is also given in Chapter 5. Chapter 6 provides a Summary and Conclusions.

Acknowledgements

I extend my gratitude to the following people for help with this dissertation. Henk Tiggelman, for helping with the time-consuming initial selection of the coastal low cases used in this study, John Carter for help with database manipulation and to Greg Clarke for help with Linux scripting and assistance with the Eta mesoscale model. I extend thanks to Professor Mark Jury, as supervisor of this study, to Robin Mountford for input on spreadsheets, to Warren Tennant for help with locating reanalysis data and for advice on the manipulation of vector winds. I wish to thank Matthew Pyle for the provision of the Eta model binaries, Michael de Villiers, Ian Hunter and Chris Reason for input on theory. I would like to thank Sheugnet Carter for help with English grammar and Professor Tyson for affording me the initial opportunity to pursue this study. I also thank Garth Sampson, Brent Appel and Louis Vermaak, who helped with locating data at various times. Finally, I would like to extend my sincere thanks to the staff at the climate section, and particularly to the helpful librarians, of the South African Weather Service.

CONTENTS

Page

ABSTRACT.....ii

PREFACE.....iii

Acknowledgements.....v

CONTENTS.....vi

List of figures.....x

List of tables.....xv

CHAPTER 1: INTRODUCTION AND LITERATURE REVIEW

1.1 Introduction.....1

1.2 Literature review.....4

1.3 Theoretical framework of this study.....18

CHAPTER 2: DATA, METHODOLOGY AND BACKGROUND CLIMATOLOGY

2.1 Meteorological data.....22

2.1.1 Surface observations (station data).....22

2.1.2 Upper air observations (station data).....24

2.1.3 NCEP Reanalysis data.....24

2.1.4 Model display and analysis programs used.....25

2.1.5 Numerical forecast models.....25

2.1.6 Topographical data.....27

2.2 Methodology.....27

2.2.1 Defining strong cases.....29

2.2.2 Upper air study on 10-year data.....29

2.2.3 September, October and November season (SON).....30

2.2.4 Propagation of the coastal low.....30

2.2.5 SON Upper air profile.....31

2.2.6 Inversions.....33

2.2.7 Temperature effects on coastal low intensity.....33

2.2.8 Composite NCEP climatology.....34

2.2.9 Case study.....37

2.3 Limitations of the study.....38

2.4 Background climatological overview of Southern Africa.....39

CHAPTER 3: COASTAL LOW CLIMATOLOGY RESULTS

3.1 Introduction.....41

3.2 Station climatology.....42

3.2.1 General profile.....42

3.2.2 Frequency of coastal low occurrence.....46

3.3 Upper air (NCEP Reanalysis 1 data) for all 642 coastal lows over the 10-year period 1987 - 1996.....47

3.4 September, October and November (SON) season climatology.....48

3.4.1 Station climatology.....48

3.4.1.1 Frequency of coastal low occurrence.....48

3.4.1.2 Propagation.....48

3.4.2 SON Sonde climatology.....50

3.4.2.1 Inversions.....50

3.4.2.2 Sonde profiles.....51

3.5 Summary.....55

3.5.1 Climate summary for all 642 coastal lows during the 10-year period from 1987 to 1996 (including comparisons for the top 5% of cases) 55

3.5.2 Climate summary of the SON (September, October and November) season during the 10-year period from 1987 to 1996.....56

CHAPTER 4: COMPOSITE COASTAL LOW PATTERNS, SON 1987 – 1996

4.1 Introduction.....61

4.2 Plan view composites of 500 hPa heights and surface pressure.....62

4.3 Cross-section composites.....78

4.4 Regional Composites.....84

4.5 Summary.....93

CHAPTER 5: COASTAL LOW CONCEPTUAL MODEL, CORRELATIONS NUMERICAL MODEL CASE STUDY AND MATHEMATICAL FRAMEWORK

5.1 Introduction.....97

5.2 Correlations.....98

5.3 Conceptual model.....100

5.4 A numerical model case study of a strong coastal low on the 14th of November 2003....110

5.4.1 Introduction....110

5.4.2 Case study....110

5.5 Mathematical framework....126

5.6 Summary....128

CHAPTER 6: SUMMARY AND CONCLUSIONS

6.1 Summary....131

6.1.1 General overview....131

6.1.2 Summary of most significant findings....132

6.2 Conclusions and discussion....135

6.3 Recommendations for operational practice....138

6.4 Further research....139

References....141

Appendix A: List of all 642 coastal lows for 1987 – 1996....151

Appendix B: Condensed notes on forecasting strong coastal lows along the southeastern coastal belt from Cape St. Francis through to East London for operational forecaster use....163

List of figures

Figure Description Page

Figure 1.1 Map of the world showing various orographically trapped disturbance sites....1

Figure 1.2 Shaded relief map of South Africa with overlaid contours in meters...5

Figure 1.3 Conceptual view of the atmospheric and topographic conditions associated with coastally trapped disturbance propagation as a distortion of the base of a subsidence enhanced marine inversion....7

Figure 1.4 Spectral analysis of surface pressure oscillations....8

Figure 1.5 Time section to show wind components parallel to the coast (a), and wind direction (b), during the passage of a coastal low past Durban on 1st July 1969....10

Figure 2.1 Wind speed monthly averages for the Port Elizabeth Weather Office....31

Figure 2.2 Locations of the weather stations and sites used in the temperature gradient hypothesis section of the study....32

Figure 2.3 Monthly observations count of land (colour filled) and ship and buoy stations (contours) used by the reanalysis project for October 1991....36

Figure 2.4 Monthly observations count of satellite wind (colour filled) and temperature (contours) used by the reanalysis project for October 1991....36

Figure 3.1 Average wind speed time series of all coastal lows in bold black line with profile of the top 5% coastal lows in thin black line....42

Figure 3.2 True vector average wind direction time series of all coastal lows in bold black line with profile of the top 5% coastal lows in dotted thin black line....43

Figure 3.3 Temperature time series of all coastal lows in bold black line with the profile of the top 5% coastal lows in dotted thin black line....44

Figure 3.4 Surface pressure time series of all coastal lows in bold black line with the profile of the top 5% coastal lows in dotted thin black line....45

Figure 3.5 Yearly spread of coastal low occurrence for all 642 coastal lows and for the top 5% of all 642 coastal lows....46

Figure 3.6 Wind roses for the upper winds at 700hPa and at 850hPa for all 642 coastal lows for the 12-hour period before, during and after coastal low passage at Port Elizabeth....47

Figure 3.7 Temperature (°C), humidity (%) and wind ($m.s^{-1}$) plots of the top and median 10% of SON upper air ascents.....53

Figure 4.1 Composite mean of all 160 SON coastal lows, on the day of coastal low passage at Port Elizabeth.....62

Figure 4.2 Composite mean of the top 10% of coastal lows, on the day of passage of the coastal lows at Port Elizabeth.....63

Figure 4.3 Sea level pressure composite anomalies of the top 10% cases in solid black contours, and of all 160 SON coastal lows in dotted lines, with all units in hPa.....64

Figure 4.4 Composite anomalies of the 500 hPa contours for the top 10% of cases in solid black contours, and of all 160 SON coastal lows in dotted lines.....65

Figure 4.5 Differential anomaly of the sea level pressure anomalies (strong minus the mean).....66

Figure 4.6 Differential anomaly of the 500 hPa contour anomalies (strong minus the mean).....66

Figure 4.7 Surface air temperature anomalies from two days before (D-2) to the day after (D+1) coastal low passage at Port Elizabeth.....67

Figure 4.8 Sea level pressure anomalies from two days before (D-2) to five days after (D+5) coastal low passage at Port Elizabeth.....69

Figure 4.9 500 hPa height (gpm) anomalies from two days before (D-2) to the day after (D+1) coastal low passage at Port Elizabeth.....71

Figure 4.10 Surface mean vector wind composites for two days before (D-2) to the day after (D+1) coastal low passage at Port Elizabeth.....72

Figure 4.11 850 hPa mean vector wind and height (gpm) composites for two days before (D-2) to the day after (D+1) coastal low passage at Port Elizabeth.....74

Figure 4.12 700 hPa mean vector wind and height (gpm) composites for two days before (D-2) to the day after (D+1) coastal low passage at Port Elizabeth.....76

Figure 4.13 Wind shear between 700 hPa and 850 hPa, from two days before (D-2) to the day after (D+1) coastal low passage at Port Elizabeth.....77

Figure 4.14 Height of land surface for 30°, 32° and 34° South between 18° East and 28° East.....78

Figure 4.15 Cross-sectional display along 18°E to 30°E of the air temperature anomalies for the day before (D-1) to the day after (D+1) coastal low passage at Port Elizabeth.....79

Figure 4.16 Cross-sectional display of the wind anomalies at 34°S along 18°E to 28°E for the day before (D-1) to the day after (D+1) coastal low passage at Port Elizabeth.....81

Figure 4.17 Cross-sectional display of the air temperature anomalies along 39°S to 29°S for the day before (D-1) to the day after (D+1) coastal low passage at Port Elizabeth.....82

Figure 4.18 Map of Southern Africa showing the areas used for the 10° by 10° degree, system-following, regional composite display areas.....84

Figure 4.19 System following composites of sea level pressure from two days before (D-2) to the day after (D+1) coastal low passage at Port Elizabeth.....86

Figure 4.20 System following composites of the surface wind (predominantly alongshore flow at the coast) from two days before (D-2) to the day after (D+1) coastal low passage at Port Elizabeth.....87

Figure 4.21 System following composites of the mean surface vorticity from two days before (D-2) to the day after (D+1) coastal low passage at Port Elizabeth.....88

Figure 4.22 System following composites of air temperature at 850 hPa from two days before (D-2) to the day after (D+1) coastal low passage at Port Elizabeth.....89

Figure 4.23 System following composites of the 850 hPa wind (predominantly offshore flow at the coast) from two days before (D-2) to the day after (D+1) coastal low passage at Port Elizabeth.....90

Figure 5.1 Schematic drawing of the major wind flow associated with the coastal low.....101

Figure 5.2 Schematic presentation of day 1 for the strong case coastal lows at sea level, 850 hPa and 700 hPa showing the isobars and contours in the conventional manner.....103

Figure 5.3 Schematic presentation of day 2 for the strong case coastal lows at sea level, 850 hPa and 700 hPa showing the isobars and contours in the conventional manner.....104

Figure 5.4 Schematic presentation of day 3 for the strong case coastal lows at sea level, 850 hPa and 700 hPa showing the isobars and contours in the conventional manner.....106

Figure 5.5 Schematic presentation of day 4 for the strong case coastal lows at sea level, 850 hPa and 700 hPa showing the isobars and contours in the conventional manner.....108

Figure 5.6 Sea level pressure (hPa) at 06:00 UTC on the 14th November 2003 (CDC NCEP Reanalysis data). 111

Figure 5.7 500 hPa contours (gpm) at 06:00 UTC on the 14th November 2003 (CDC NCEP Reanalysis data)....112

Figure 5.8 Horizontal time section plot of sea level pressure showing the progression and intensification of the coastal low along the south coast of Africa....113

Figure 5.9 Vertical time section plot at Port Elizabeth with wind barbs (each feather is 10 knots) and temperature (°C)....113

Figure 5.10 10m wind barbs (each feather is 10 knots) and sea level pressure (hPa) for 06Z on the 13th of November 2003....114

Figure 5.11 10m wind barbs (each feather is 10 knots) and sea level pressure (hPa) for 21Z on the 13th of November 2003....114

Figure 5.12 10m wind barbs (each feather is 10 knots) and sea level pressure (hPa) for 09Z on the 14th of November 2003....115

Figure 5.13 10m wind barbs (each feather is 10 knots) and sea level pressure (hPa) for 06Z on the 14th of November 2003....117

Figure 5.14 10m wind barbs (each feather is 10 knots) and 1000 hPa temperature (°C) for 06Z on the 14th of November 2003....118

Figure 5.15 10m wind barbs (each feather is 10 knots) and 1000 hPa temperature (°C) for 11Z on the 14th of November 2003....118

Figure 5.16 Time Section at Port Elizabeth with temperature (°C), and wind barbs (each feather equal to 10 knots)....119

Figure 5.17 Tephigram at Port Elizabeth with temperature and dew point (°C) and wind (each feather is 10 knots) for 00Z on the 14th (solid black lines and black barbs) and for 12Z on the 13th (dotted lines and gray barbs)....120

Figure 5.18 Tephigram at Port Elizabeth with temperature and dew point (°C) and wind (each feather is 10 knots) for 12Z on the 14th (solid black lines and black barbs) and for 00Z on the 14th (dotted lines and gray barbs)....120

Figure 5.19 10m wind barbs (each feather is 10 knots) and sea level pressure (hPa) at 06Z on the 14th of November 2003....121

Figure 5.20 10m wind barbs (each feather is 10 knots) and sea level pressure (hPa) at 13Z on the 14th of November 2003....122

Figure 5.21 Cross section display at 25.6°E for 06Z on the 14th of November 2003....122

Figure 5.22 Time section display for Port Elizabeth with wind barbs (each feather is 10 knots) and vertical velocity vertical velocity ($Pa.s^{-1}*10^{-3}$) is displayed (red is upwards).....123

Figure 5.23 Wind at 10m (black), 850 hPa (blue) and 700 hPa (red) in knots with the 10 knot isotachs at 850 hPa.....124

Figure 5.24 Wind at 10m (black), 850 hPa (blue) and 700 hPa (red) in knots with the 10 knot isotachs at 850 hPa.....124

Figure A1 Aeronautical diagram of the averaged ascents at Cape Town (blue), Port Elizabeth (gray) and Durban (red) with the darker shades showing the top 10% of coastal lows and light the mean 10% of the coastal lows.....155

Figure A2 Aeronautical diagram of the averaged ascents at 24 hours before coastal low passage at Port Elizabeth (blue), 12 hours before coastal low passage (red) and at coastal low passage (gray) with the darker shades showing the top 10% of coastal lows and light the mean 10% of the coastal lows.....156

Figure A3 Aeronautical diagram of the averaged ascents at 24 hours before coastal low passage at Port Elizabeth (blue), at coastal low passage (gray) and at 24 hours after coastal low passage (red) with the darker shades showing the top 10% of coastal lows and light the mean 10% of the coastal lows.....157

List of tables

Table	Description	Page
Table 2.1	Coastal stations used for surface data	23
Table 3.1	Results of the propagation study for the top 10% of coastal lows	49
Table 3.2	Results of the propagation study for the mean 10% of coastal lows	49
Table 5.1	Correlations between 850 hPa wind speed, 700 hPa wind speed and the interior surface temperature against the strength of the coastal low	99
Table A1	Top 10% of SON coastal lows tracked from Cape Town (C) to George (G), to Port Elizabeth (P), to East London (E) and on to Durban (D)	158
Table A2	Mean 10% of SON coastal lows tracked from Cape Town (C) to George (G), to Port Elizabeth (P), to East London (E) and on to Durban (D)	159
Table A3	Temperature inversions on the top 10% of SON upper air ascents at Cape Town (CTT), Port Elizabeth (PET) and Durban (DNT) within the 12-hour period preceding coastal low passage at the stations	160
Table A4	Temperature inversions on the mean 10% of SON upper air ascents at Cape Town (CTM), Port Elizabeth (PEM) and Durban (DNM) within the 12-hour period preceding coastal low passage at the stations	161
Table A5	Legend for Tables A3 and A4	162

CHAPTER 1

INTRODUCTION AND LITERATURE REVIEW

1.1 Introduction

The coastal low is a local weather scale phenomenon along the coast of southern Africa (Fig. 1.1) that transits from the Namibian coast to the east coast of South Africa. Coastal lows are shallow, mesoscale systems that form part of the family of coastally trapped disturbances which, in turn, fall within the family of orographically trapped disturbances. Orographically trapped disturbances are found in various places across the world (Ruttland, 1983; Reason, 1993; Baines, 1980; Colquhoun *et al.*, 1985; McInnes, 1993).

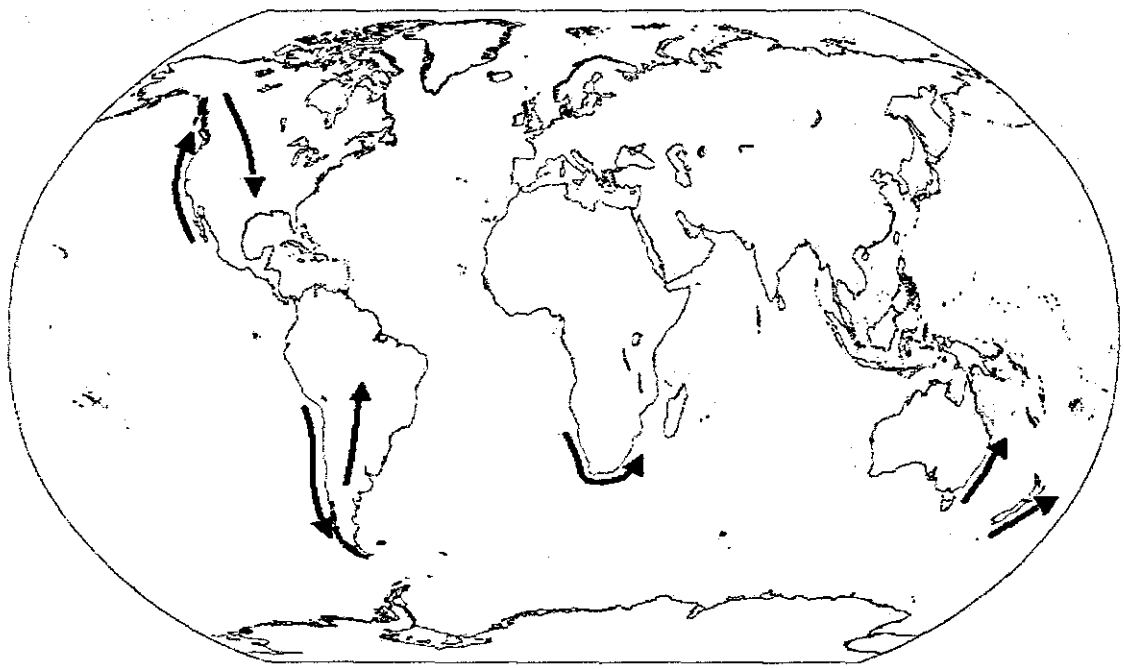

Fig. 1.1 Map of the world showing various known orographically trapped disturbance sites.

Coastal lows are a feature of the subtropical westerlies on the South African coast and are important in coastal weather forecasting. The coastal lows that occur along the South African coastal belt are local shallow systems, which produce intense and rapid weather change. This is always in the form of a change in wind direction and speed and a temperature change from relatively hot, to cool post-low conditions. This may be accompanied by low cloud, fog or drizzle. The rapid change has various economic and societal implications, but the one aspect that holds the most danger for the coastal environment is the change in wind. This change in wind speed and direction is potentially dangerous, mainly to shipping and aviation (Estie, 1990).

Low level wind shear is significant to aviation due to its effect on aircraft performance and hence its potentially adverse affect on flight safety. Wind shear in the lowest 500 m is of particular importance to aircraft landing and take-off. During the climb-out and approach phases of flight, aircraft airspeed and height are near critical values, thus rendering the aircraft especially susceptible to the adverse affects of wind shear. The response of aircraft to wind shear is complex and depends on many factors including the type of aircraft, the phase of flight, and the scale on which the wind shear operates relative to the size of the aircraft and the intensity and duration of the wind shear encountered. A general description of wind shear is a change in horizontal wind speed and/or direction in space, but also including updrafts and downdrafts (ICAO Circular, 1987).

When the post-coastal low wind takes the form of a sudden jump in wind speed from near calm to over 10 $m.s^{-1}$, it is known as a "buster" (Hunter, 1987). The National Research Institute for Oceanology had advised mariners to "stand inshore of the

continental shelf (where the Agulhas current will be much weaker) between Richard's Bay and Great Fish Point when steaming towards the south-west with the barometer falling, a fresh NE'ly wind is blowing and a change to fresh or strong SW'ly winds are forecast within the next 24 hours" (Torrance (1995). This is the typical signature of an approaching coastal low.

Operational weather forecasters rely heavily on numerical weather prediction models. As the movement of the coastal low is forced by synoptic scale systems, the initial position and propagation of the coastal low is predicted well by the models which forecast synoptic scale systems well. However, the intensity and east coast propagation of the coastal low is not forecast well due to a discrepancy between the small size of the coastal lows and NWP model grid scales (COMET, 1999), and their inability to trap energy vertically.

It is also difficult to analyse the coastal lows properly due to a lack of sufficient data from the standard weather observing networks, particularly over the sea itself where ship (and other) weather reports are scarce. This leads to feedback problems, as the numerical models need sufficient input data at the correct mesoscale density to resolve and forecast a coastal low (Jascourt *et al.*, 2001). Most of the manned coastal observing stations operated by the South African Weather Services are not well placed for a proper representation of the marine environment. It is quite common, for example, for the Port Elizabeth Weather Office to experience an early winter morning calm whilst a wind of over 20 knots is being experienced just offshore. A main difficulty in identifying the time of passage of the coastal low is undercutting caused

by the mesoscale land breeze, which causes the southwesterly wind to appear to be delayed.

1.2 Literature review

Orographically trapped disturbances, with similar characteristics to the South African coastal lows, occur along the coast of Chile and also on the eastern side of the South American Andes (Meteorological Reports, 1948), along the Australian Great Dividing Range (e.g., Holland and Leslie, 1986), the North American west coast mountains (e.g., Dorman, 1985, 1987; Mass and Albright, 1987; Reason and Dunkley, 1993), the "backdoor" fronts on the eastern side of the Appalachian mountains of the United States (Carr, 1951; Bosart *et al.*, 1973), the eastern side of the Rocky mountains of the United States (Lilly, 1981), the Pacific coast of the United States (Mass and Albright, 1987), the South Island of New Zealand (Smith *et al.*, 1991), the Himalayas and their southeast Asian extension (Chang *et al.*, 1979; Webster and Stephens, 1980) and the Alaskan Ranges (Overland and Bond, 1993). Only the South African and the South American (coastal) disturbances are coastal lows, the other coastal cases indicated tend to be produced by coastal ridging (Reason and Steyn, 1990).

Orographically trapped disturbances in the lower atmosphere propagate along sufficiently large mountain barriers and are trapped vertically by stable stratifications and laterally, by Coriolis effects against the mountains. OTD are typically generated by interaction of a large synoptic scale feature with the mountains, have length scales in the along-mountain direction of 1000 – 4000 km but are considerably smaller in the

across-mountain direction and usually propagate over a period of 2 – 6 days. In the vertical, they are generally confined in the lowest 1 – 2.5 km but sometimes in a layer only a few 100's of meters thick. The generation of OTD can be described in terms of two dynamic parameters, which depend on the latitude, the atmospheric stratification, the mountain half-width and height – these parameters are the Rossby number and the ration of the Rossby to the Froude number. With the exception of the South African case, none of the above mountain ranges is broad enough for the dynamics to be quasi-geostrophic during OTD generation (Reason, 1993).

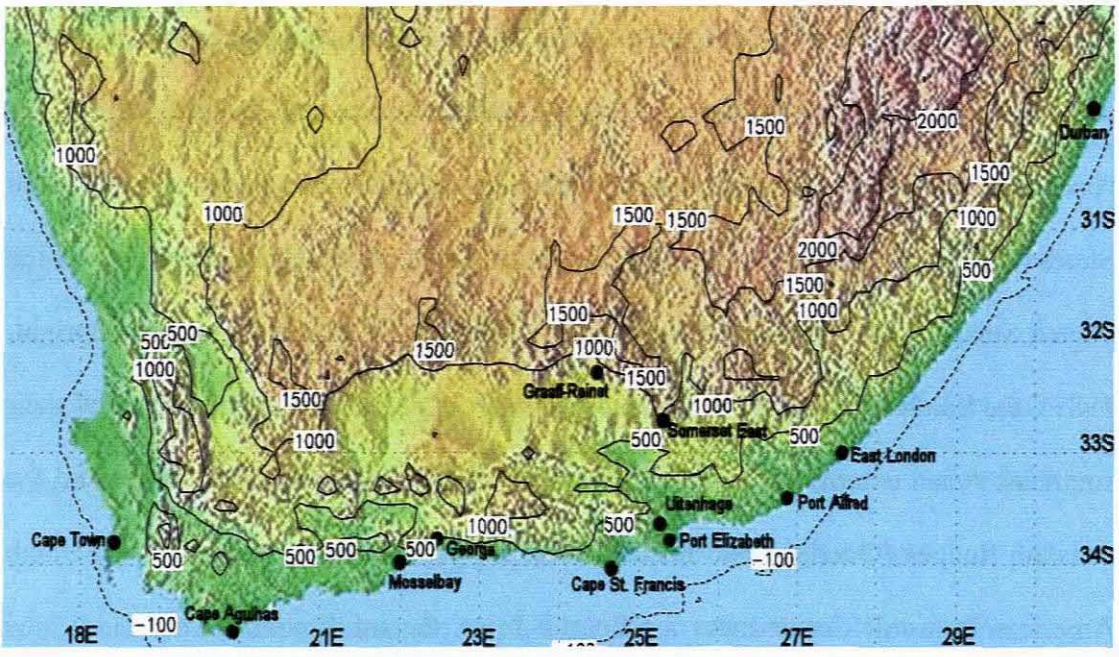

Fig. 1.2 Shaded relief map of South Africa with overlaid contours in meters.

Low-level coastal weather is steered efficiently around the periphery of the South African interior plateau and escarpment (Taljaard, 1972). As the air descends in South Africa over the escarpment from the high interior plateau to the coast, cyclonic vorticity is generated and coastal lows form. Without the topographical configuration of interior plateau, escarpment and coastal littoral, they would not come into being.

The coastal lows are usually initiated on the west coast near Walvis Bay and then propagate southwards to Cape Town as internal Kelvin waves trapped vertically beneath a strong low-level subsidence inversion and horizontally on the landward side against the escarpment or coastal mountains. They then move east and north-eastwards along the coast. Coastal lows are shallow (seldom deeper than 850hPa, i.e. about 1500 m), are decoupled from the synoptic-scale subtropical westerly wave usually present above the surface layer, and seldom produce precipitation in excess of mist or fine drizzle (Preston-Whyte and Tyson, 1988).

The main topographical features of southern Africa are the inland plateau with an average height of about 1500 meters, and its convex coastline. South Africa as a whole resembles a dome with a horizontal radius of curvature of about 900 km with coastal mountains forming the edge of the dome, allowing low-level coastal weather to be steered efficiently around its periphery (Taljaard, 1972). Along the south coast, the edge of the dome is separated from the sea by ranges of fold mountains (Fig. 1.2), which form a more or less effective barrier to the inland movement of maritime air. These fold mountains also serve to deflect and distort the off-plateau winds (Van Lingen, 1944). The coastal low is trapped beneath the elevated temperature inversion at the top of the marine layer, average height approximately 1200 m at Port Elizabeth (Preston-Whyte, Diab and Tyson, 1977), and against the mountain barrier where the one kilometre contour (Fig. 1.2) is, on average, approximately 70 km from the coastline (Estie, 1990).

Another significant feature is the difference between the inversion level on the west coast, and that of the south and east coasts where greater surface heating on the Indian

Ocean with its warm Agulhas Current is typically 10°C warmer than on the South Atlantic side with its cold Benguela Current, which is often reduced further by coastal upwelling (CLW, 1984). This difference in inversion heights may be the single most significant reason why coastal lows on the west coast have lower propagations speed than the ones on the south and east coasts (Reason and Jury, 1990). The other main reasons would include differences in the topography and in the synoptic forcing.

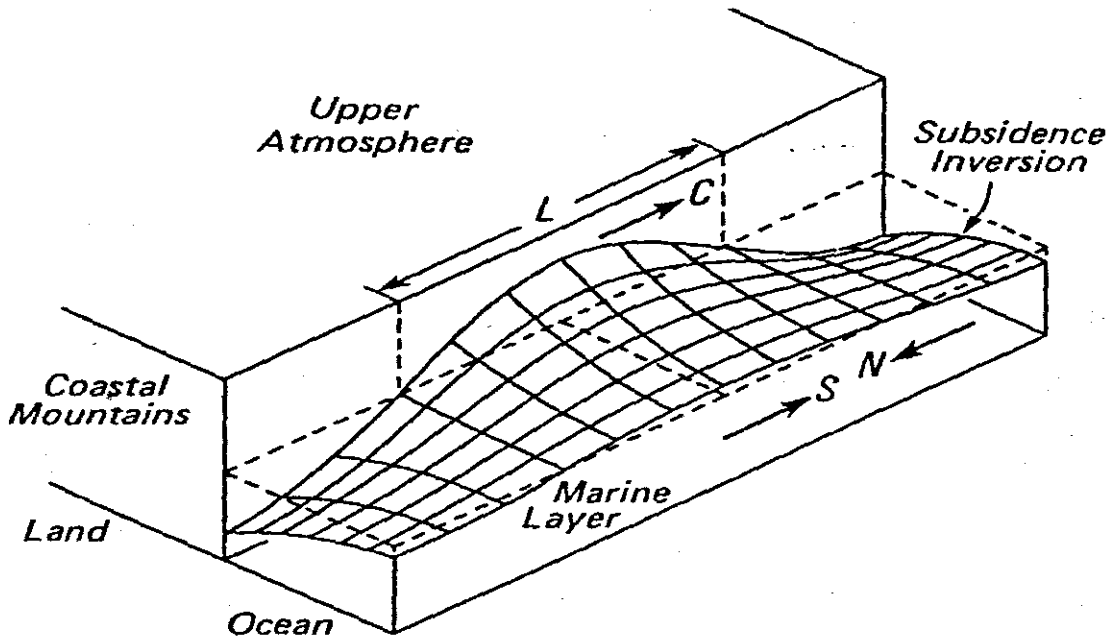

Fig. 1.3 Conceptual view of the atmospheric and topographic conditions associated with coastally trapped disturbance propagation as a distortion of the base of a subsidence enhanced marine inversion, - L is the alongshore length scale, C the propagation speed, N the northerly surface wind and S the southerly surface wind for a Southern Hemisphere coastally trapped disturbance (Reason and Steyn, 1990).

The effect of latitude on the south coast of South Africa is that the Coriolis force causes the pole-wards moving offshore pre-coastal low air to become convergent (Preston-Whyte and Tyson, 1988), and cyclonic vorticity is associated with convergence (Preston-Whyte and Tyson, 1988). In this way an additional amount of vorticity may be generated along the south coast of Africa.

The buoyancy advection derived from the dynamically and adiabatically heated, pre-coastal low offshore winds, together with the cyclonic vorticity acquired during the descent from the interior plateau to the coast, leads to coastal low rather than coastal high formation. The descending air mass will lead to an area of cyclonic vorticity at the coast which, together with the falling pressures resulting from the lower density of this airmass, will give rise to a coastal low pressure cell (Reason and Jury, 1990).

Coastal disturbance intensity is at a maximum near the coast and decays seawards (Anh and Gill, 1981). The coastal low is trapped (Fig. 1.3) to within a Rossby radius (approximately between 100 and 200 km) of the escarpment or blocking mountains through Coriolis force effects on the along shore flow and reduction of across-shore flow at the coastal mountains (Anh and Gill, 1981; Reason and Jury, 1990).

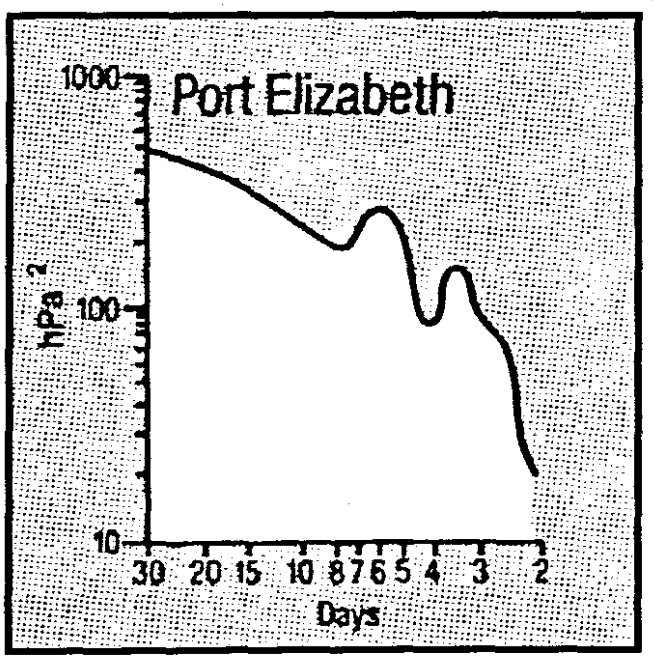

Fig. 1.4 Spectral analysis of surface pressure oscillations (Preston-Whyte and Tyson, 1988).

Coastally trapped disturbances are confined to the coastal zone and propagate horizontally along the shore with the coast on the left in the southern hemisphere until frictional or orographic effects lead to the dissipation of the disturbance. Another cause for dissipation of the coastal low northwards of Durban would be the diverging nature of the coastline and plateau (Reason and Steyn, 1990).

If the coastal low becomes coupled to the wave above, it may develop into a coastal depression that will produce rainfall on a larger scale (Estie, 1984). Apart from the normal summer thunderstorms moving over the coast, there should be no significant precipitation with coastal low (Hunter, 1987).

Co-spectra of pressure fluctuations at Cape Town and some east coast stations reveal that, on average, disturbances take 1.2 days to travel from Cape Town to Port Elizabeth. The perturbation time series show prominent spectral peaks at about 3 and 6 days at Port Elizabeth (Fig. 1.4) and at various other coastal stations (Preston-Whyte and Tyson, 1988).

Propagation speeds for a 5 – 6 day oscillation along the coast of 6.3 $m.s^{-1}$ have been obtained by making use of the phase lag between coastal stations (Preston-Whyte and Tyson, 1973). A limited number of events were studied with propagation speeds of 17 – 54 $m.s^{-1}$ found between Cape Town and George/Port Elizabeth (Shillington, 1984), although the latter speed was possibly due to a coastal low that reformed further along the coast, or that it was a separate low entirely. Propagation speeds of 6.9 $m.s^{-1}$ to 25 $m.s^{-1}$, excluding outlyers, were found by Hunter (1987). An analysis of hourly pressures from Durban and Port Elizabeth gave a phase speed of 29 $m.s^{-1}$ with a

propagation speed virtually independent of frequency (Schumann, 1983). The propagation speed of three case studies showed a change from around 10 $m.s^{-1}$ on the west coast to over 20 $m.s^{-1}$ on the east coast (Jury, MacArthur and Reason, 1990).

The development of coastal disturbances along the South African coast is dependent on the forcing function, which is a function of the orographic gradient and the component of the flow down the gradient—the steeper the gradient, or the stronger the flow, the larger the forcing function and the resulting disturbance (de Wet, 1983). Due to their mesoscale properties, only the coarsest features of orographically trapped disturbances can be captured by standard weather observing networks and forecasting by numerical weather prediction models is difficult (Reason, 1993; COMET, 1999).

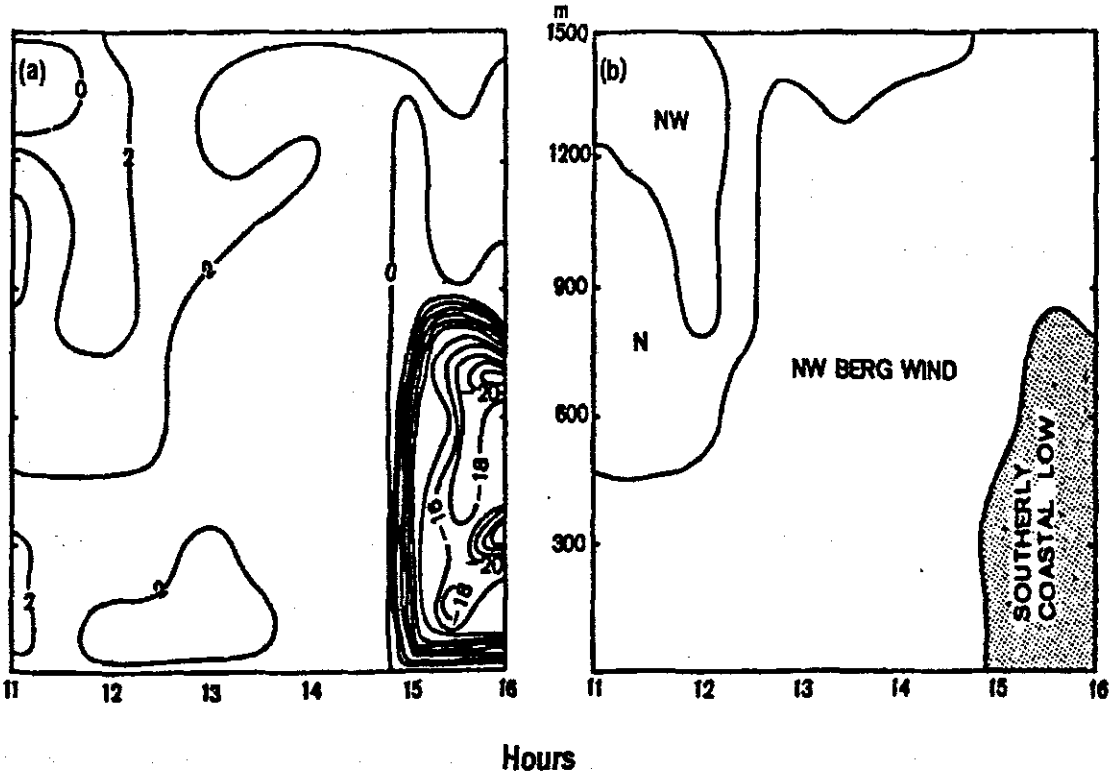

Fig.1.5 Time section to show wind components ($m.s^{-1}$) parallel to the coast (a) and wind direction (b) during the passage of a coastal low past Durban on 1st July 1969 (Preston-Whyte, 1975).

The main objective of this study is to improve analysis and forecasts of the very strong winds that occur after coastal lows passage. The change from pre-coastal low offshore flow to the sideshore post-low winds is abrupt, and the change in wind direction may be as much as 180 degrees. Very strong post-coastal low winds do not occur often, but when they do occur, the effects have the potential to be hazardous. An example of these strong winds is given in Figure 1.5(a). The temperatures over the interior ahead of the coastal low are warm to hot during the day due to dynamic warming and are enhanced by the adiabatic warming of offshore northerly flow. Berg wind type offshore pre-low wind flow is indicated in Figure 1.5(b).

Sea surface temperatures are influenced by the longshore wind flow and Ekman transport (Schumann *et al.*, 1995). A sea surface temperature change of more than 10°C is possible within a few hours (Schumann *et al.*, 1995). Goshen and Schumann (1995) state that cold water upwelling would emerge within a day of easterly flow along the Algoa Bay shore of Cape Recife, and as upwelling-generating easterly winds generally last between one and three days, it would be possible for a Kelvin wave to transport water upwelled along the southern shoreline of Cape Recife into the south-western corner of Algoa Bay. Easterly flow is often in the order of two to three days ahead of the coastal lows and this would cause a significant change in the boundary layer temperature fields. A shelf wave in the ocean propagates with the coastal low in the atmosphere (Jury, MacArthur and Reason, 1990)

In the case of the South African coastal low, symptoms such as the symmetric adjustment of the inversion layer, the east/west wind switch below that, continuous propagation and a drop in the near-surface temperature was found to be consistent

with the coastal low as an internal Kelvin wave propagating in the marine layer (Jury *et al.*, 1990; Reason and Jury, 1990). Two other crucial properties of Kelvin waves were also satisfied. That the coastal low propagates downstream with the coast on the left (southern hemisphere) and that the coastal low should decay offshore from the coast within a Rossby radius (Gill, 1982; Reason and Jury, 1990). The time-height structure of the coastal low was found to resemble a continuously forced Kelvin wave, particularly with regard to the symmetric shape and temporal behaviour of the inversion. The theoretical Kelvin wave phase speed;

$$c = (g'H)^{0.5}$$

where **g'** is related to the inversion strength and **H** is the height of the inversion, was compared to synoptic scale observations and agreement was found both in the consistent propagation and coherent structure of the system (Reason and Jury, 1990). The fact that the low propagates around the pronounced bend in the mountains east of Cape Town supports it being a forced linear Kelvin wave as opposed to an impulsive solitary Kelvin wave (Reason and Jury, 1990).

Using the Colorado State University Regional Atmospheric Modelling System (RAMS), the influence on the propagation of coastally trapped disturbances (CTD) by large gaps in the bounding coastal mountains was studied (Reason, Jackson and Hai Fu, 2000) and it was found that the gaps weaken the intensity of the coastally trapped disturbances and slowed its propagation. Since coastally trapped disturbances (which include the coastal low of South Africa) are mesoscale systems trapped laterally against coastal mountain ranges by Coriolis effects and vertically by stable stratifications, the effect that a break in the lateral trapping mechanism has is of great interest. It was found that the larger the gap, the more pronounced the effect turned

out to be. Gaps in the order of 25 – 50% of the Rossby radius were found to be important (Reason, Jackson and Hai Fu, 2000).

Observations (Reason and Dunkley, 1993) show that OTD often slow near major topographical variability, i.e. in areas where one might expect frictional effects to be the greatest (Reason, 1993).

A definition of the coastal low used by the forecasting meteorologists at the South African Weather Bureau (Estie, 1984), was stated as a small area of relatively lower pressure which appears in the lower levels of the atmosphere (below 700hPa) along the coast. It is associated with subsidence off the interior escarpment. The accompanying inversion and wind shear in the lower levels strengthen the recognition of the coastal low for the forecaster, but the essential features of the coastal low are the pressure minimum and the shallowness of the system. This definition excludes any low-pressure system situated on the coast which is supported by an upper air trough or cut-off low in vertical alignment. It is important in identifying a coastal low to confirm that the upper trough tilts significantly to the west and is not in vertical alignment above the coastal low (CLW, 1984).

Further, three classes of coastal low were established at the workshop (CLW, 1984).

- Class one: the "summer" west coast low, taking place predominantly in summer.
- Class two: the travelling coastal low, where the high pressure ridges to the south, leading to the formation of the coastal low on the west coast, with the coastal low moving down the west coast as a trough of low pressure while its

associated cold front approaches from the west; thereafter, the forcing function shifts to the south coast and the coastal low propagates in front of the trough, along the south and southeast coasts as long as the following function precedes it.

- Class three: the "winter" south coast low taking place predominantly in winter. Here the South Atlantic High takes up a more northerly position and does not ridge in south of the continent, a series of cold fronts associated with a single westerly wave can pass over the south of the country. Prior to the passage of the first cold front, the forcing function will be established on the south coast and the coastal low will act as a leader cell on the east coast. It was noted that any of the three synoptic situations, and hence the three classes of coastal lows, can occur at any time of the year.

Other significant characteristics of the coastal low noted at the coastal low workshop were that the coastal low would, depending on the wave length of the synoptic-scale ridge/trough system, develop on the South Coast in the Mossel Bay area when a well-defined frontal system is 12 to 15 degrees of longitude west of Cape Town (Estie, 1984), with the coastal low preceding the passage of a frontal trough by roughly 10 – 16 hours (Hunter, 1984). There is often no link between the coastal low on the west coast and the one on the south coast, with the west coast low remaining semi-stationary and the south coast coastal low forming ahead of the approaching front (CLW, 1984). The change in wind direction is the sure signal of a coastal low (Estie, 1984), and the pressure minima is usually synonymous with a coastal low but is perhaps not suitable as a signature due to interference of diurnal effects and to interior or mid-latitude trough interactions (CLW, 1984). Rapidly falling coastal pressure

(high negative pressure tendency) associated with an intensifying coastal low is usually linked to an intensifying frontal system (Hunter, 1987).

The relationship between the upper atmospheric Rossby waves and coastal trapped waves were investigated with significant energy contributed by waves of length 8000 km (Wave 4) to the pulsing of the physical environment in the southern Benguela region (Jury *et al.*, 1990).

A grid-point based numerical weather prediction (NWP) model can resolve features as small as about four grid lengths. Anything smaller than the four grid lengths will be "aliased", which means that it will be misinterpreted as having a longer wavelength than it really does. Features that span less than 8 – 10 grid points, although fairly well represented initially, will quickly degrade with time. A feature will be well forecast (resolved with enough definition in the model's initial analysis that it will be carried forward in time with reasonable accuracy in the subsequent model integration), over 1 – 2 days forecast length, if it spans at least 8 – 10 grid points. Even if a feature meets the resolvable size criteria, it may still be inadequately resolved based on its orientation and juxtaposition within the model grid. Models also have difficulty in resolving features influenced or caused by the interface between land and large bodies of water (including oceanic coastal regions). This can be improved by increasing the horizontal resolution (Jascourt *et al.*, 2001; COMET, 1999).

However, the biggest factor in obtaining improved forecasts from high-resolution models is that high-resolution data must be available and the data assimilation system must handle those data correctly at the resolution of the model (Jascourt *et al.*, 2001).

f budgetary issues do not allow for an increase in high-resolution data, increasing the esolution of the model will be the next-best option. Computing resources ultimately imit the resolution of NWP models. The additional computing resources required to un a model at half its current horizontal resolution increase by a factor of eight, ıssuming no change to the vertical resolution or domain size (COMET, 1999).

The coastal low is a mesoscale system with a cross-shore width of approximately 100 to 200 km (Anh and Gill, 1981; Reason and Jury, 1990), away from the escarpment or blocking mountains. With an average cross shore size of 150 km, and taking a median of 9 grid points, a 10 or 15 km grid point model would be required to provide a good one to two-day forecast of the coastal low.

Coastally Trapped Wind Reversals (CTWR's) along the California coast are compared to coastally trapped disturbances in a mesoscale model training module on CTWR's, which includes the South African coastal low along the west coast of South Africa (COMET, 2003). In the summary section some of the findings include; that the wind reversal defines the event, that the disturbances propagate faster than the wind which suggests that they are internal wave-like disturbances trapped against the coast (i.e., a Kelvin wave) and that the disturbances occur very low in the atmosphere – typically below 850 hPa – within the marine boundary layer and its capping inversion. Also found is that the low pressure associated with the disturbance is located near the point of strongest offshore flow, and that the wind reversal propagates along the coast, underneath the region of strongest offshore flow. Suggestions for forecasting the low includes that the synoptic scale models will give reasonably good guidance for the area of the strongest offshore flow (that the synoptic scale forcing is handled well by

mesoscale models); however, mesoscale models tend to overemphasize sea breezes and diurnal forcing, which can mask some of the features of coastally trapped wind reversals. It is also cautioned that mesoscale models may not depict the timing and location of the disturbances well. Another significant point made in the module is that the offshore flow at 850 hPa (forcing function) goes accompanied by an extension of warm temperatures and that the region of strongest offshore flow marks the region of greatest warming and largest pressure falls along the coast.

A debate exists about the relative importance of synoptic-scale forcing versus variations in the MBL depth and inversion strengths in the generation and propagation of mesoscale coastally trapped disturbances similar to the coastal low (Nuss *et al.*, 2000; Mass and Bond, 1996).

Mass and Bond, 1996, gave three reasons for the dominance and direct effect of synoptic forcing and its modulation of the climatological thermal trough, which creates the Coastally Trapped Wind Reversal on the West Coast of North America. They stated that the composite pressure anomalies that weakened or reversed the climatological coastal pressure gradients were clearly synoptic in scale and not restricted to the coastal zone where trapped marine-layer effects may be significant. Secondly, application of the hydrostatic equation indicates that gradients in the marine-layer depth are generally not large enough to reverse the climatological alongshore pressure gradient over a significant horizontal domain. They used the example that even a large 400m upward displacement of a marine layer capped by a 7°C inversion results in a surface pressure change of only about 1.2 hPa, in comparison to an approximately 5 hPa climatological pressure difference between

iorthern California and San Diego. The last reason given was that several mesoscale nodel simulations had produced realistic trapped southerlies without adequately simulating the topology of the marine layer. They did state however that even if the synoptic scale forcing was the dominating factor, the gradients in marine-layer height could be concentrated over relatively limited domains, and that the resulting pressure gradients and their influences on the wind fields could be quite large (Mass and Bond, 1996).

1.3 Theoretical framework of this study

Upper air convergence on the lee side of Rossby waves in the westerly jet stream of the Southern Hemisphere's lower latitudes drives the surface anticyclones that dominate the southern parts of Africa and the southern Indian and Atlantic Oceans (Preston-Whyte and Tyson, 1973). It is the usual progression of the eastwards ridging of the AOA (South Atlantic Ocean Anticyclone), budding off into and strengthening the IOA (South Indian Ocean Anticyclone), which then in turn causes offshore flow from the interior plateau of southern Africa.

Coastal lows are essentially Kelvin waves generated by the interaction of synoptic-scale systems with the topography (e.g., Gill, 1977; Anh and Gill, 1981). The coastal lows are forced by the synoptic-scale pressure systems which are affected by the presence of the elevated land mass (Gill, 1977; Anh and Gill, 1981; Reason, 1993; Reason and Jury, 1990; Reason and Steyn, 1990). In Southern Africa, ridging of the AOA south of the landmass drives the offshore flow that results in the coastal low. It

is also this synoptic forcing that determines where the coastal low ceases and propagation dissipates (Reason and Jury, 1990).

Mass and Bond (1996) considers the synoptic flow to be the dominant factor (forcing function) in the generation of the coastally trapped wind reversals (CTWR's) of the western American coast, and that the propagation speeds of the CTWR's depend on the movement of the synoptic-scale features. The CTWR's and the coastal low of Southern Africa are both coastally/orographically trapped disturbances and are similar in many respects (Reason and Steyn, 1990).

This study focuses on changes in the synoptic-scale offshore flow, as it is this flow that is the forcing function that generates, maintains and effectively steers the coastal low eastwards along the South Coast. The coastal low is caused primarily through lee side and thermal troughing, based on the arguments of CTD generation as presented by Mass and Bond (1996) for the west coast of America's CTWR's. The resultant dynamic and internal structure of the coastal low, as an internal Kelvin wave, is not considered and neither are the changes in and to the marine layer.

A primary reason for concentrating on the synoptic scale flow is a lack of fine temporal and spatial data over the study region. The numerical model data used is very coarse (2,5 X 2,5 km grid) and for that reason these data are more applicable to synoptic scale parameters. The coastal stations with appropriate data (surface and upper air) are far apart, and are themselves often not sited very close to the ocean, and are in places (particularly George and Cape Town) therefore a poor reflection on the marine environment.

The lee side troughing is caused through buoyancy advection of the previously dynamically warmed air (originating over the interior of South Africa) moving out almost orthogonally over the coast. This area of lowered pressure along the coast is then further affected by adiabatic heating of the offshore flow on descent from the interior plateau, sometimes heating adiabatically by as much as 10°C, which results in a deepening of the coastal surface pressure in the area of the strongest offshore flow. These processes give rise to the coastal low-pressure minimum. Positive vorticity is generated through vortex stretching as the offshore flow (at around 850 hPa) moves from the interior plateau out over the coastal belt. The resultant coastal low is then trapped to within a Rossby radius of the escarpment through Coriolis effects on the along-shore flow and the vanishing of the across-shore flow at the coastal mountains (Reason and Jury, 1990).

Along the southern parts of Africa, the IOA and the following interior thermal trough on its western edge over the interior plateau retreats eastwards, ahead of the approaching frontal system (or ridging AOA in the cases where the front passes by to the south of land). As the interior trough retreats eastwards, the coastal low propagates eastwards underneath the tongue of warm, relatively strong offshore flow along the eastern edge of the interior thermal trough.

The inversion at the top of the marine boundary layer is higher along the southeast coast than along the west coast primarily because the sea surface temperatures are higher. Another factor which may affect the height of the inversion is upwelling caused by the pre-coastal low easterly flow. The strength of the inversion is modified by the warm offshore flow, which depresses and strengthens the inversion in the

vicinity of the minimum pressure associated with the coastal low. The Kelvin wave's theoretical phase speed (propagation speed of the coastal low) is based on the height and strength of this inversion layer.

The coastal low could not exist in its present form without this combination of the warm offshore flow, the marine boundary layer (MBL) and the coastal mountains along the periphery of the interior plateau which rise above the top of the marine layer, allowing the coastal low to be trapped below the MBL inversion in the vertical and against the mountains in the horizontal.

The hypothesis is that a stronger and warmer offshore flow should lead to more intense coastal lows.

CHAPTER 2

DATA, METHODOLOGY AND BACKGROUND CLIMATOLOGY

2.1 Meteorological data

Daily synoptic weather charts for 12:00 UTC as published by the South African Weather Service (hereafter SAWS) in their Monthly Newsletter for the 10-year period from 1 January 1987 to 31 December 1996 were used for preliminary subjective identification of coastal lows. Thereafter the coastal low passages were pinpointed using hourly observations at the various observing stations.

2.1.1 Surface observations (station data)

This study used hourly surface weather observation data for the 10-year period from 1 January 1987 to 31 December 1996 of temperature, humidity, pressure and wind as measured at the official weather stations at Cape Town, George, Port Elizabeth, East London, Durban, Somerset East, Uitenhage and Graaff-Reinet (Table 1.1). A Dines anemometer measured surface wind speed and direction at 10 meters AGL, a Kew barometer was used for atmospheric pressure recordings, and standard wet and dry thermometers were used to determine humidity and dew point temperature values using hydrometric tables.

Table 2.1 Particulars of weather stations used in study. Latitude and longitude is in decimal degrees.

Weather Station	Elevation (meters)	Latitude	Longitude
Cape Town	46	33.96° S	18.6° E
George	218	33.96° S	22.417° E
Cape St. Francis	7	34.12° S	24.50° E
Graaff - Reinet	784	32.2° S	24.55° E
Uitenhage	157	33.7° S	25.433° E
Somerset East	717	32.733° S	25.583° E
Port Elizabeth	66	33.98° S	25.6° E
East London	130	33.03° S	27.833° E
Durban	8	29.96° S	30.95° E

After October 1992, when the switch over to AWS (Automatic Weather Station) and EWOS (Electronic Weather Observing System at airports) took place, measurements in both systems were by PRT sensor PT100/1000 with model accuracy of 0.2°C for temperature, Vaisala PTB 200 with accuracy of 0.2 hPa for pressure and RM Young model 105 with a wind direction accuracy of 5° and wind speed accuracy of 2 $m.s^{-1}$ for wind speed.

The highest wind gust was recorded for each day; with the wind gust defined as the instantaneous wind rising to 5 $m.s^{-1}$ above the average wind. While the airports switched to EWOS in 1992, Uitenhage became an AWS station on 1 September 1985 and Graaff-Reinet switched to AWS on 1 July 1992. Somerset East had previously been a 1st order station with the SAWS.

2.1.2 Upper-air observations (station data)

Radiosonde upper-air data for the three national weather offices at Cape Town, Port Elizabeth and Durban airports (within Table 1.1) for the same 10-year period were used. The ascents at all three locations were released twice daily, at approximately 00:00 UTC and 12:00 UTC. The ascent data were obtained from the SAWS in standard and significant level format bulletins. The tracking equipment used during this period by the SAWS was the Omega system (to determine upper winds) and Vaisala receiving equipment was used with the Vaisala RS-80 sondes. Data included profiles of temperature, dew point temperature, wind speed and direction.

2.1.3 NCEP Reanalysis data

NCEP Reanalysis data provided by the NOAA-CIRES Climate Diagnostics Centre (CDC), Boulder, Colorado, USA, from their web site at http://www.cdc.noaa.gov was extensively used in Chapter 3. Composites of the NCEP/NCAR Reanalysis 1 daily averaged data, with a 2.5-degree latitude by 2.5-degree longitude global grid for the SON season from 1987 – 1996 was used between 10°S to 60°S and 10°W to 60°E. The available dataset has a temporal coverage from 1/1/1948 to present with output every six hours. The full spatial coverage is global at a 2.5-degree latitude by 2.5-degree longitude grid.

The model parameters consist of three principal parameters. The SSI analysis, Global Spectral Model and the observation quality control programs of the NMC data assimilation system. The system cycles on itself. The Global model moves the system

along in time; then the SSI corrects the time integration toward the observed values, providing the initial conditions for the next 6-hour integration.

Wind speed and direction reanalysis data at 850 and 700 hPa for Port Elizabeth was obtained from the South African Weather Service, for both 850 and 700hPa, for the 10-year period 1987 – 1996.

2.1.4 Model display and analysis programs used

GrADS – Grid Analysis and Display System. Program and user's guides available on http://grads.iges.org/grads/grads.html All model analysis and topographical displays were done using GrADS (COLA/IGES) unless otherwise specified.

PcGRIDDS – PC Gridded Interactive Diagnostic and Display System. User's guide available on http://www.lib.noaa.gov/pcgridds

2.1.5 Numerical forecast models

The EMC/NCEP Eta Workstation mesoscale numerical weather forecast model version 0.2 (http://wwwt.emc.ncep.noaa.gov/mmb/wrkstn_eta/) was used for particular case studies. A full description of the Eta model is available (Rogers et al., 1996).

A short description of the model configuration used includes (Matthew Pyle, 2002):

- Default convective scheme – Betts-Miller-Janjic parameterization
- Boundary layer – Mellor-Yamada Level 2.5 scheme
- Hydrostatic version
- Mass based vertical coordinate (pressure-based)
- Step topography
- Microphysics – Zhao scheme (relatively simple with few hydrometeor species in order to run with the speed necessary for operational modelling)
- Various grid resolutions including 20 vertical layers and 15 km horizontal layers
- Input and boundary layer data was obtained from the FTPPRD server, boundary files used were the early release (T+4), limited AVN for every 6 hours during the 48 hour forecast period.
- The output forecast time was set at T+48, with a forecast output file for every hour during the 48-hour forecast period.
- The operating system used was Linux RH-8 using a Pentium 111, 800 MHz computer.

GFS (Global Forecast System) – The NCEP (National Centers for Environmental Prediction) GFS model data was used. This model is a combination of the AVN (Aviation model) and the MRF (Medium Range Forecast) models.

The GFS is a Spectral model with transformation to a Gaussian grid for the calculation of nonlinear quantities and physics.

The horizontal resolution of the GFS is approximately 0.5 X 0.5 degrees latitude/longitude with a vertical resolution of 64 unequally-spaced sigma levels.

2.1.6 Topographical data

All topographical data were obtained from the Internet site http://cola8.iges.org:9191/dods/topo/topo05 consisting of the 0.08° average resolution topography dataset, and was displayed using GrADS (COLA/IGES).

2.2 Methodology

To perform comparative studies between average coastal lows and strong case coastal lows, it was necessary to identify a ten-year period, in order to have as large a population size as possible that also had the best available data.

The single most limiting factor was upper air data, as the SAWS had significantly reduced the amount of upper air ascents performed, due to budgetary constraints, in the latter 1990's. The period chosen was the ten-year period from 1 January 1987 to 31 December 1996.

The initial identification procedure involved using two operational forecasters from the Port Elizabeth Weather Office to independently select coastal lows from the 1200 UTC daily synoptic weather charts of the SAWS for this 10-year period. Any coastal

minima cases that may possibly have been the remains of cold fronts, or did not have the typical visual signature of coastal lows, were discarded. As suggested by participants at the (CLW, 1984) any coastal minima that had linked to the approaching westerly trough above, or were connected with an upper level low, were also not included.

Individual coastal lows were marked by noting the point (hour) where the surface wind at the Port Elizabeth Weather Office changed to southwesterly on the hourly observation records. In this study the surface wind change was used as the primary indicator of coastal low passage, with the surface pressure minimum being the secondary indicator.

In some of the cases, in particular during the early morning hours, the arrival of southwesterly winds is delayed by a nocturnal inversion, and here the pressure minima were used to be representative of the passage of the coastal low.

To study the nature and evolution of the coastal lows, the surface temperature, surface atmospheric pressure, wind speed and wind direction (10 m) data for a period of 48 hours before passage to 24 hours after passage were averaged for 642 cases, and also for the strongest 5% of cases (strongest 32 coastal lows), using the mean strength of the 8-hour average wind speed of the southwesterly post coastal low passage as the defining factor for the strong coastal lows.

The wind direction averages were obtained by reducing the original wind records to their U and V (meridional and zonal) components, in order to do a true vector analysis

for the average wind directions. The diurnal variation (monthly averaged long-term diurnal variation) was filtered from the temperature and pressure data before averages were calculated.

As the wind gust data were only recorded once per day, 12% of the data had to be discarded due to uncertainty whether the gusts were associated with the post-coastal low southwesterly winds, or due to missing data.

2.2.1 Defining strong cases

The mean of the 8-hour post-coastal low passage wind speed for each coastal low was used to represent the long-shore southwesterly wind surge strength in order to differentiate between coastal lows. This period was chosen as the wind speed time series (Fig. 3.1) shows that the average southwesterly wind speed drops significantly at around 8 hours after the coastal low passage at Port Elizabeth. The top 5% of these 8-hour means were selected to represent the strong cases out of all 642 coastal lows during the 10-year period, and the top 10% of the 8-hour means represent the strong cases during the SON season.

2.2.2 Upper air study on 10-year data

NCEP reanalysis data were used to plot 700 and 850hPa wind roses at coastal low passage, for 12-hours before and also 12-hours after passage for all 642 cases. The 12-

hour periods were made up by averaging all coastal lows which fell within six hours, either way, of the passage points.

2.2.3 September, October and November Season (SON)

Due to the higher frequency of strong coastal lows during the SON season (Fig. 3.5), coupled with the fact that the SON season contains the strongest average hourly surface wind speeds at Port Elizabeth (Fig. 2.1), the rest of the coastal low analysis concentrates only on SON season data.

2.2.4 Propagation of the coastal low

To study the propagation of the coastal low a 10% sample (16 cases) of the strongest and a 10% sample (16 cases) of the median coastal lows cases, for the 10-year period from 1987 to 1996, were used for comparison purposes. The coastal lows were tracked back from their passage at Port Elizabeth to Cape Town, noting when that particular low or pressure minima had previously passed Cape Town from the hourly surface data taken at that station. Then the passage at George, East London and Durban were also noted in the same way.

Only coastal lows that had visible signatures at all four of the other weather stations were used. At Cape Town the signature of the coastal low was weak in general, and often the "switching off" of the SE'ly wind was used to signal passage (Hunter,

1987). At times the pressure minima were used to signal passage at George, which is set away from the coast and into the base of the southern Cape fold mountains. At East London and Durban the coastal low was defined by the wind switch to SW'ly (as at Port Elizabeth), and that was used as the signature for coastal low passage.

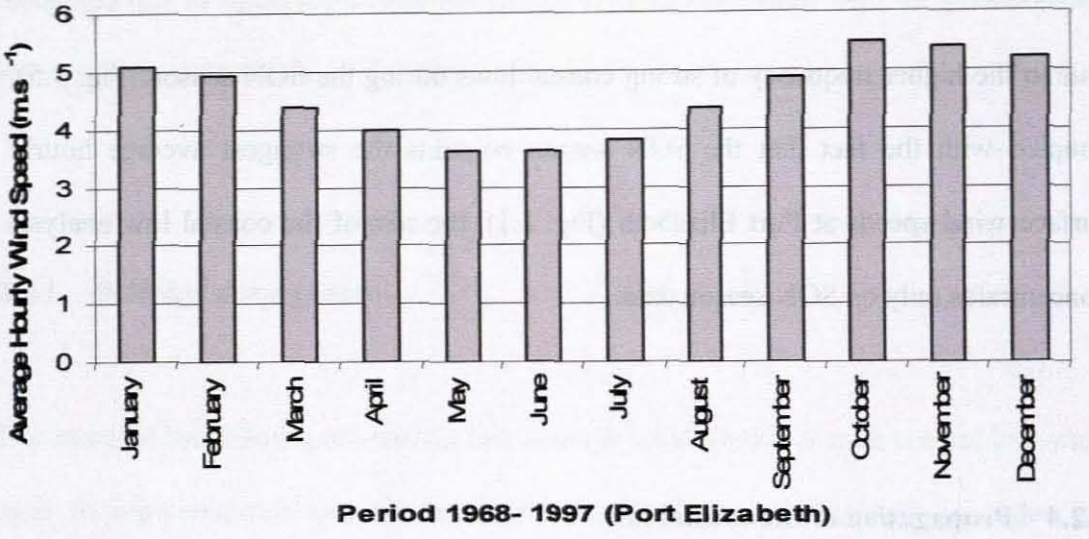

Fig. 2.1 Wind speed monthly averages for the Port Elizabeth Weather Office. The airport has an elevation of 67 meters and is situated approximately 6 km (to the east) and 10 km to the south away from the coast. The windy season is from September to February.

2.2.5 SON Upper air profile

To study the upper air features of the coastal low, and the changes in the upper air associated with the coastal low along the south and southeast coasts, time-height and aeronautical diagrams were created using ascent data (SON) for Cape Town, Port Elizabeth and Durban Weather Offices. These are the only regular radiosonde releasing stations along the south and southeast coasts. The strongest 10% and the median 10% composite samples of coastal low sonde data, using the mean 8-hour post

coastal low wind speed as criteria, were considered. The same coastal low sonde composites, tracked back from passage at Port Elizabeth, were then followed along the coast eastwards until they passed Durban.

For a particular ascent, the passage of the coastal low at the surface at a station was noted, then the ascent done within the 12-hour period before that passage was used as indicative of the state of the atmosphere immediately before coastal low passage.

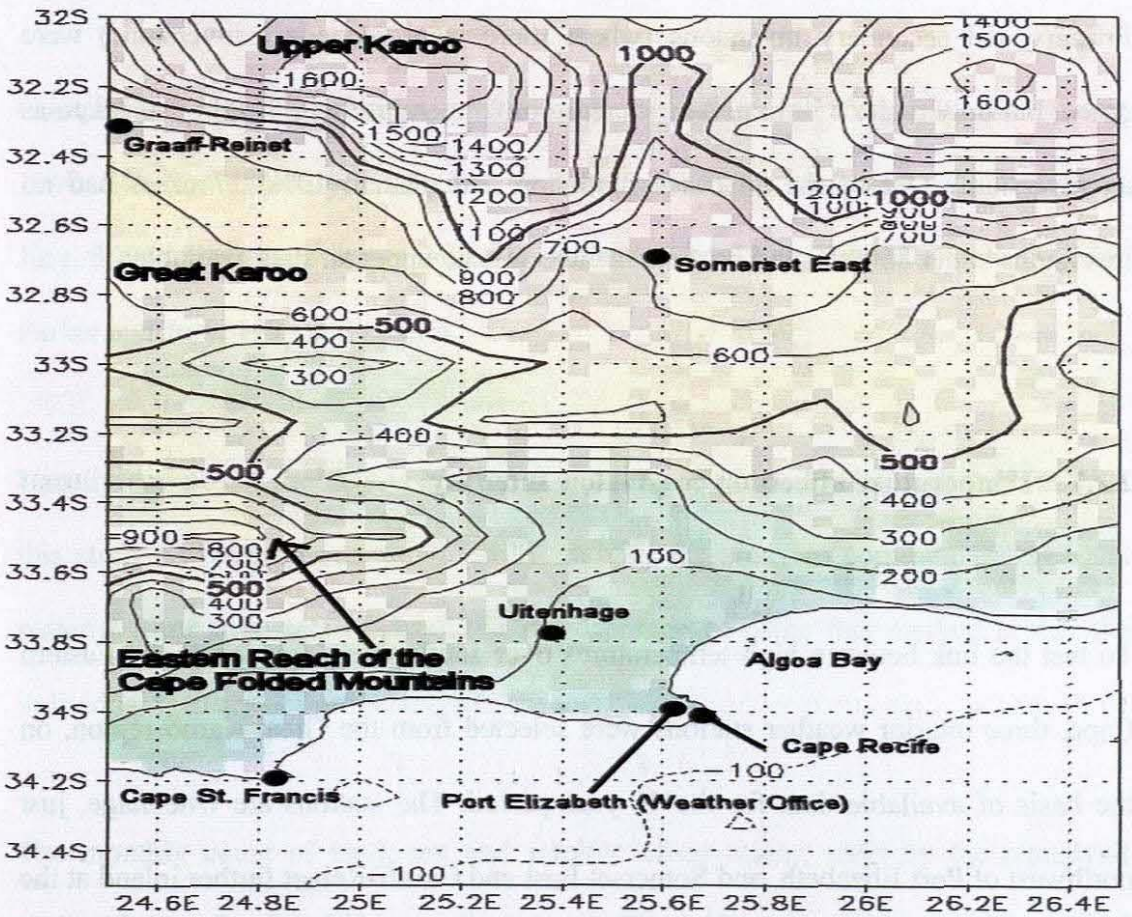

Fig. 2.2 Locations of the weather stations and sites used in the temperature gradient hypothesis section of the study. Contours are in meters.

Out of the possible 96 cases, there were 4 occasions where no upper air data were available. At Port Elizabeth, diagrams were also created for 24 hours before, 12 hours

before and for 24 after coastal low passage for both the top 10% and median 10% of cases.

2.2.6 Inversions

The significant level data at Cape Town, Port Elizabeth and Durban were used to trace temperature inversions for the top 10% and the median 10% cases (SON). Primary and secondary inversions (where there were secondary inversions) were noted, but only under 850 hPa. Any increase in temperature with height was taken as an inversion. Out of the 96 cases (both top and median 10%) 17 cases had no inversions under 850 hPa and on 4 cases there was no upper air data available.

2.2.7 Temperature affects on coastal low intensity

To test the link between high temperatures over southeastern interior of the Eastern Cape, three interior weather stations were selected from the Great Karoo region, on the basis of available data for the 10-year period. The stations are Uitenhage, just northwest of Port Elizabeth, and Somerset East and Graaff-Reinet further inland at the southern base of the escarpment leading to the Upper Karoo (Fig. 2.2). The average of the daily maximum temperatures at these stations was used to represent the interior temperature.

Using data from the 10-year period from 1 January 1987 to 31 December 1996, correlations were then calculated between the post coastal low southwesterly wind speed and the average maximum temperatures. Other correlations were also drawn between the post coastal low southwesterly wind speeds and upper winds and also surface pressures.

2.2.8 Composite NCEP climatology

Composite analysis has been used by many researchers including (Rui and Wang, 1990; Matarira and Jury, 1992; Jury and Pathack, 1993; Majodina and Jury, 1996; Jury, 1996; Levey and Jury, 1996; Nassor and Jury, 1997; Naeraa and Jury, 1998; Parker and Jury, 1999 and others).

Usually composite analysis is applied at monthly resolution to climate problems, in this study daily resolution was used to simplify the study of common features and patterns from large sets of data. The disadvantage of using this method is that the individual features of particular cases are lost.

The monthly count of land, sea and satellite observations, used by the reanalysis project during October 1991, are displayed in Figure 2.3 as an example of the spread and density of the input data used during the 10-year period from 1987 to 1996.

The satellite data are spread evenly over the region, and land station observations are spread fairly well along the south coast. The ship and buoy count are also well spread along the south coast.

The composites of the top 10% (16 cases) strong coastal low cases were compared, using against the composite of all 160 cases that took place over the 10-year period from 1987 -1996 for the SON season using the NCEP Reanalysis data and imagery (Kalnay et al., 1996), as provided by NOAA-CIRES Climate Diagnostics Center, Boulder Colorado from their Web site at http://www.cdc.noaa.gov/

The mean was derived by first adding all individual cases together (of either the 10% strongest SON cases or all 160 SON cases), the result was then divided by the total number of cases (depending on the sample size) to get a mean value per selected climatic variable at each grid point.

Subtracting the composite mean of either the composite mean of the 10% strongest SON cases, or the composite mean of all 160 SON cases, from the composite mean of all the corresponding days in the NCEP reanalysis database (from 1968 to 1996) produced the composite anomalies.

Subtracting the composite anomaly of all 160 cases from the composite anomaly of the 10% strongest SON cases produced the "differential anomaly" which was used to highlight the deviation of the strong case coastal low from the norm.

Cross-sectional analyses were used to indicate the change in low-level atmospheric structure with height along either latitude or longitude.

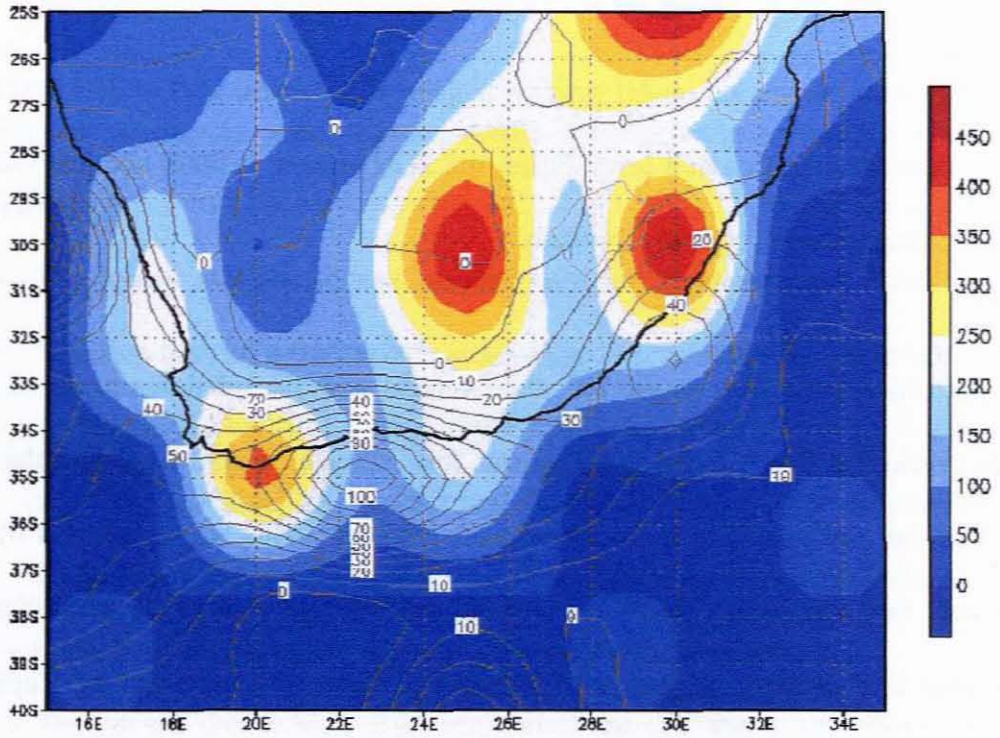

Fig. 2.3 Monthly observations count of land (colour filled) and ship and buoy stations (contours) used by the reanalysis project for October 1991.

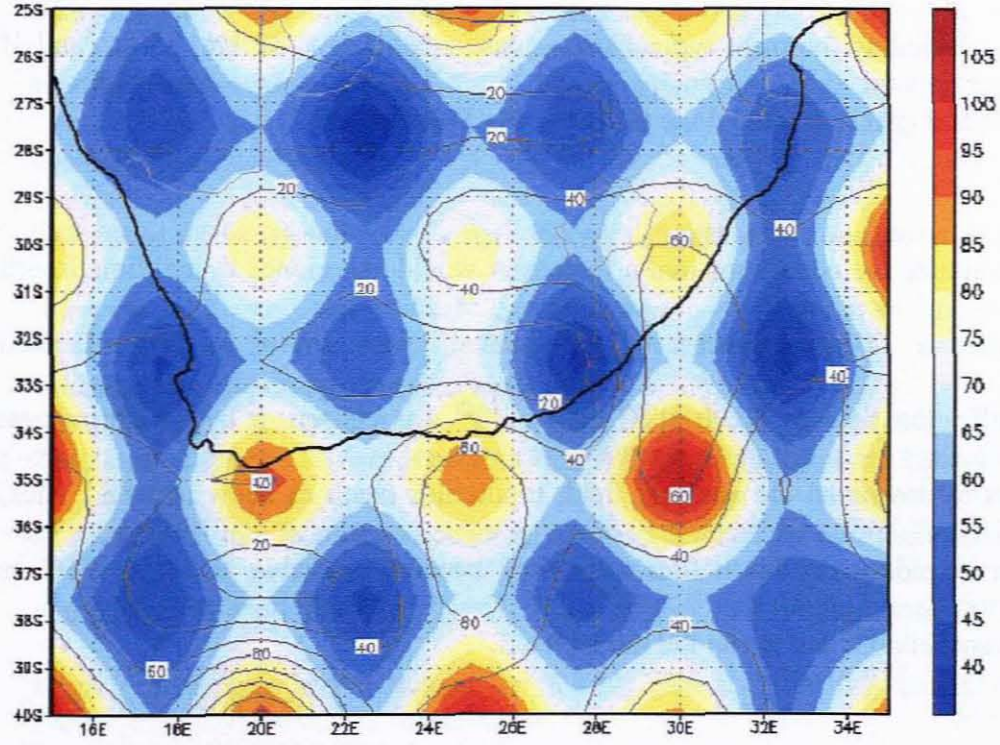

Fig. 2.4 Monthly observations count of satellite wind (colour filled) and temperature (contours) used by the reanalysis project for October 1991.

2.2.9 Case study

Eta workstation mesoscale model runs were done at a vertical grid of 32 kilometers for the three strongest coastal lows during the SON season of 2003 and analyzed in order to select the most typical case study.

The low which took place on the 17th of November was discarded due to the surface winds veering at Port Elizabeth on coastal low passage, which suggested that the centre of the low passed to the north of Port Elizabeth. This was confirmed by the mesoscale run. The low on the 24th of October was also not used due to an anomalous mesoscale low pressure region approximately 2 degrees southwards of Cape St. Francis at the time of coastal low passage at Port Elizabeth.

The coastal low which passed Port Elizabeth at 07:00 UTC on the 14th of November was selected as the most typical strong case coastal low. 32 km, 15 km and 10 km horizontal grid runs were done using the Eta Workstation.

To simulate the conditions that a forecaster would experience in real time in order to produce a 24-hour forecast of the coastal lows' arrival at Port Elizabeth an initialization time of 00:00 UTC on the 13th was chosen. It takes approximately 2 hours to download the analysis field, input files (such as snow and SST files) and main boundary condition files after they become available at 04:00 UTC on the relevant servers, and to run the model itself.

2.3 Limitations of the study

In order to assess the value of this study, the following limitations should be considered.

1. The hourly surface observation data used are from the main South African Weather Service's observing sites along the coastal belt. In places, most notably in the cases of George and Cape Town, these sites are situated away from the coastline, and are for that reason not always representative of the marine environment. In these cases, local effects (such as land breezes) could make it difficult to identify coastal low passage at the coast.
2. The ascent data which also originate from the above stations were only available for every 12 hours, which means that there is little likelihood of any particular ascent coinciding with the passage of a coastal low.
3. The reanalysis numerical model data used for compositing purposes are a relatively coarse data set (2.5 X 2.5 degree grid spacing) in relation to the scale of the coastal low.
4. The speed of the coastal lows is such that one ideally needs observations at 5' intervals with wind data, which includes average and gusts to accurately estimate time of passage between stations.
5. This study uses the 8-hour average of the SW'ly wind following the passage of the coastal low in order to differentiate between coastal low intensities. In some cases, it is possible that the winds associated with the following front or ridging high may arrive within the 8-hour period following coastal low passage already, and therefore may affect the wind speeds within this period.

6. A 24-hour gap between analyses is generally too long to follow the passage of a coastal low; it is possible for one coastal low to have filled and another to have formed along the Cape South Coast within the 24 hours.

2.4 Background climatological overview of Southern Africa

Away from the surface, the mean circulation of the atmosphere over southern Africa is anticyclonic throughout the year. In winter the mean anticyclone intensifies and moves northward. The near surface circulation at 850 hPa in January consists of a weak heat low centred over the central. In contrast to the January situation, the low level July mean pressure field at 850 hPa is strongly anticyclonic, and the equator ward extension of the westerly wind belt is dominant as far northwards as 23°S. At the surface level the dominant features are the semi-permanent South Atlantic Anticyclone and the South Indian Anticyclone. Both cells move about 6 ° northwards in winter (Preston-Whyte and Tyson, 1988).

Underlying a considerable day-to-day variability in the weather, it is possible to discern a tendency for the occurrence of typical sequences in the passage of disturbances to the south of the subcontinent. These sequences seldom occur for long enough to impose a predictable regularity on the coastal weather, although occasionally they may establish themselves clearly for short periods.

On day 1 of such a sequence, the circulation is dominated by subtropical highs. Thereafter a low in the westerlies drifts eastward to trail its cold front across the

southern part of South Africa by day 3. By day 4 the low is moving off the east coast and strong southerly meridional flow sweeps across the subcontinent. At the same time the Atlantic high begins to ridge eastward towards Cape Town. By day 5 a large ridging anticyclone has broken free of its parent Atlantic high and is drifting around the tip of Africa and into the Indian Ocean. By day 6 the ridging high has been amalgamated into the Indian high and the circulation pattern has reverted to one similar to that prevailing originally on day 1 (Preston-Whyte and Tyson, 1988).

CHAPTER 3

COASTAL LOW CLIMATOLOGY RESULTS

3.1 Introduction

The ten-year period contains 642 individual coastal lows, roughly 64 per year or 5 per month. On average, a coastal low passes Port Elizabeth every six days, which compares favorably with the spectral peak found by Preston-Whyte and Tyson (1988) for Port Elizabeth. In reality, the coastal lows would have passed slightly more often, as the basic procedure for choosing the individual lows, as described in the method section, was conservative.

The fact that a coastal low passes Port Elizabeth approximately every six days also compares well with the general climate overview section described in the previous chapter. While there are many variations on the general theme, using the sequence of events described by Preston-Whyte and Tyson (1988), as a template, offshore flow due to the continental high will lead to coastal low formation on day 1 on the west coast. As the continental high retreats and the cold front to the west of land approaches, the coastal low moves southwards and then eastwards to be situated on the south coast on day 2, (ahead of the cold front by approximately 11 degrees longitude). By day 3 the coastal low will have moved northwards along the east coast and is situated somewhere along the Natal coast after which it will dissipate. By the end of day 4 any sign of the coastal low will have vanished and on day 6 the next coastal low will start forming on the west coast.

3.2 Station climatology

3.2.1 General profile

The basic meteorological variables for Port Elizabeth: wind speed, wind direction, temperature and pressure are averaged for all 642 cases out of the 10-year period. The average of the 8-hour wind strength after coastal low passage as the criteria for discerning between coastal low intensities is used. This is overlaid by the top 5% cases of coastal lows.

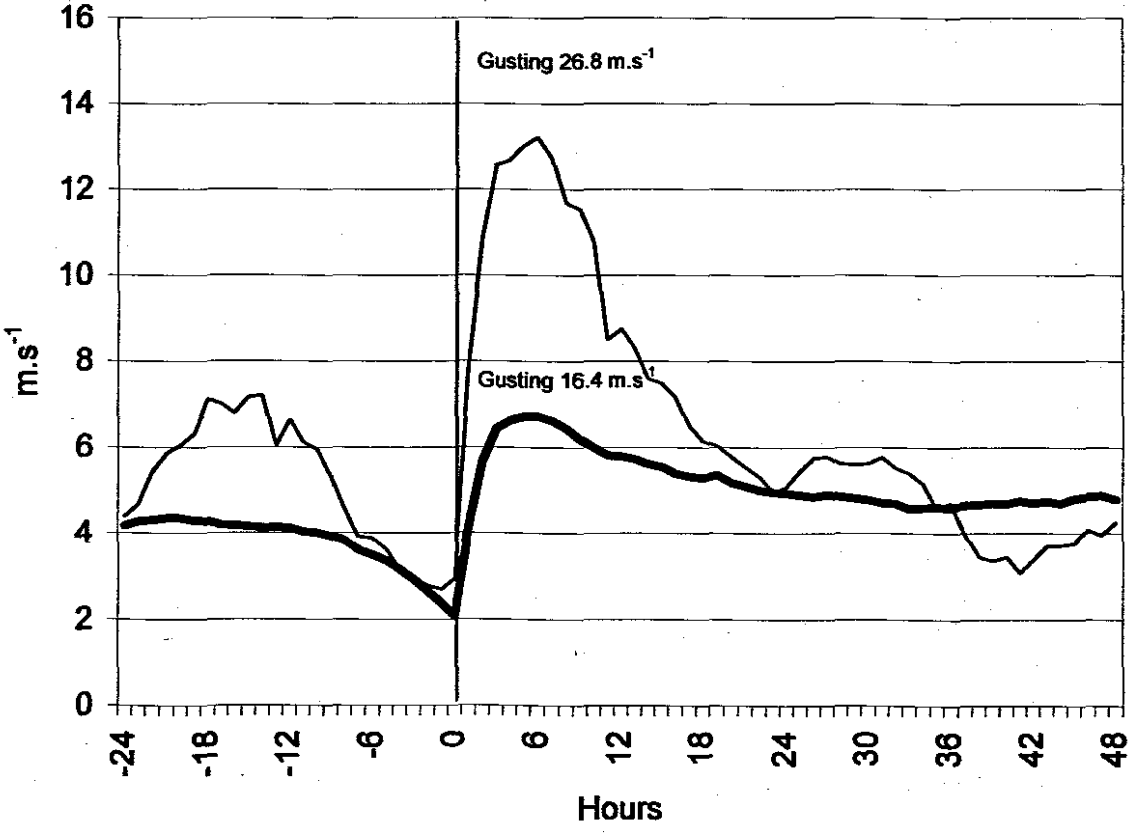

Fig. 3.1 Average wind speed time series of all coastal lows in bold black line with profile of the top 5% coastal lows in thin black line. The peak wind gust averages are printed above the respective traces. Coastal low passage at Port Elizabeth is at hour zero with the time series starting at 24 hours before passage and terminating at 48 hours after coastal low passage.

The wind speed graph (Fig. 3.1) also shows the results of the average wind gust data for all 642 cases and for the top 5% of the coastal lows. The graphs span the 24-hour period before and the 48-hour period after coastal low passage. The arrival of the southwesterly winds at hour zero marks the coastal low passage.

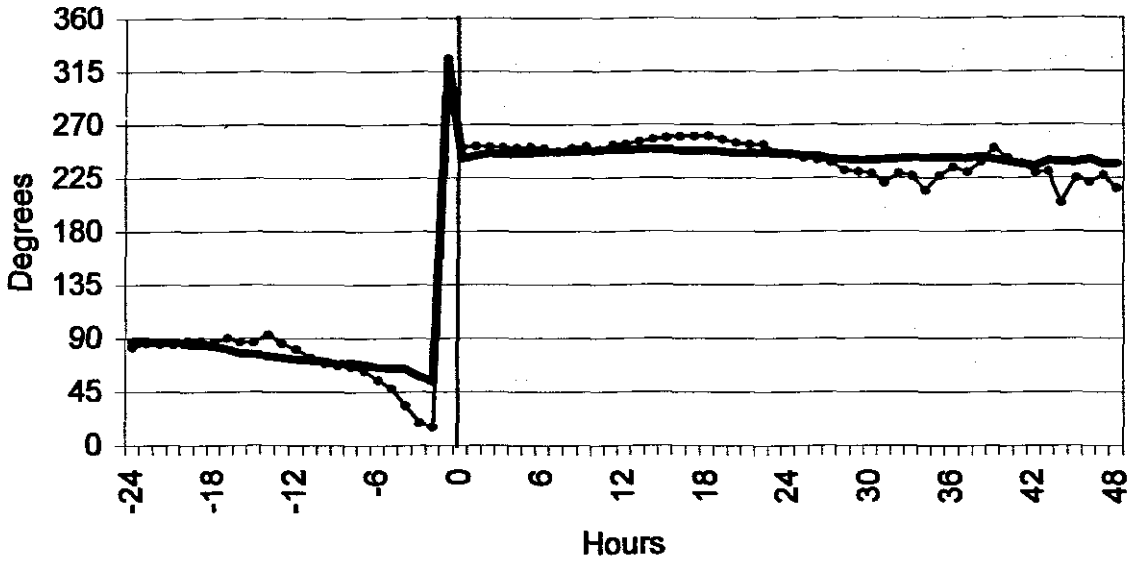

Fig. 3.2 True vector average wind direction time series of all coastal lows in bold black line with profile of the top 5% coastal lows in dotted thin black line. Coastal low passage at Port Elizabeth is at hour zero with the time series starting at 24 hours before passage and terminating at 48 hours after coastal low passage.

Notable is the significantly stronger pre-coastal low passage wind on the stronger cases (Fig. 3.1). The length, time-wise, of the coastal low's relatively strong post-low wind speed period is very similar in both the average and the strong cases, with a steep decrease in wind speed visible around 11 hours after coastal low passage, particularly so in the top 5% trace. The peak gust averages are more than twice as strong as the mean wind traces for both the average and the strong cases. This

suggests that the coastal low is significantly stronger than the average wind speed trace alone would suggest.

The top 5% coastal low average wind direction profile indicates a more gradual progression from an easterly flow (Fig. 3.2), which backs slowly through north and then northwest before the coastal low passage. On the average wind direction trace, the switch from northeasterly to southwesterly is more abrupt.

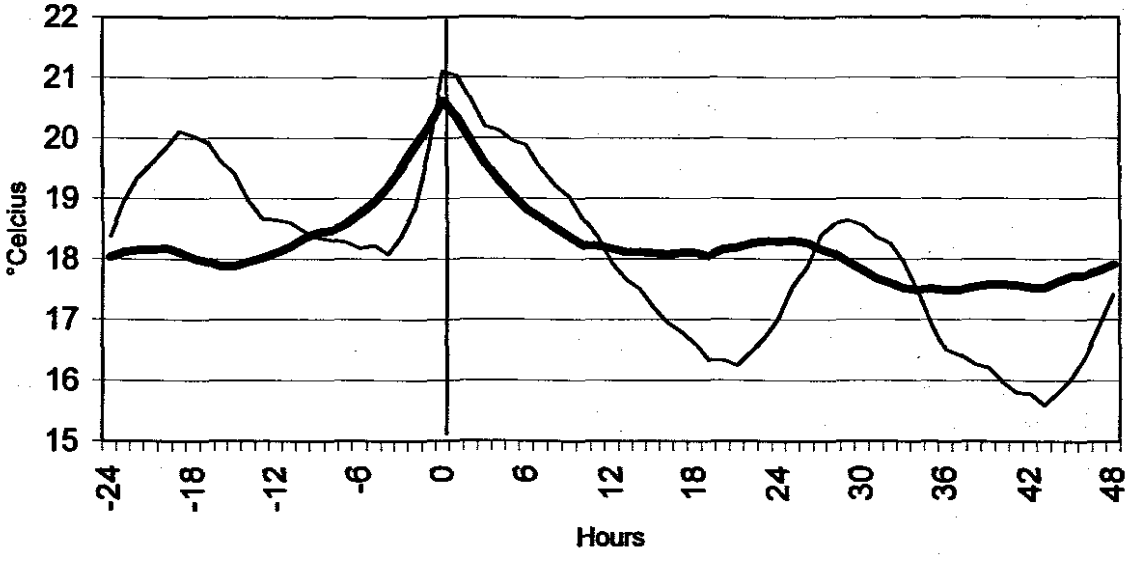

Fig. 3.3 Temperature time series of all coastal lows in bold black line with the profile of the top 5% coastal lows in dotted thin black line. Coastal low passage at Port Elizabeth is at hour zero with the time series starting at 24 hours before passage and terminating at 48 hours after coastal low passage.

The temperature peak at about 17 hours before coastal low passage on the top 5% profile (Fig. 3.3) is coincidental with the stronger than average easterly flow (Fig. 3.1). A higher temperature peak is noted at coastal low passage (hour zero, Fig. 3.3) due to the more prominent (adiabatic and dynamically warmed) offshore flow (Fig.

3.2) just ahead of coastal low passage. From hour zero up to hour 20 (Fig. 3.3) there is significantly more cooling due to the stronger southwesterly wind associated with the top 5% cases (Fig. 3.1). The top 5% cases show a more diurnal variation.

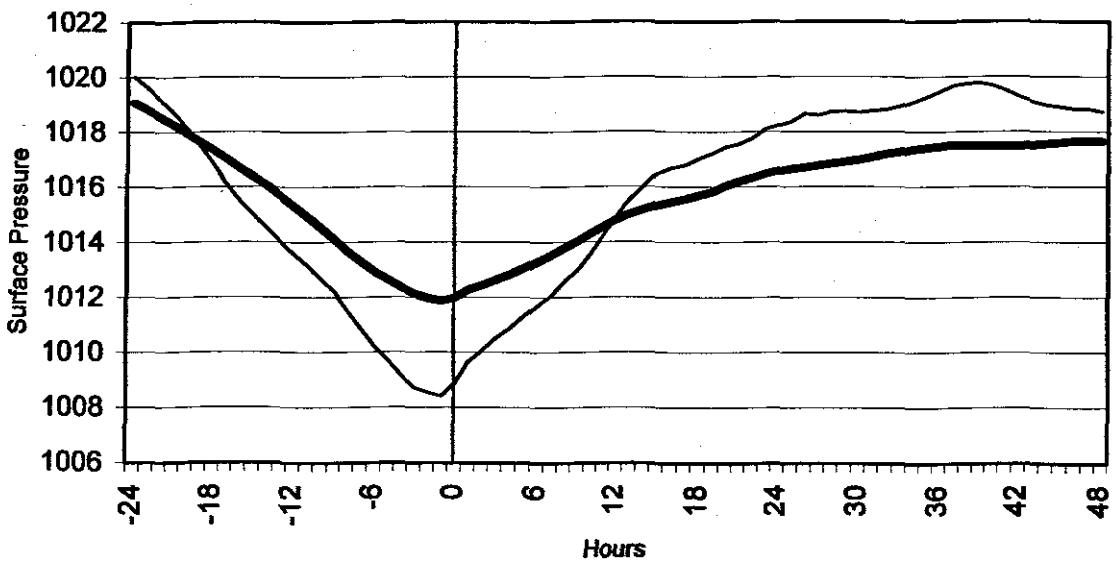

Fig. 3.4 Surface pressure time series of all coastal lows in bold black line with the profile of the top 5% coastal lows in thin dotted black line. Coastal low passage at Port Elizabeth is at hour zero with the time series starting at 24 hours before passage and terminating at 48 hours after coastal low passage.

The drop in temperature (Fig. 3.3) after approximately hours 28 – 34, and the slight rise in wind speed (Fig. 3.1) during the same period coupled with a backing to the south in wind direction (Fig. 3.2), may be due to the following frontal passage and ridging of the Atlantic Ocean Anticyclone (AOA). It is likely that the frontal passage or ridging of the AOA behind the front is more visible in the strong case profile due to the fact that these coastal lows are better defined. This is contrary to the mean profile trace of all 642 cases for the whole period, which would include a significant proportion of weak and poorly defined coastal lows.

The atmospheric pressure profile of the top 5% strong case average clearly indicates a steeper drop ahead of the coastal low passage in pressure (hour zero, Fig. 3.4) and a steeper rise after the passage of the coastal low. The core minimum pressure of the top 5% strong case average profile is almost 4 hPa deeper than that of the average coastal low profile. The top 5% coastal low pressure maxima at 24 hours before coastal low passage (Fig. 3.4) linked to the Indian Ocean Anticyclone (IOA), and at 40 hours after coastal low passage (AOA ridging), are 1 – 2 hPa stronger respectively than that of the average coastal low pressure profile.

3.2.2 Frequency of coastal low occurrence

The coastal lows pass Port Elizabeth every 5.7 days, which translates to 5 every month, or 64 per year. For all 642 cases, the coastal lows occur more frequently in summer, from December through to February. The top 5% of coastal lows occur more frequently during the September to November season (Fig. 3.5).

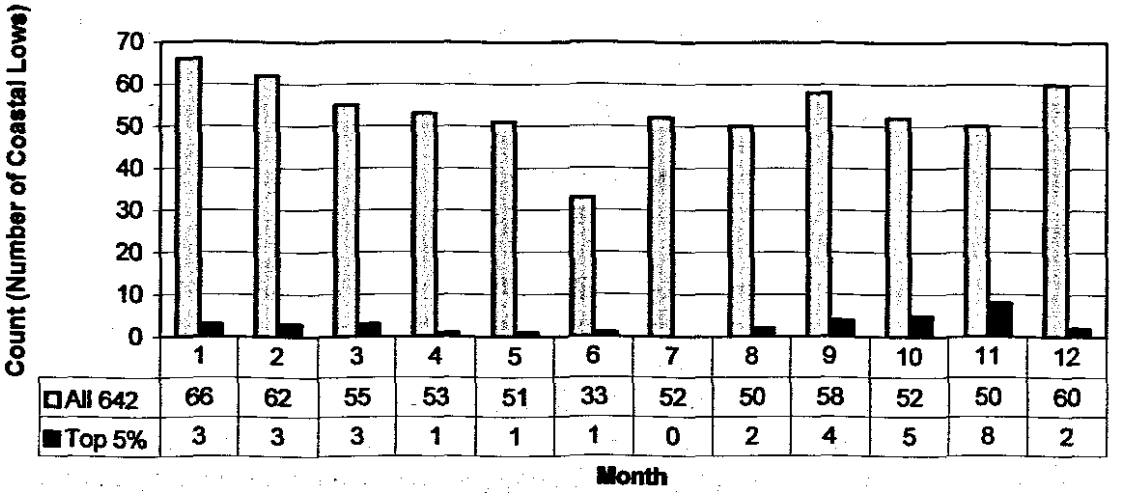

	1	2	3	4	5	6	7	8	9	10	11	12
All 642	66	62	55	53	51	33	52	50	58	52	50	60
Top 5%	3	3	3	1	1	1	0	2	4	5	8	2

Fig. 3.5 Yearly spread of coastal low occurrence for all 642 coastal lows and for the top 5% of all 642 coastal lows.

3.3 Upper air (NCEP Reanalysis 1 data) for all 642 coastal lows over the 10-year period

The shift in wind speed and direction during coastal low passage (Fig. 3.6) shows the strong westerly to northwesterly flow at 700hPa veering to the northwest after coastal low passage. This fits with the wind shift expected from an approaching upper trough as it moves closer 12 hours after passage of the coastal low. At 850 hPa the flow before coastal low passage is mostly north to northwesterly before coastal low passage, backing to the west after coastal low passage.

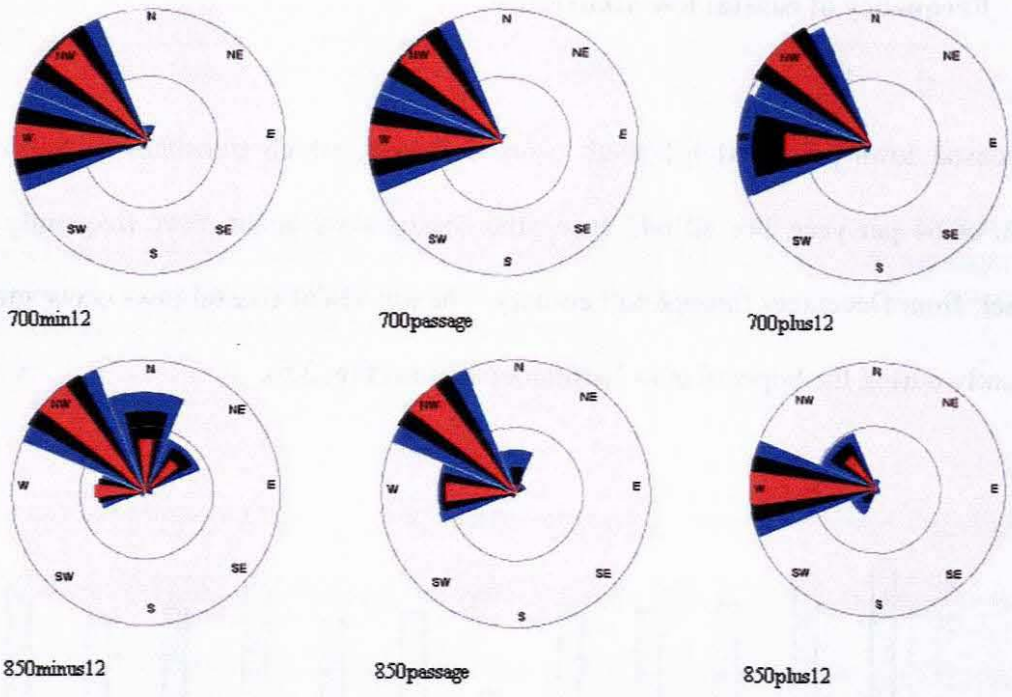

Fig. 3.6 Wind roses for upper winds at 700 hPa and 850 hPa for all 642 coastal lows for the 12-hour period before, during and after coastal low passage at Port Elizabeth. For each of the sectors the outermost wedge (blue) shows the wind frequency distribution, the middle wedge (black) shows the distribution of the product of the wind speed times the frequency and the innermost wedge (red) shows the distribution of the wind speeds bed (i.e. the energies) multiplied by the frequencies.

3.4 September, October and November (SON) season climatology

3.4.1 Station climatology

3.4.1.1 Frequency of coastal low occurrence

There were 160 coastal lows, out of the 642 total cases for the 10-year period from 1987 – 1996, which occurred during the SON season. The SON coastal lows display the same general frequency as that of all 642 cases; approximately 5 per month or a coastal low passing Port Elizabeth every 5.7 days on average.

3.4.1.2 Propagation

The propagation speed of the coastal low along the coast from Cape Town through to Durban on the East coast is calculated for the strongest 10% of SON coastal lows (Table A1) and for the median 10% of coastal lows (Table A2). The result is shown for the strong 10% (Table 3.1) and the median 10% of cases (Table 3.2), where the time taken in hours, the distance, and propagation speed in knots and in $m.s^{-1}$ is tabled.

The mean of the 8-hour average wind speed for the post coastal low southwesterly winds at Port Elizabeth for the median 10% of SON coastal lows is 6.9 $m.s^{-1}$ and for the top 10% of coastal lows it is 11 $m.s^{-1}$. The coastal low propagation speed for the top 10% of coastal lows is 28% faster than that of the mean 10% of coastal lows. The

fastest coastal low propagation speed for both mean and top 10%, takes place between Port Elizabeth and East London (Tables 3.1; 3.2). The slowest propagation speed is between Cape Town and George. The sectors with the best orographical barriers are from George to Port Elizabeth and from East London to Durban. These sectors produced similar propagation speeds in the mean 10% of cases (Table 3.2) and also in the top 10% of cases (Table 3.1).

Table 3.1 Results of the propagation study for the top 10% of coastal lows. CT refers to Cape Town, GG to George, PE to Port Elizabeth, EL to East London and DN to Durban.

Top 10% of SON	CT to GG	GG to PE	PE to EL	EL to DN	CT to PE	PE to DN	CT to DN
Average time taken in hours	15.1	6.8	3.6	10.6	21.9	14.2	36.1
Approximate Distance (km)	410	290	240	450	700	690	1390
Propagation speed ($m.s^{-1}$)	7.6	11.8	18.5	11.8	9	13.5	10.7

Table 3.2 Results of the propagation study for the mean 10% of coastal lows. CT refers to Cape Town, GG to George, PE to Port Elizabeth, EL to East London and DN to Durban.

Mean 10% of SON	CT to GG	GG to PE	PE to EL	EL to DN	CT to PE	PE to DN	CT to DN
Average time taken in hours	23.3	8.8	6.2	12.1	32.1	18.3	50.4
Approximate Distance (km)	410	290	240	450	700	690	1390
Propagation speed ($m.s^{-1}$)	4.9	9.2	10.8	10.3	6.1	10.5	7.7

In both the mean and the strong 10% cases, the propagation speed of the system is faster than the mean of the 8-hour averaged post coastal low's surface southwesterly wind speed at Port Elizabeth.

The fastest propagation speeds take place between Port Elizabeth and East London. Particularly noteworthy is the propagation speed of the top 10% coastal lows for this section of the coast of 18.5 $m.s^{-1}$, which is almost twice as strong as the mean of the 8-hour post coastal low surface southwesterly winds at Port Elizabeth of 11.1 $m.s^{-1}$ (Table 3.1).

3.4.2 SON Sonde climatology

3.4.2.1 Inversions

The inversions for the top 10% cases (Table A3) were lower on average during the 12 hours preceding coastal low passage than the corresponding inversions for the mean 10% of coastal low cases at Port Elizabeth and Durban (Table A4). For the 10% strongest coastal lows, the inversions at Port Elizabeth were also notably lower than at Cape Town and Durban.

There were two nil inversions at Cape Town in the top 10% inversion study (Table A3), three at Port Elizabeth and three at Durban. On one occasion no data was available at Port Elizabeth and Durban. There were nine surface inversions at Cape Town, but only one at Port Elizabeth and three at Durban. For the mean 10%

inversion study (Table A4), three nil inversions occurred at Cape Town, two at Port Elizabeth and four at Durban. Port Elizabeth had two occasions with no ascent data. Four surface inversions were recorded at Cape Town, four at Port Elizabeth and two at Durban.

Signs of persistence were noted where strong coastal lows followed relatively closely after one another. There were two coastal lows during September 1994, two during September 1995, two during November 1993 and two during November 1994 out of the total of 16 cases for the top 10% of SON coastal lows. Half of the strong coastal lows occurred within 13% of the available months.

3.4.2.2 Sonde profiles

Two views of the temperature, humidity, height and wind fields are presented from surface level to 700 hPa using upper ascent data. The first set shows the change that takes place to these variables from 24 hours before to 24 hours after coastal low passage at Port Elizabeth. This includes the data from 12 hours before coastal low passage and the data at coastal low passage at Port Elizabeth. The second set presents the data on coastal low passage at Cape Town, Port Elizabeth and Durban, following the coastal low as it propagates eastwards along the coast.

There is an increase in temperature (Fig. 3.7) of 3 – 4°C from PE-24 to PE-12 for the median 10% of cases below 700 hPa. The strong cases show a further positive temperature departure of 1 - 1.5°C between 750 hPa and 925 hPa at PE-12. At PE0

this region of warmer air above Port Elizabeth cools somewhat already in westerly rather than the offshore northwesterly flow. By PE+24 significant cooling of 8 – 10°C takes place in the cooler southwesterly onshore post-coastal low flow.

The humidity fields (Fig. 3.7) shows the same trend, with 10% drier air for the median 10% of cases at PE-12 within the warmer offshore air continental origin air between 850 and 950 hPa. For the strong cases, this air has an added negative departure of 5 – 10%.

The composite wind plots (Fig. 3.7) show that the winds start off slightly weaker - both below 850 hPa in the easterly flow, and in the westerly flow above that at PE-24. By PE-12 this changes as the flow above 950 hPa becomes north to northwesterly up to 700 hPa, with the wind speed for the strong cases showing a positive departure of 1 - 2 $m.s^{-1}$. At PE0 the strongest departure is seen, with 2 - 5 $m.s^{-1}$ stronger winds throughout the column to 700 hPa. The peaks are at 925 hPa and surface levels.

The northwesterly winds between 700 hPa and 850 hPa are vertically aligned at PE-12 (Fig. 3.7). The flow just below that, between 900 hPa and 925 hPa has a more northerly component, but as the interior trough moves eastwards from PE-12 to PE0, this wind will back to the west (as shown at PE0), with a point reached between PE-12 and PE0 where all of the winds above 925 hPa up to 700 hPa will be vertically aligned from the northwest.

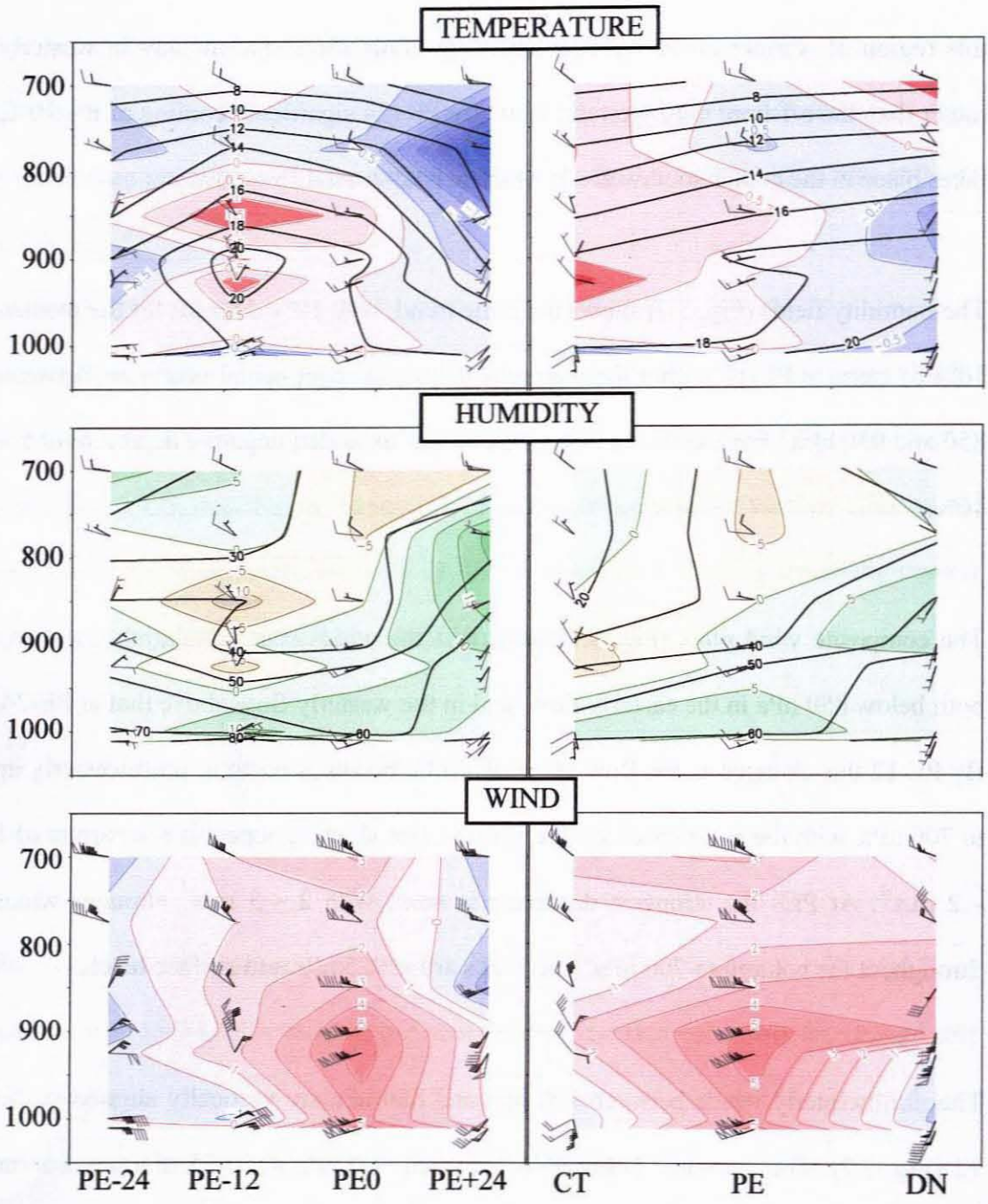

Fig. 3.7 Temperature (°C), humidity (%) and wind ($m.s^{-1}$) plots of the top and median 10% of SON upper air ascents. The solid lines represent the composites of the mean 10% of coastal low cases, while the colour filled contours represent the departure of the top 10%. Each full feather on the wind barbs on the temperature and humidity plots equals 10 $m.s^{-1}$, while the full feathers on the wind plots equal 1 $m.s^{-1}$ with the dark barbs showing the strong cases, and the gray the median. Passage of the lows at Cape Town (CT), Port Elizabeth (PE) and Durban (DN) are shown and the 48-hour passage of the low at Port Elizabeth is marked by PE-24, PE-12, PE0 and PE+24.

For the strong cases (Fig 3.7), the wind above 850 hPa is weaker than that of the median 10% of cases by PE+24, showing that the upper trough has weakened. The wind direction still shows a slightly more northerly component to the composite of the mean cases, indicating that the upper trough still lies to the west of Port Elizabeth at PE+24.

The temperature plot (Fig. 3.7) shows a weak positive departure at Cape Town for the strong case coastal lows from 925 hPa to 700 hPa with a peak of 1.5 °C at 925 hPa due to the winds at that level being northwesterly for the strong cases, while it is still easterly for the median 10% of cases.

By the time the coastal low reaches Durban, the departure of the top 10% wind speed shows that the strong case coastal low surface wind speed has significantly eased, with the wind speed for the mean cases being stronger on average than that of the top 10% coastal lows at 1000 hPa. However, the upper winds between 775 hPa and 900 hPa are stronger for the stronger coastal lows.

An alternate view of the upper air sonde composite data, in more conventional aeronautical diagram format, is presented in the appendix (Figs. A1, A2 and A3).

3.5 Summary

3.5.1 Climate summary for all 642 coastal lows during the 10-year period from 1987 to 1996 (including comparisons for the top 5% of cases).

A coastal low passes Port Elizabeth every 5.7 days on average, or approximately five times per month. This compares well with the 6-day spectral peak found by Preston-Whyte and Tyson (1988) for Port Elizabeth. The reason for the other 3-day spectral peak is not clear; it could possibly be found that (given more representative coastal data) coastal lows move through at the lower frequency, or may well be found that the 3-day peak is a combination of coastal low and frontal pressure minima. Coastal lows occur more frequently from December to February, but for the top 5% of cases the peak period is between September and November (SON).

At the peak wind strength period, between hours 3 and 10 after coastal low passage, the top 5% of coastal lows register an average wind speed of about 13 $m.s^{-1}$, gusting at 27 $m.s^{-1}$. The average coastal low registers around 7 $m.s^{-1}$, gusting 16 $m.s^{-1}$.

The easterly wind (negative zonal component) ahead of the coastal low passage from 20 to 10 hours before coastal low passage is 2 - 3 $m.s^{-1}$ stronger than that of the mean for the top 5% of coastal low cases.

On average, the wind direction backs from easterly through the north to southwesterly during coastal low passage, confirming that the coastal low minimum pressure passes southwards of Port Elizabeth.

The duration of the post-coastal low southwesterly wind for both the average and the top 5% cases are very similar, however the top 5% of coastal lows shows a decrease in speed at around 11 hours after coastal low passage.

The wind associated with the top 5% coastal lows backs gradually from an easterly to a northwesterly direction during the 12 hours before coastal low passage, while the average coastal lows back rapidly from an east-northeasterly direction to northwesterly during the six hour preceding coastal low passage.

The top 5% of coastal lows show a higher peak surface temperature of 0.5 °C on coastal low passage, just ahead of coastal low passage, than the average coastal lows.

The core minimum pressure associated with the top 5% of coastal lows is almost 4 hPa deeper at 1008 hPa than that of the average coastal low minimum of 1012 hPa. The sea level pressure at 24 hours before coastal low passage, associated with the IOA, and at about 40 hours after, associated with the ridging AOA, are both around 1 hPa stronger than that of the average coastal low's pressure profile.

3.5.2 Climate summary of the SON (September, October and November) season during the 10-year period from 1987 to 1996.

The frequency of occurrence is similar to that of all 642 cases.

The propagation speed from Cape Town to Durban for the median 10% of SON coastal lows is 7.7 $m.s^{-1}$; while that of the strongest 10% is 10.7 $m.s^{-1}$ (the top 10% of cases are 28% faster).

The fastest propagation speed takes place between Port Elizabeth and East London, with 18.5 $m.s^{-1}$ for the strong cases (where the mean of the 8-hour post low surface southwesterly wind speed at Port Elizabeth is 11 $m.s^{-1}$) and 10.8 $m.s^{-1}$ for the median 10% of cases (where the mean of the 8-hour post low surface southwesterly wind speed at Port Elizabeth is 6.9 $m.s^{-1}$). This result shows that the coastal lows propagate faster than the surface wind speed within the system.

The strongest cases are also the ones that propagate faster along the coast. One reason for this may be that the synoptic systems which create the offshore flow that bring about the coastal lows move faster eastwards during strong case coastal low events, effectively dragging the coastal low eastwards faster.

West of Port Elizabeth, the fold mountains adjacent to the coast provide an effective vertical trapping barrier, which is one of the boundaries needed for maintaining the Kelvin wave (the other boundary apart from the surface itself is the horizontal inversion layer). The orography then steepens close to the coast again near to Port Alfred, where the combination of the steep orography close to the coast (vertical trapping barrier), the warmer waters and the convex coast all combine to allow for a stronger buster and therefore allows for faster propagation of the coastal low as it moves north-eastwards towards East London and the Transkei coast.

The segment from Port Elizabeth to Port Alfred along the south coast, where the coastal trapping mountains retreat well northward to the escarpment close to Somerset East, also falls within the region where the fastest propagation speeds for both the top 10% and the median 10% of cases occur (between Port Elizabeth and East London). The RAMS study (Reason, Jackson and Hai Fu, 2000) showed that gaps in the vertical trapping barrier should weaken the intensity of the coastally trapped disturbances and slow its propagation. However, between Port Elizabeth and Port Alfred (which is equal to about half the distance from Port Elizabeth to East London), where the vertical trapping barrier has retreated well away from the coast, the opposite occurs.

The slowest propagation speeds are recorded between Cape Town and George where the coast is concave and the water is colder than to the east. The coastal sections with orographic trapping mountain barriers close to the coast, from George to Port Elizabeth, and again from East London to Durban, produce similar propagation speeds for both the median and for the top 10% of cases.

During the top 10% of cases, the inversions at Port Elizabeth (555 m) are notably lower than those at Cape Town (887 m) and Durban (658 m).

The data shows a 50% chance of one strong coastal low being followed by another within the same month.

The temperature field already shows a positive anomaly for the median 10% of coastal lows as the coastal lows pass Cape Town, with a further 1.5°C positive

departure for the strong 10% of cases at 925 hPa due to the northwesterly wind at that level. This positive anomaly is somewhat visible at PE-24 at 850 hPa, but the anomaly increases significantly by PE-12 when the temperature increases by 4°C for the median 10% of cases, with a further 1 to 1.5°C positive departure for the strong 10% of cases between 850 and 925 hPa.

When the coastal lows pass Port Elizabeth, the warmer air is still apparent overhead, but this air has cooled somewhat from PE-12 due to the winds aloft at those levels having backed to the west during the 12-hour period. By the time the coastal low reaches Durban, the positive anomaly is apparent for the median 10% of cases, but there is a negative temperature departure of 0.5 to 1°C for the top 10% of coastal lows below 775 hPa.

The wind fields follow the same trend; with stronger winds of 1 – 2 $m.s^{-1}$ for the strongest 10% of coastal lows at Cape Town above 925 hPa as the coastal lows pass. The same positive departure persists as the coastal low moves along the coast up to PE-12, particularly between 850 and 925 hPa. As it takes the strong coastal lows about 22 hours on average to get to Port Elizabeth from Cape Town (Table 3.1), PE-12 would be roughly equal to 10 hours after the coastal low has left Cape Town. The strong cases are 3 - 5 $m.s^{-1}$ stronger than the median 10% of cases below 850 hPa on coastal low passage at Port Elizabeth. By the time the coastal lows reach Durban, the top 10% of cases are weaker than the median 10% of coastal lows below 900 hPa.

Twenty-four hours after coastal low passage at Port Elizabeth, the top 10% of cases show weaker winds at Port Elizabeth above 850 hPa than that of the median 10% of coastal low cases.

CHAPTER 4

COMPOSITE COASTAL LOW PATTERNS SON 1987 - 1996

4.1 Introduction

In order to find the synoptic scale distinctions that characterize strong coastal lows, composite analysis is used in various forms. While the use of composites allows for robust analysis of bulk data, noteworthy features associated with particular cases may be lost. This, however, is offset by the fact that batches of similar events will display similar general characteristics.

By comparing the composite characteristics of different meteorological variables of the top 10% of coastal lows (using the mean 8-hour wind speed after the passage of the coastal lows to differentiate between coastal lows), against the same variables displayed by the composite of all of the SON (160 cases) coastal lows, the distinctions which characterize the strong coastal lows may be discovered.

The anomalous or mean composites of different meteorological variables are displayed on large-scale plan views for the initial analysis. Cross-sectional displays which show the variables by height along either longitude or latitude, and also system-following, small-scale plan views are then utilized for more detailed analysis.

Subtracting the composite anomaly of all 160 SON coastal lows from the composite anomaly of the 16 top 10% SON coastal lows produces the "differential anomaly" which highlights how the general characteristics of strong coastal lows differ from those of the mean coastal lows.

4.2 Plan view composites of 500 hPa heights and surface pressure

The composite mean of all 160 SON coastal lows (Fig. 4.1) shows the Indian Ocean Anticyclone (IOA) and the Atlantic Ocean Anticyclone (AOA), with the frontal trough in between the two high-pressure cells, just west and southwest of land on the day of coastal low passage at Port Elizabeth.

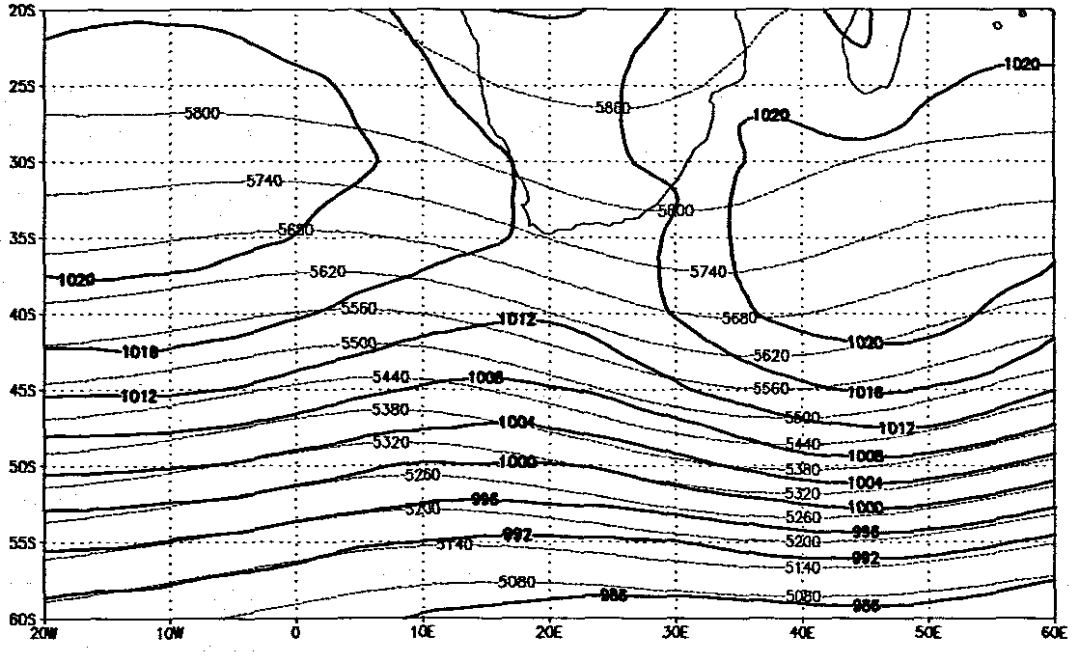

Fig. 4.1 Composite mean of all 160 SON coastal lows, on the day of coastal low passage at Port Elizabeth. Sea level pressure (hPa) is displayed in solid black contours and the overlay of the height of the 500 hPa contour (gpm) in dotted lines.

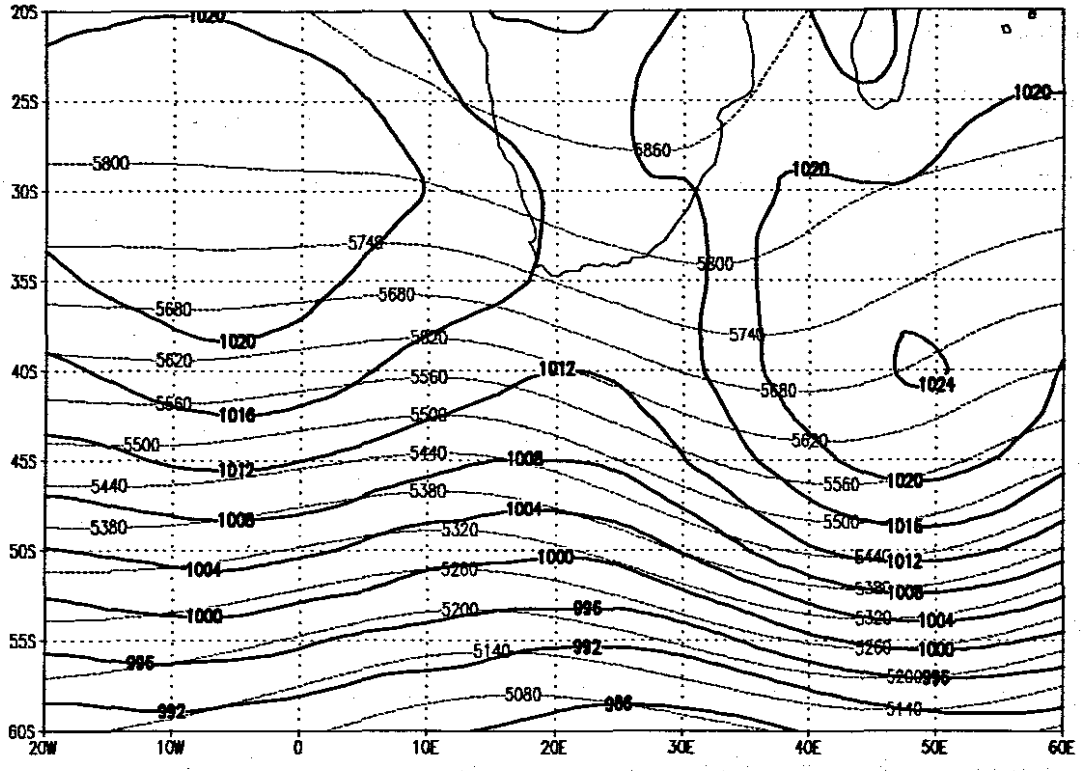

Fig. 4.2 Composite mean of the top 10% of coastal lows, on the day of coastal low passage at Port Elizabeth. Sea level pressure (hPa) is displayed in solid black contours and the overlay of the height of the 500 hPa contour (gpm) in dotted lines.

On the overlay (Fig. 4.1) the approaching Rossby wave is apparent at about 5°E just west of land. The coastal low is on Port Elizabeth, but is not clearly visible from the sea level pressure data; one can only infer its position as lying between the IOA and AOA, and over Port Elizabeth, ahead (eastwards) of the frontal trough.

The composite mean (Fig. 4.2) of the strong 10% of SON coastal lows show one significant departure from that of the mean cases, where the Indian Ocean Anticyclone (IOA) has a center of 1024 hPa, well southeast of South Africa. The upper trough is more pronounced, due to the fact that both the IOA and the AOA are more pronounced on the composite mean of the strong cases.

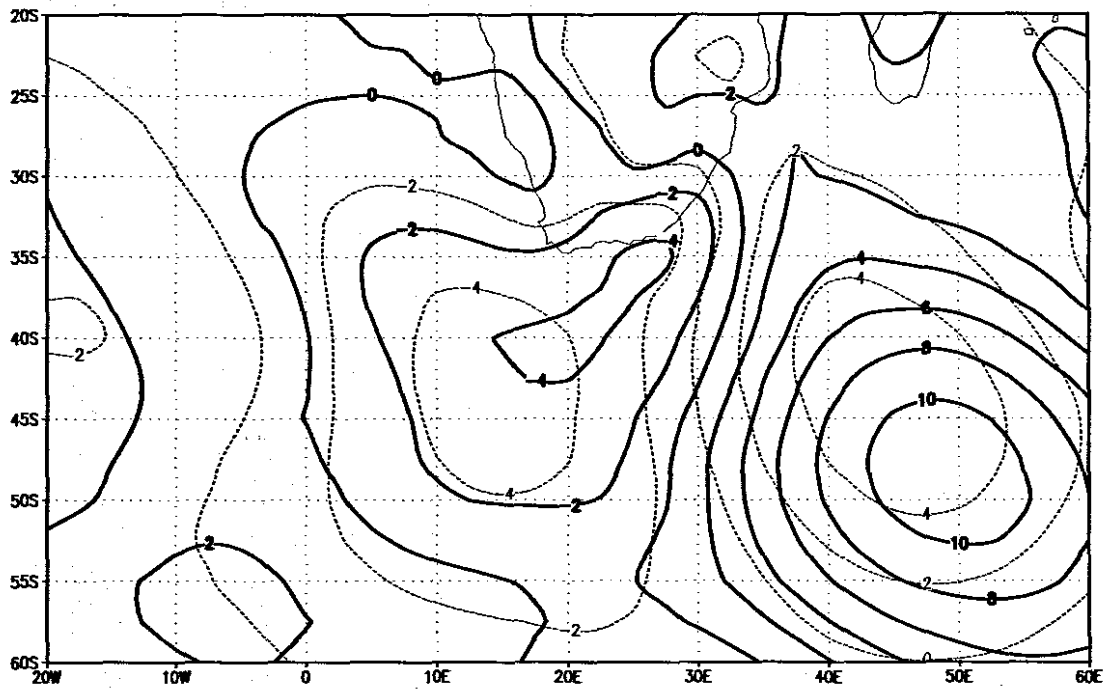

Fig. 4.3 Sea level pressure composite anomalies of the top 10% cases in solid black contours, and of all 160 SON coastal lows in dotted lines, with all units in hPa.

Both composite anomalies clearly show the higher pressure southeast of land associated with the IOA (Fig. 4.3) and the lower pressure of the frontal system southwest of land. The lower pressure region associated with the coastal lows is also well depicted on both composite anomalies. Significantly, the composite anomaly of the top 10% SON strong cases show both a stronger IOA region and a deeper low pressure in the coastal low region. However, the composite anomaly of all 160 SON cases depicts a deeper frontal trough to the southwest of land.

The upper ridge (Fig. 4.4) is clearly visible stretching out southeast of land, with the ridge associated with the composite anomaly of the top 10% SON cases significantly more pronounced and centered southeastwards of that of the mean case upper high. The trough associated with the mean cases is better defined and leans back to the west

while the anomaly of the top 10% strong cases is centered further eastwards and also does not extend as far northwards.

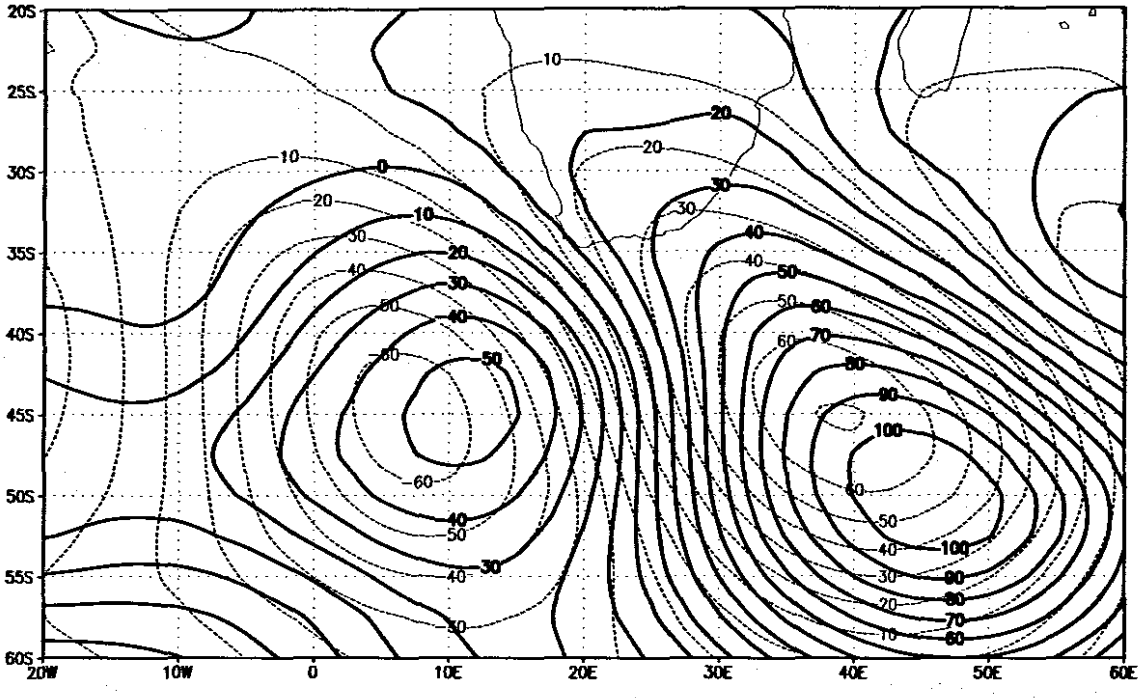

Fig. 4.4 Composite anomalies of the 500 hPa contours for the top 10% of cases in solid black contours, and of all 160 SON coastal lows in dotted lines, with all units in gpm.

The differential anomaly (Fig. 4.5) of the sea level pressure anomalies highlights the weak area of lower pressure on the southeast coast and the substantially higher pressure well to the southeast of land, suggesting that a significantly more dominant IOA southeast of land is generally associated with strong case coastal lows. The positive values (Fig. 4.5) to the west of land show that a slightly weaker trough is also associated with the strong coastal lows.

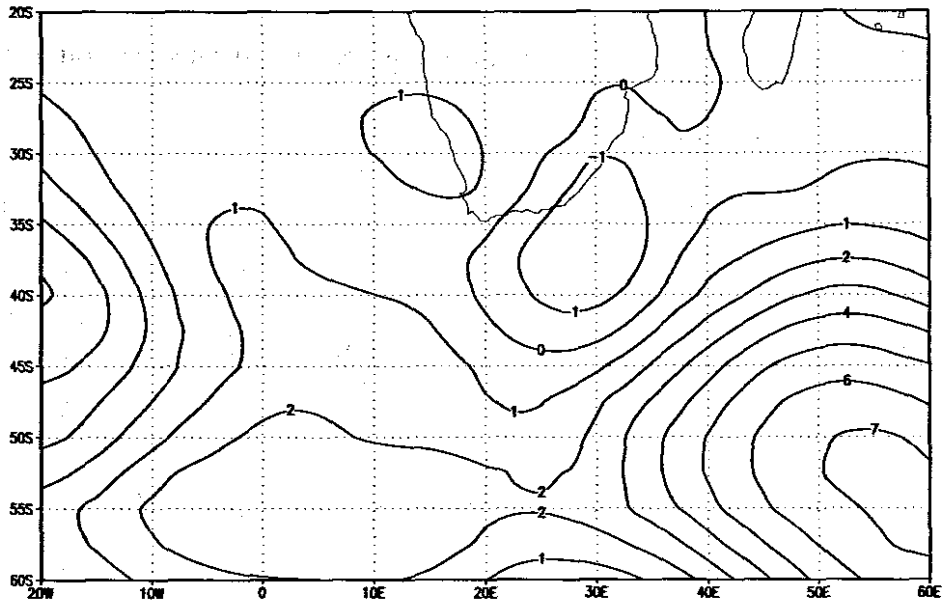

Fig. 4.5 Differential anomaly of the sea level pressure anomalies (strong minus the mean).

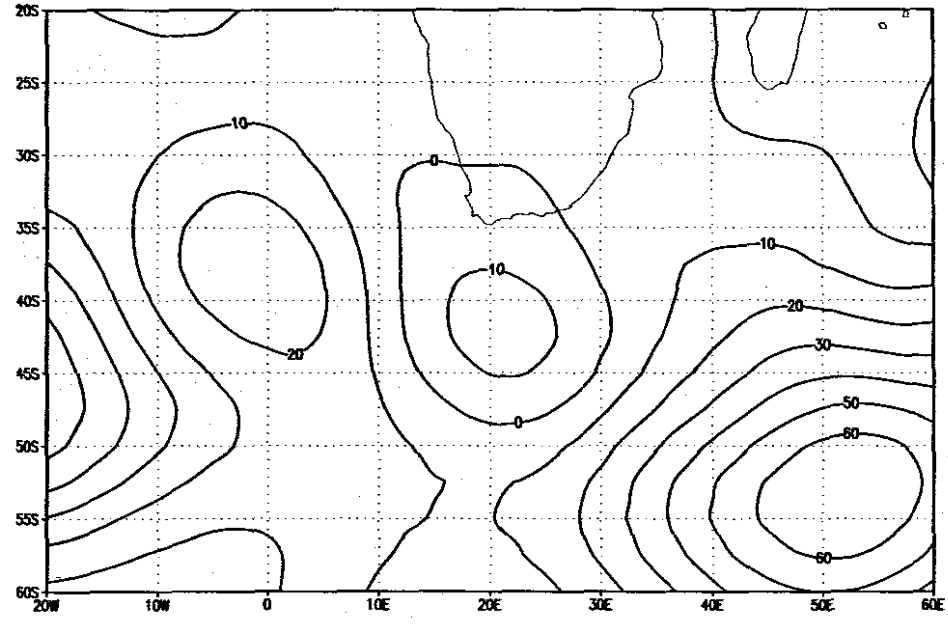

Fig. 4.6 Differential anomaly of the 500 hPa contour anomalies (strong minus the mean).

At 500 hPa (Fig. 4.6), the higher differential anomaly well southeast of land and the slightly higher anomalies at 0° longitude, combined with the lower values to the south of land, show that the Rossby wave is not as dominant during strong coastal low days,

and that the core placement of the trough is almost 20° to the east and 10° to the south.

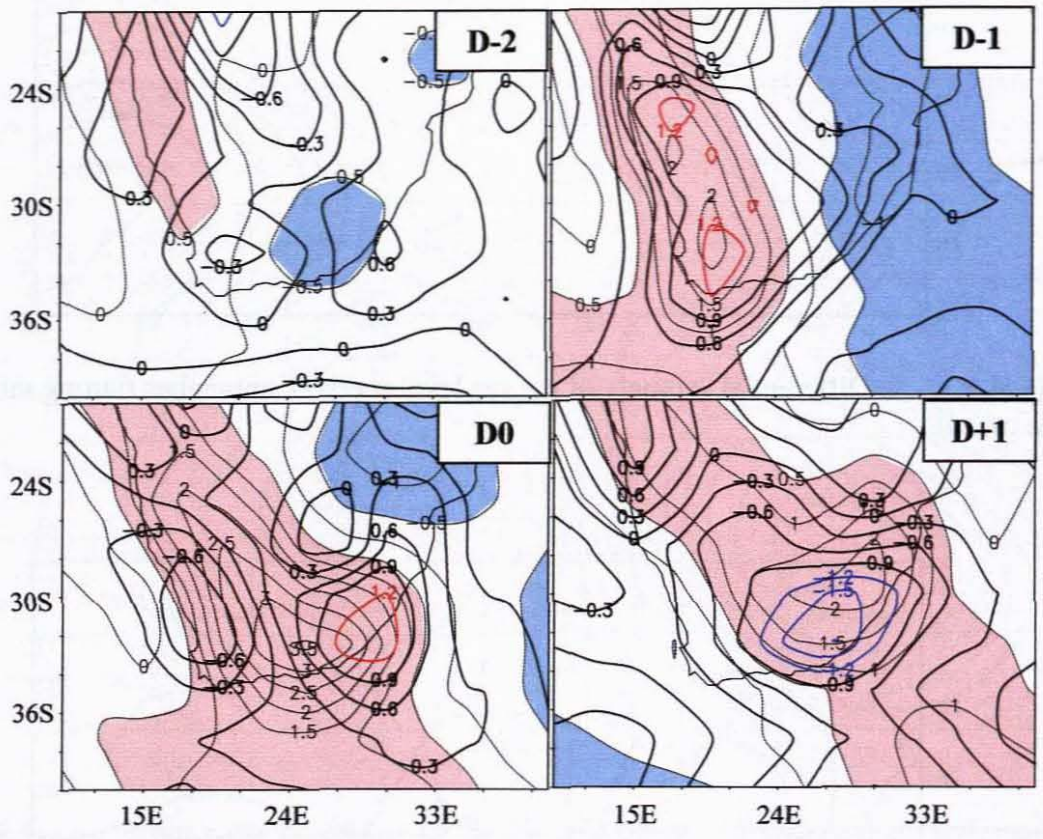

Fig. 4.7 Surface air temperature anomalies from two days before (D-2) to the day after (D+1) coastal low passage at Port Elizabeth. The dotted and colour filled contours represent the composite anomaly of all 160 SON coastal lows. The solid black with highlighted contours shows the differential anomaly that represents the departures of the top 10% SON coastal lows.

The air temperature anomalies at surface level show the warmer region starting to develop on the west coast two days before coastal low passage at Port Elizabeth (Fig. 4.7, D-2). At one day before coastal low passage (D-1), the warmer temperatures associated with adiabatic and dynamic heating has spread southwards along the west coast, with the strong coastal lows showing significantly higher temperatures at the surface.

This trend continues on the day of coastal low passage at Port Elizabeth (Fig. 4.7, D0), where the core of higher temperatures associated with the stronger coastal lows is now depicted ahead (eastwards) of that of the mean of the SON cases.

There is also a pool of colder air visible on the west coast for the strong cases, while the mean cases still have slightly warmer than average temperatures. This significant pool of colder air spreads eastwards on the day after coastal low passage (D+1), while the anomaly of the mean 160 SON cases is still warmer than average according to the NCEP model assimilated data fields (Fig. 4.7, D+1).

The same trend is shown by the sea level pressure anomalies at two days before coastal low passage at Port Elizabeth (Fig. 4.8, D-2), where the surface pressure drops northwards of 28°S along the west coast, then spreading to the southwestern tip of South Africa by the day before coastal low passage. On this day, the strong positive departure to the southeast of land is visible for all 160 SON coastal lows, and more so for the differential anomaly of the strong cases.

The negative departure of the coastal low's minimum pressure region also strengthens as it moves southwards on the day before passage (Fig. 4.8, D-1), and then strengthens further as it moves eastwards along the South Coast on the day of coastal low passage (D0), with the core of the negative departure 5° eastwards (away from land) from the core of the minimum pressure associated with the mean coastal low's anomaly according to NCEP model analyses.

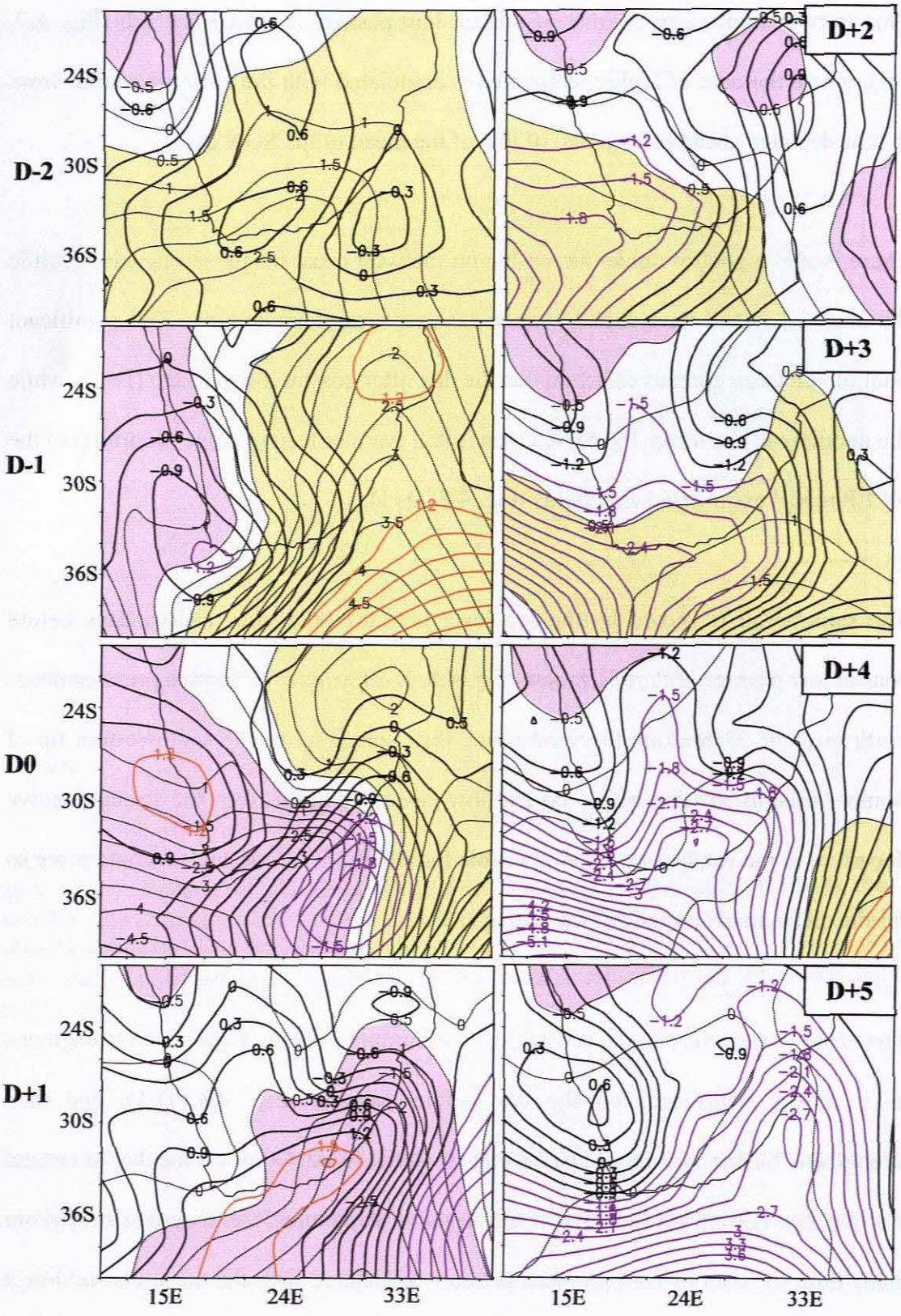

Fig. 4.8 Sea level pressure anomalies from two days before (D-2) to five days after (D+5) coastal low passage at Port Elizabeth. The dotted and colour filled contours represent the composite anomaly of all 160 SON coastal lows. The solid black with highlighted contours shows the differential anomaly that represents the departure of the top 10% SON coastal lows.

The stronger pressure rise region behind the strong case coastal lows (Fig. 4.8, D+1), on the day after coastal low passage, moves northwards along the east coast by the second day after coastal low passage (D+2) when pressure is still only starting to rise along the south coast for the mean of all 160 SON coastal lows.

The anomalies for days 3, 4 and 5 after coastal low passage (Fig.8; D+3 to D+5) were included to show the following sequence of events with the next coastal low (for the strong cases particularly) visible by D+4 along the south coast again, moving northwards along the east coast to about 31°S on day five after the first coastal lows' passage at Port Elizabeth. This indicates, for the strong coastal lows, a 4 -5 day periodicity of strong case coastal low passage. The mean of all 160 SON coastal lows is not as clear on the surface pressure anomalies.

The 500 hPa anomalies (Fig. 4.9) for the mean case coastal lows shows the upper ridge moving past, centered at around 50° south, and intensifying as the trough moves eastwards, with the converse happening to the trough, where the trough is at its most intense on the day before coastal low passage, then weakening and slipping southeastwards.

For the strong case coastal lows (Fig. 4.9), the differential anomaly shows a stronger IOA, with the AOA ridging well to the south of land, further strengthening the more intense IOA well southeast of land, and in the process, trapping a region of lower pressure ahead of, and northwards from where the mean case's coastal low trough lies.

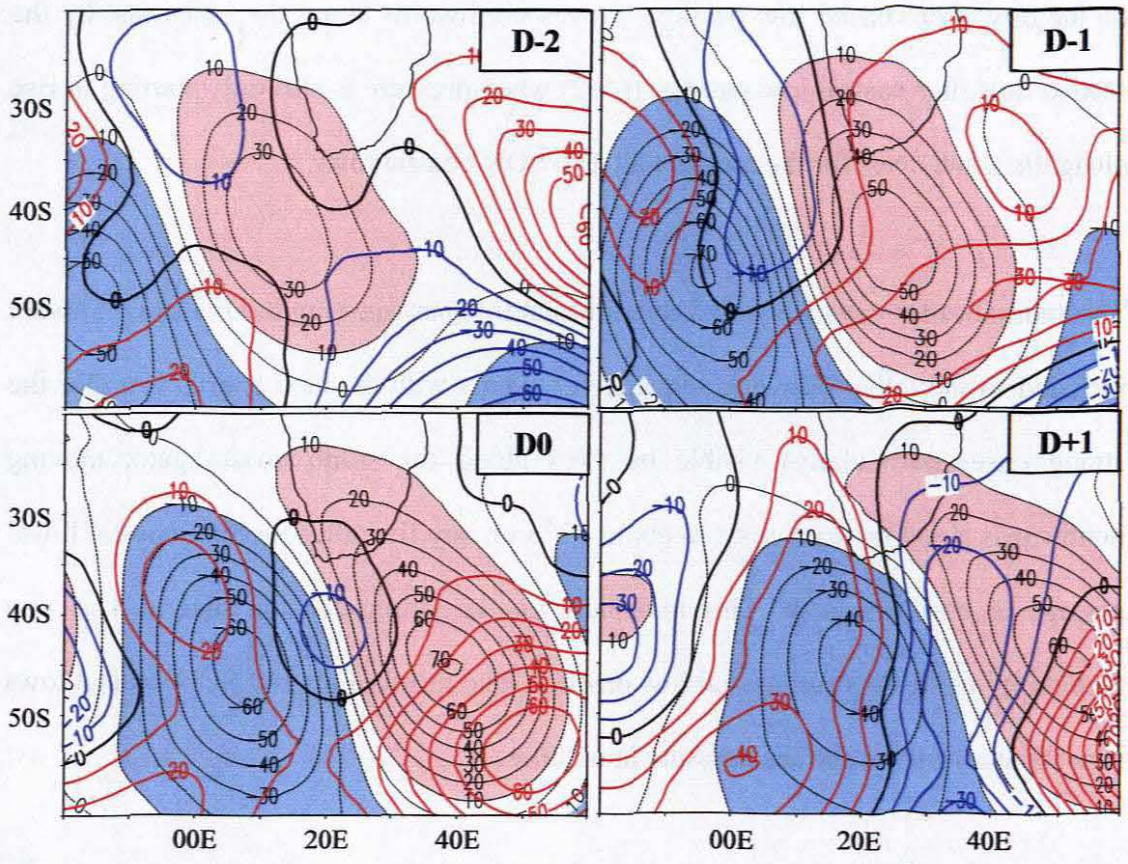

Fig. 4.9 500 hPa height (gpm) anomalies from two days before (D-2) to the day after (D+1) coastal low passage at Port Elizabeth. The dotted and colour filled contours represent the composites of all 160 SON coastal lows. The solid black with blue and red highlighted contours represents the differential anomalies that show the departure of the top 10% SON coastal lows.

The northwesterly flow at 25°S 19°E (Fig. 4.10, D-2) is already stronger for the strong case coastal lows than for the mean 160 SON cases two days before coastal low passage at Port Elizabeth, and this trend continues on the day before passage (D-1). Although the central and western parts of the land (over the interior trough region) are now covered by northwesterly flow, there is a core of maximum northwesterly flow just south of the south coast.

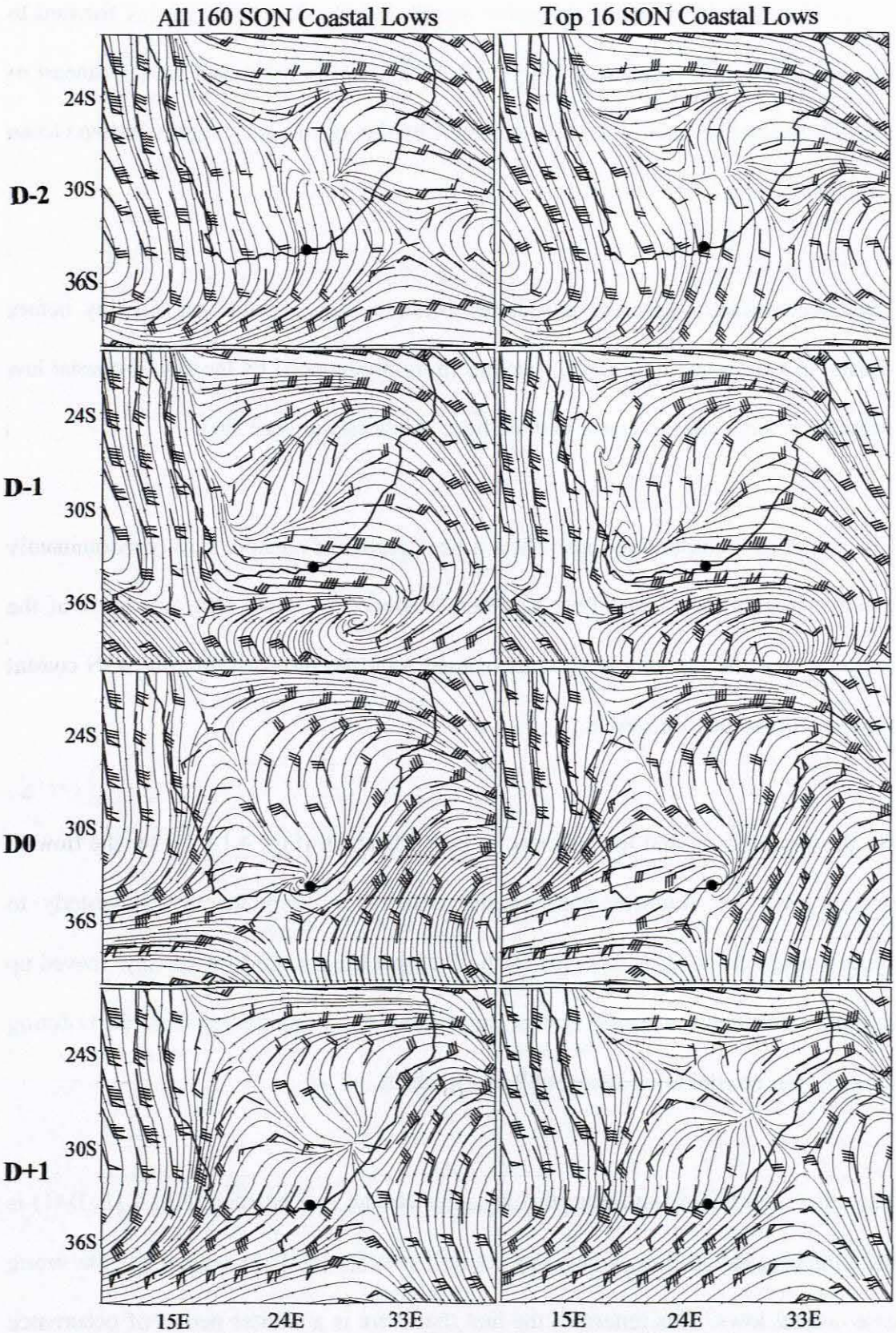

Fig. 4.10 Surface mean vector wind composites for two days before (D-2) to the day after (D+1) coastal low passage at Port Elizabeth. Each full feather on the wind barbs is equal to one meter per second. The black dot represents Port Elizabeth.

In particular, the very strong (negative zonal) easterly flow wind carries forward to the day of coastal low passage (Fig. 4.10, D0), when it is situated well southeast of land for the strong case coastal lows, driven by the significantly higher Indian Ocean Anticyclone (Fig. 4.5).

The predominantly negative meridional offshore flow, visible on the day before coastal low passage (4.10, D-1), becomes more pronounced by the day of coastal low passage on the southeast coast, and offshore southeastwards of land.

The strong case coastal lows also show a peak region of onshore flow (predominantly positive meridional) in the Port Elizabeth region (Fig. 4.10, D0), just west of the region where the meridional flow associated with the mean of all 160 SON coastal lows is at its weakest negative.

By the day after coastal low passage at Port Elizabeth (Fig. 4.10, D+1), the flow in general over the southern parts of the country is dominated by a westerly to southwesterly flow, as is expected by the fact that the coastal low has now moved up the east coast with the frontal system and ridging AOA dominating these parts during the day after coastal low passage at Port Elizabeth.

The other significant feature on the day after coastal low passage (Fig. 4.10, D+1) is the similarity to the flow at two days before passage (D-2) in general for the strong case coastal lows. This reiterates the fact that there is a shorter period of occurrence for these lows.

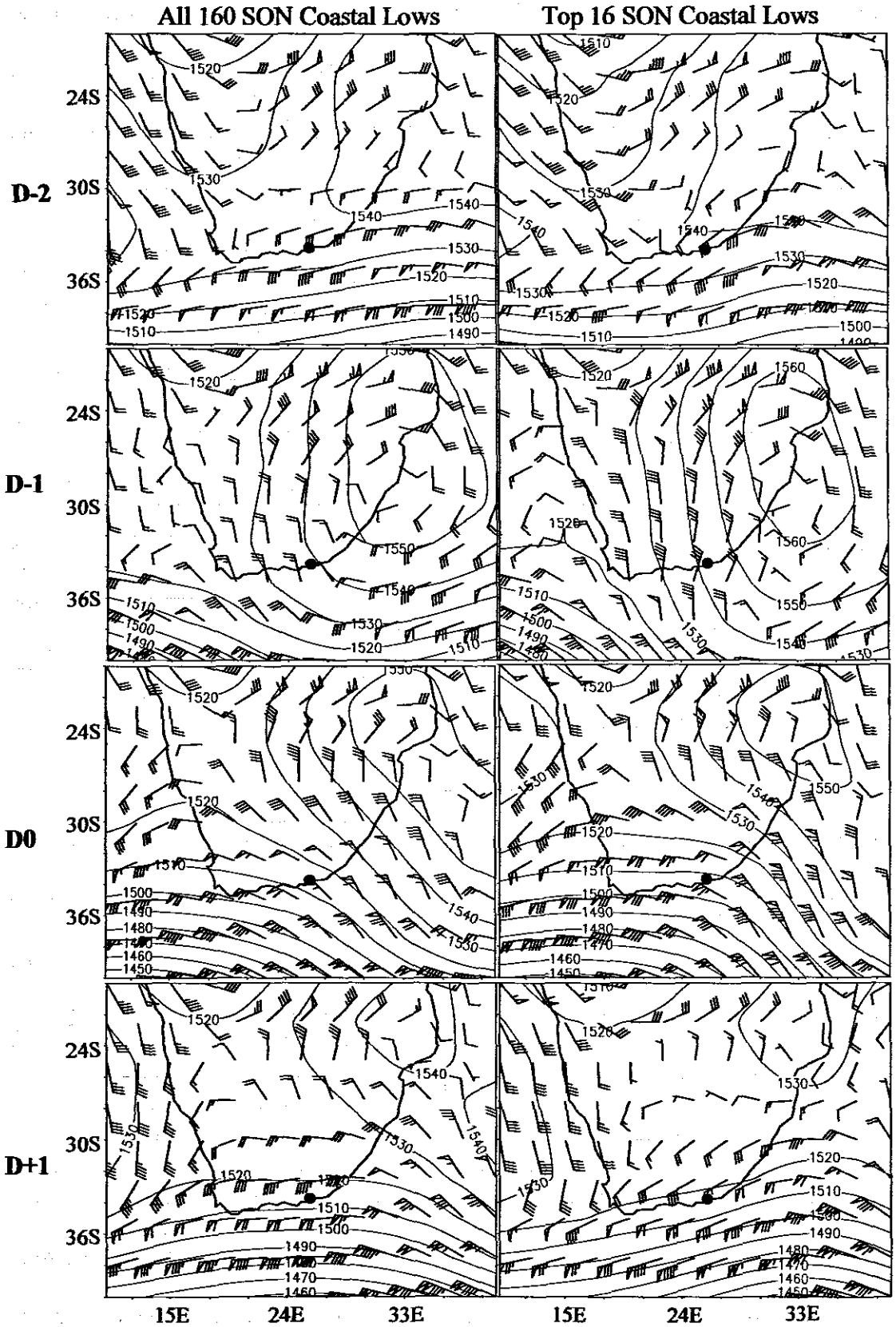

Fig. 4.11 850 hPa mean vector wind and height (gpm) composites for two days before (D-2) to the day after (D+1) coastal low passage at Port Elizabeth. Each full feather on the wind barbs is equal to one meter per second. The black dot represents Port Elizabeth.

The wind flow patterns at 850 hPa (Figs. 4.11) are very similar to those of the surface levels, particularly so in the way that the enhanced northwesterly flow dominates over the western parts of land, during the days before coastal low passage, for the strong case coastal lows. The same strong southwesterly core over the South Coast (Figs. 4.10 and 4.11, D-1) is visible from surface level up to 850 hPa (associated with the strong case coastal low anomaly).

The strong easterly to northeasterly flow south of land (Figs. 4.10 and 4.11, D-1) also dominates throughout this column for the strong case coastal lows. However, the most notable feature at 850 hPa is the strong negative meridional flow, which is twice as strong as, and slightly eastwards of that of the mean cases. This strong northerly flow advects dynamically warmed air from the interior, and as the air descends from the interior plateau, adiabatic heating further warms the air.

At 700 hPa the wind for the strong case coastal lows (Fig. 4.12, D-1) is significantly stronger over the southwestern parts of the land, and this flow has also veered more to the north from the day before (D-2), suggesting a steeper trough approaching from the west. The flow remains stronger for the day of coastal low passage over the southern parts of land (D0). At two days before passage (Fig. 4.13, D-2), there is a maximum region of shear between 850 hPa and 700 hPa over the region where the coastal low is developing. By the day before coastal low passage at Port Elizabeth (D-1), this shear maximum weakens, and by the day of passage (D0), minimum shear is visible over the central and southeastern parts of land, highlighting the fact that flow at 850 hPa and 700 hPa have aligned with each other, allowing for the possibility of downwards momentum transfer.

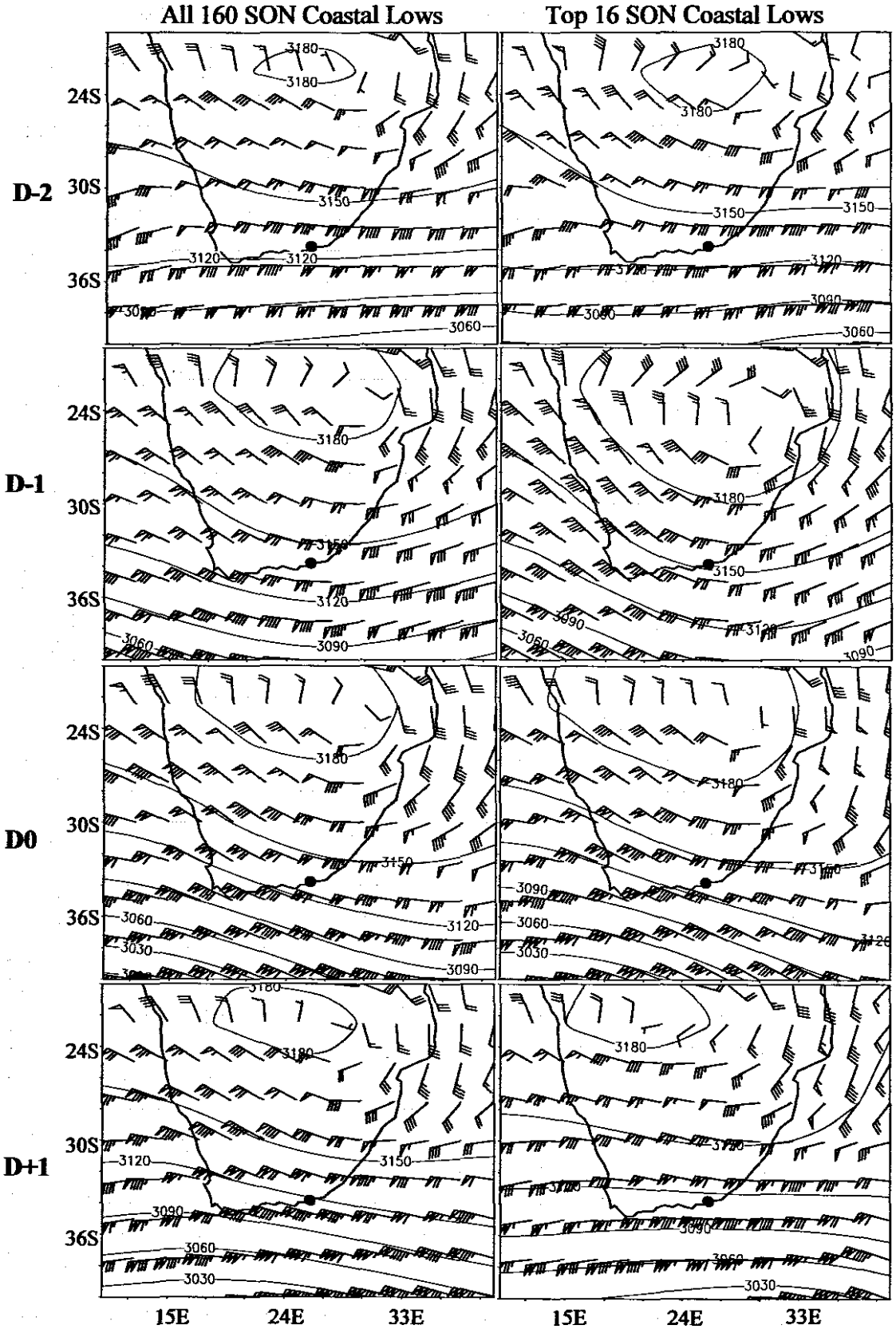

Fig. 4.12 700 hPa mean vector wind and height (gpm) composites for two days before (D-2) to the day after (D+1) coastal low passage at Port Elizabeth. Each full feather on the wind barbs is equal to one meter per second. The black dot represents Port Elizabeth

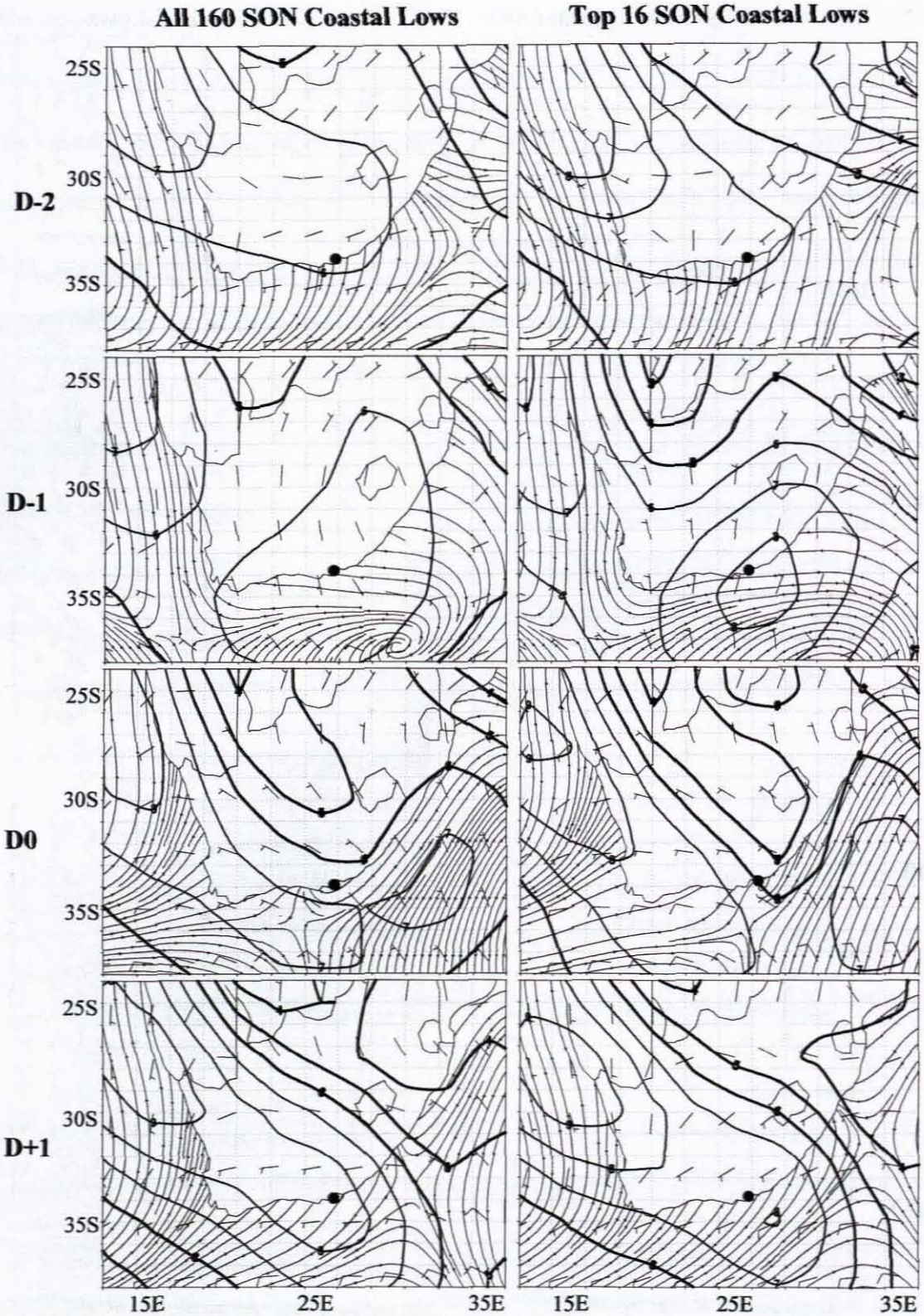

Fig. 4.13 Wind shear between 700 hPa and 850 hPa, from two days before (D-2) to the day after (D+1) coastal low passage at Port Elizabeth. The black contours represent the wind shear with minimum shear in bold black. The streamlines represent the composite mean wind flow at the surface and the barbs show the composite mean vector winds at 850 hPa, with each full feather equal to 10 $m.s^{-1}$. The black dot represents Port Elizabeth.

4.3 Cross-section composites

In order to find the vertical extent of the coastal low's anomalous characteristics the cross-sectional displays are shown for 18° to 28° East, at 30°, 32° and also 34° South. The heights of the topography for those slices (Fig. 4.15) are displayed for reference to analyze the cross-sections, as they are displayed from 1000 to 650 hPa, and the interior slices at 32° and 30° South both display data that cut the surface levels at approximately 1200 meters on average, which roughly translates to 925 hPa.

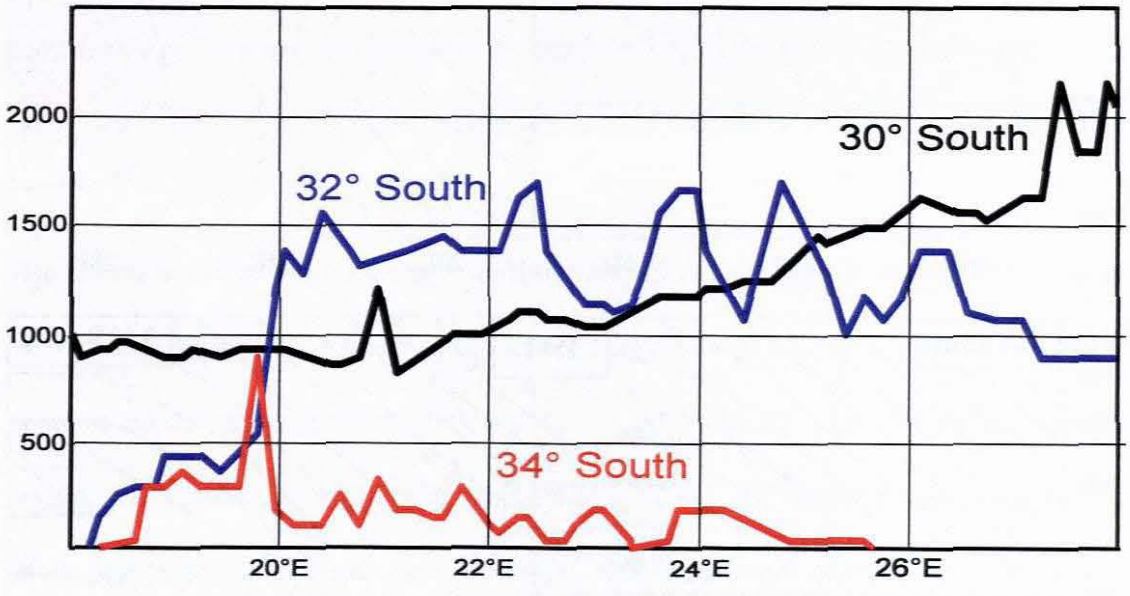

Fig. 4.14 Height of land surface for 30°, 32° and 34° South between 18° East and 28° East. Abscissa is height in meters with the ordinate longitude in degrees.

The warmer air apparent westwards of 24° East (Fig. 4.16, D-1) at both 30°S and 34°S is similar to the maximum values at around 850 hPa. On both the differential anomalies of the strong case coastal lows indicates warming eastwards of the maximum core of warmer than average temperatures, represents the region of the interior thermal trough.

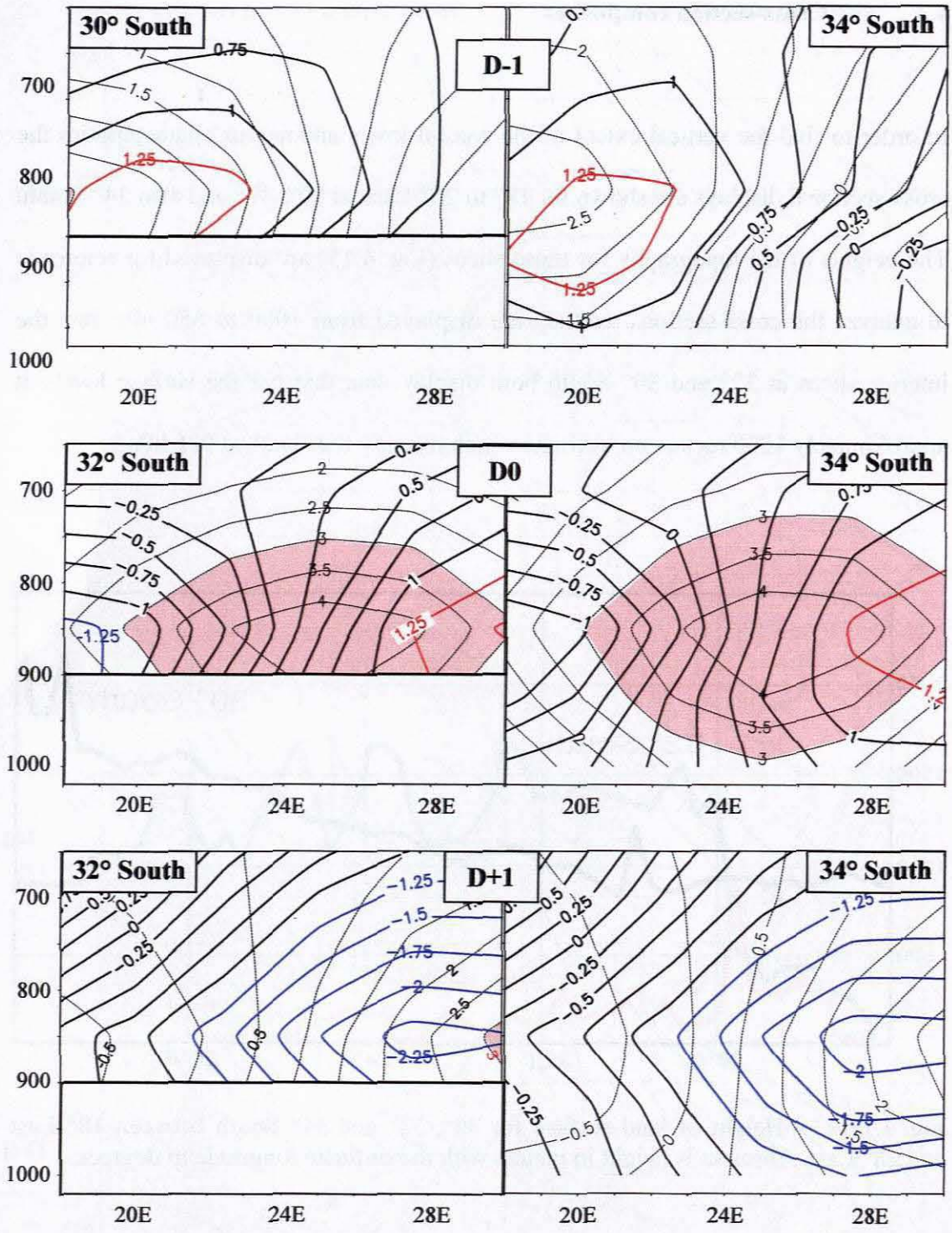

Fig. 4.15 Cross-sectional display along 18°E to 30°E of the air temperature anomalies for the day before (D-1) to the day after (D+1) coastal low passage at Port Elizabeth. The dotted and colour filled contours represent the composite anomalies of all 160 SON coastal lows and the solid black with red (warmer) and blue (colder) highlighted contours show the differential anomaly which represent the departure of the top 10% SON coastal lows. Abscissa is height in hPa. Ground level is roughly indicated by 900 hPa (approximately 1000 meters or 3200 feet) for the interior sections.

There is still some cooling over the eastern parts of Southern Africa associated with the onshore easterly flow originating with the Indian Ocean Anticyclone. By the day of coastal low passage (D0), the prominent warmer than average temperatures reach a maximum over the central regions, with a significant maximum visible for the strong case coastal lows at about 850 hPa at 28° East, between 32° and 34° South. At 32° South and 28° East, 850 hPa is about 500m above ground level, and at 34° South and 28° East; this core of warmer temperatures is at about 1500m above ground level.

By the day after coastal low passage (Fig. 4.16, D+1), a slight cooling is introduced in the west for the mean cases, while the strong case coastal lows' differential anomaly shows relative cooling already over the eastern parts of the country associated with the stronger west to southwesterly flow associated with the strong case coastal lows.

The stronger differential anomaly northeasterly flow, during the day before coastal low passage (Fig. 4.30), peaks in the lower levels below 850 hPa, with an enhanced positive zonal region (northerly flow) at 925 hPa directly over the Port Elizabeth region. On the day of coastal low passage (Fig. 4.31), the stronger case coastal lows show significantly stronger positive zonal and meridional components throughout most of the column up to 650 hPa.

By the day after coastal low passage (Fig. 4.17, D+1), the upper trough (strong case coastal lows) has also passed by as evidenced by the southerly wind anomalies above 800 hPa (also see Fig 4.9), while the anomalies for the normal case coastal lows still shows a northwesterly anomaly.

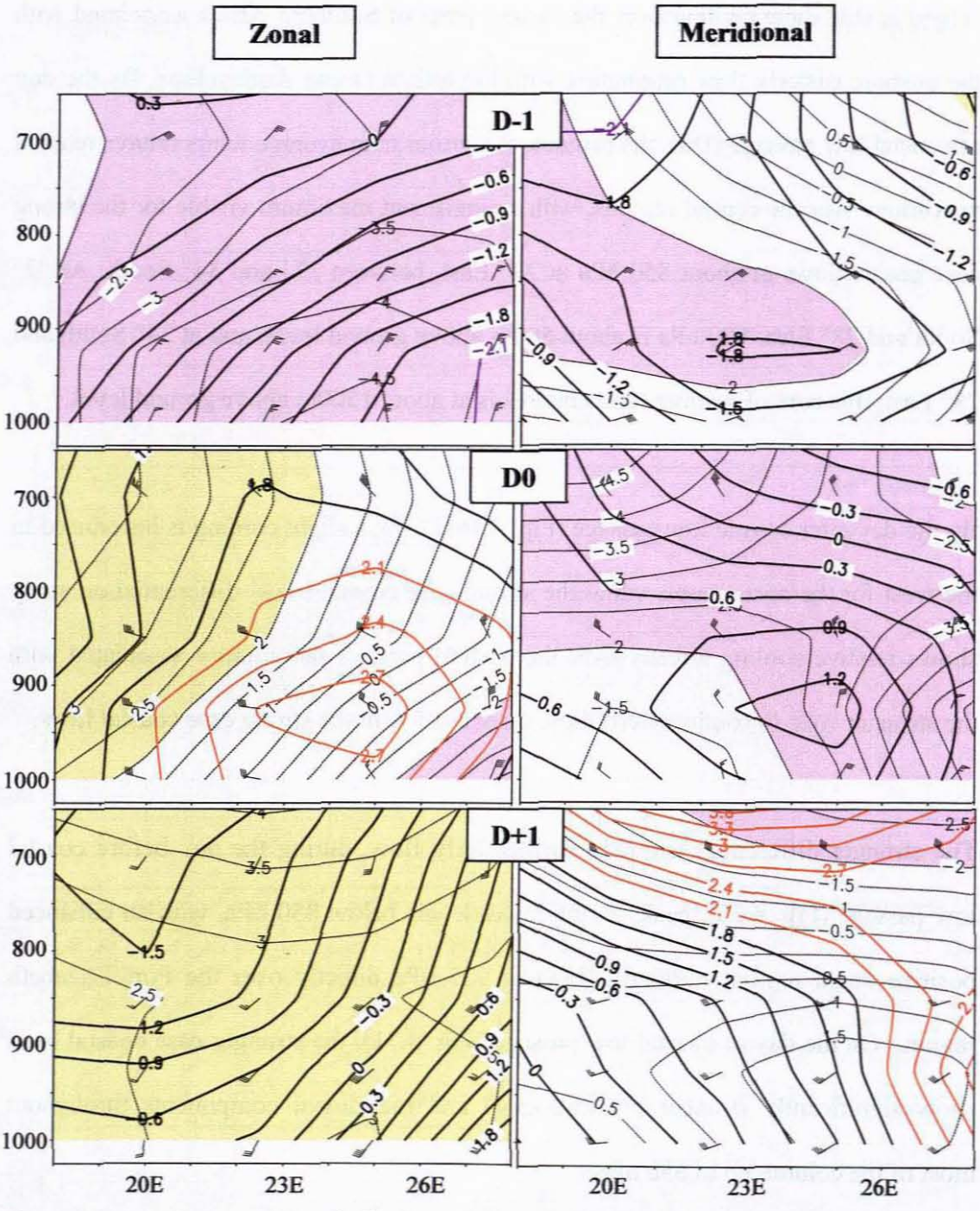

Fig. 4.16 Cross-sectional display of the wind anomalies at 34°S along 18°E to 28°E for the day before (D-1) to the day after (D+1) coastal low passage at Port Elizabeth. The dotted and colour filled contours represent the composite of all 160 SON coastal lows and the solid black with yellow and purple highlighted contours show the differential anomaly which represents the departure of the top 10% SON coastal lows. Abscissa is height in hPa. The wind barbs are a visual representation of the recombined zonal and meridional component anomalies. The barbs overlaid on the zonal sections show the top 10% of cases and the barbs overlaid on the meridional sections represent all 160 SON coastal lows. Each full feather is equal to 1 $m.s^{-1}$.

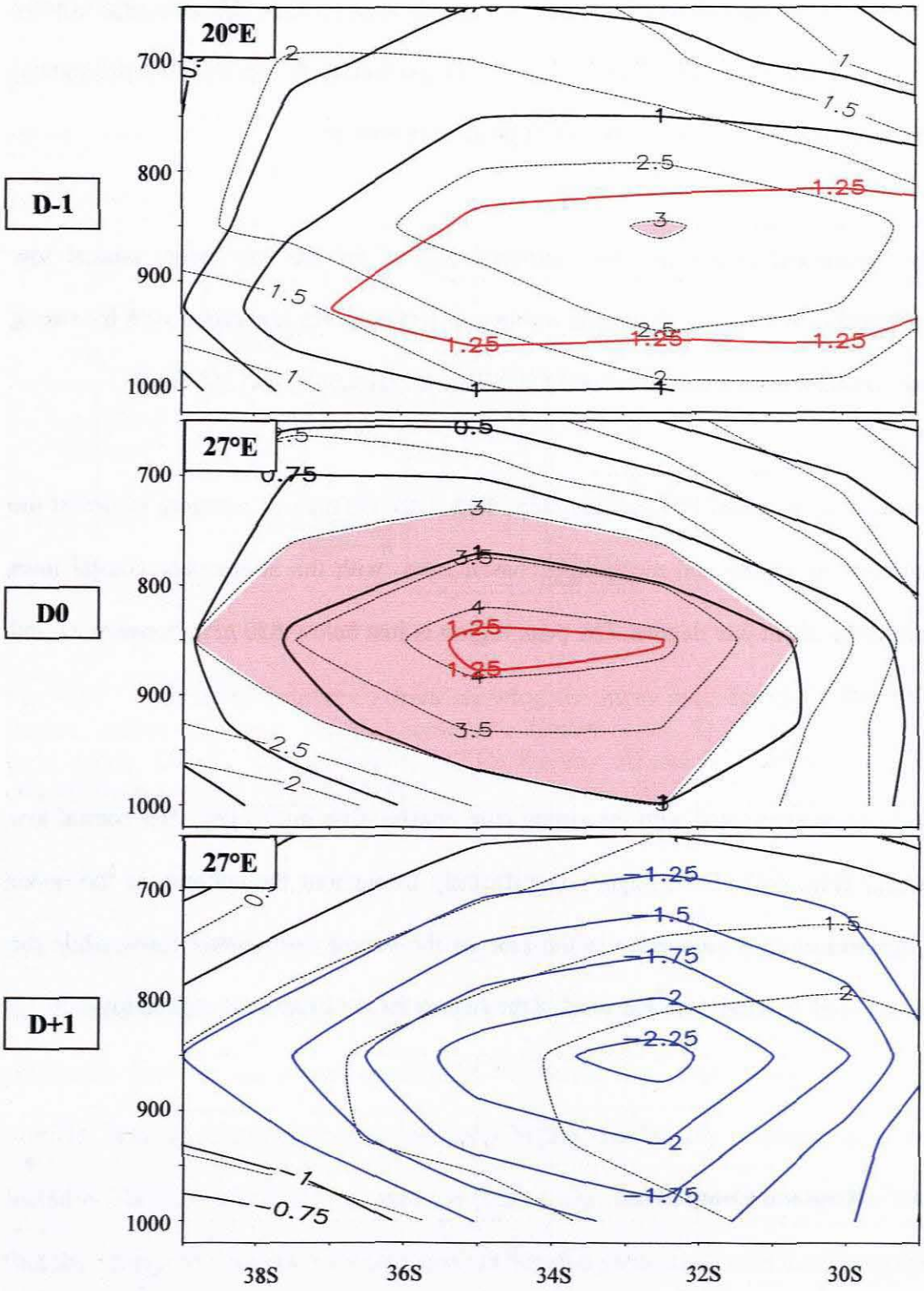

Fig. 4.17 Cross-sectional display of the air temperature anomalies along 39°S to 29°S for the day before (D-1) to the day after (D+1) coastal low passage at Port Elizabeth. The dotted and colour filled contours represent the composite anomalies of all 160 SON coastal lows, and the solid black with red (warmer) and blue (colder) highlighted contours show the differential anomaly which represent the departure of the top 10% SON coastal lows. Abscissa is height in hPa. The western interior is represented by 20°E while 27°E is representative of the central interior.

Throughout the air column the winds in general, westwards of 23E, are significantly weaker in the strong case coastal lows. This is visible on the 500 hPa differential anomalies (Fig. 4.9, D+1) as an area of positive departure.

The meridional composite cross-sectional display for the day before coastal low passage (Fig. 4.18, D-1) shows the warmer air temperatures associated with the strong case coastal lows peaking at around 850 hPa and between 30 and 35° South.

On the day of coastal low passage (Fig. 4.18, D0), the area of warming is almost the same for the strong and mean case coastal lows, with the strong case coastal lows warmer by about one degree. The peak region is just below 850 hPa, between 31 and 37° South.

The cooling associated with the strong case coastal lows on the day after coastal low passage (Fig. 4.18, D+1) departs significantly throughout the column, as the upper trough had already passed by in the case of the strong case coastal lows, while the upper trough is still just to the west of the region for the mean case coastal lows.

4.4 Regional Composites

At two days before the passage of the coastal lows at Port Elizabeth, the pressure anomalies (Fig. 4.20, D-2) are already lower in the region of the pressure minima associated with the coastal low for the stronger cases. The anomaly deepens further on

the day before coastal low passage (D-1), and further still on the day of coastal low passage (D0), indicating an intensifying system as it moves along the coast.

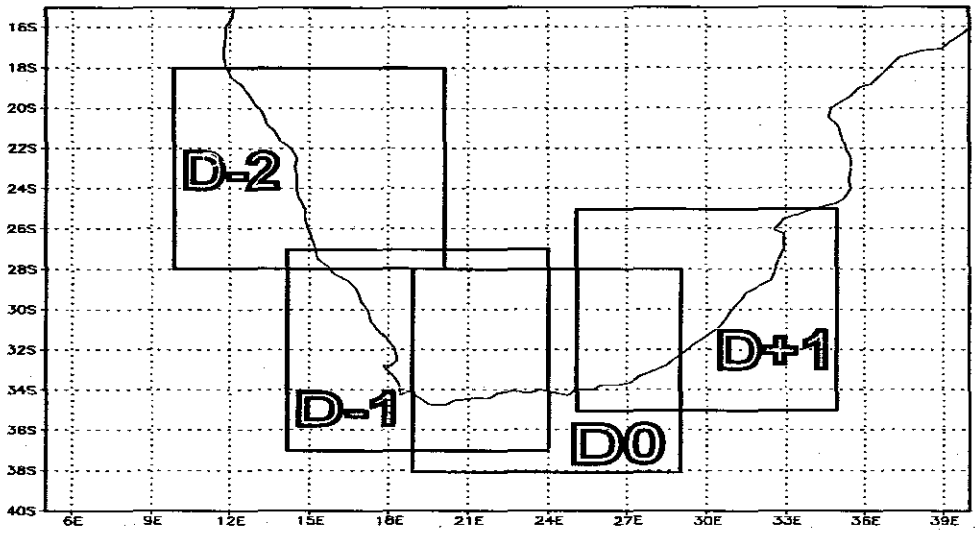

Fig. 4.18 Map of Southern Africa showing the areas used for the 10° by 10° degree, system-following, regional composite display areas. D-2 was used for two days before, D-1 for one day before, D0 for the day of, and D+1 for the day after coastal low passage at Port Elizabeth.

The composite vorticity fields show stronger negative vorticity (clockwise "spin" in the Southern Hemisphere) associated with the strong case coastal lows, but the difference between the actual amount of the strong and mean case coastal low vorticity remains unchanged from two days before coastal low passage, up to and including the day of coastal low passage (Fig. 4.22). The vorticity fields also show that the strong case coastal lows propagate faster along the coast, with the strong case coastal lows' peak regions of negative vorticity moving gradually further ahead of the mean cases throughout the four day period up to day four (D+1), when the strong case composite field shows mainly positive vorticity along the East coast in the same region where the mean case composite vorticity field still shows negative vorticity.

For the surface, the predominantly along-shore composite wind component is displayed (meridional component along the West and Southwest coasts, and zonal for the Southeast and East coasts) in order to view the most significant vector component of coastal low post and pre-low flow (Fig. 4.21).

The offshore composite wind component is displayed at 850 hPa (the zonal component for the West and Southwest coasts, and meridional for the Southeast and East coasts) in order to highlight the offshore forcing function component of the wind. The wind barbs are overlaid for both the mean and the strong case coastal low composites so as to keep a perspective of the mean vector wind flow at both surface and 850 hPa levels (Fig. 4.24).

The meridional surface wind composite (Fig. 4.21, D-2) for two days before coastal low passage at Port Elizabeth shows strong positive flow along the coast and offshore to the west of land, with just a slight clockwise kink at around 23° South suggesting the coastal low region. The wind barbs show that the wind speeds are very similar between the strong and mean cases for most of the region.

By the day before coastal low passage (Fig. 4.21,D-1), the wind barbs show a cyclonic rotation at about 34° S and 19° E for the strong cases, while a broad interior trough is apparent at around 20-21° E for the mean cases with no discernable negative meridional post-coastal low flow.

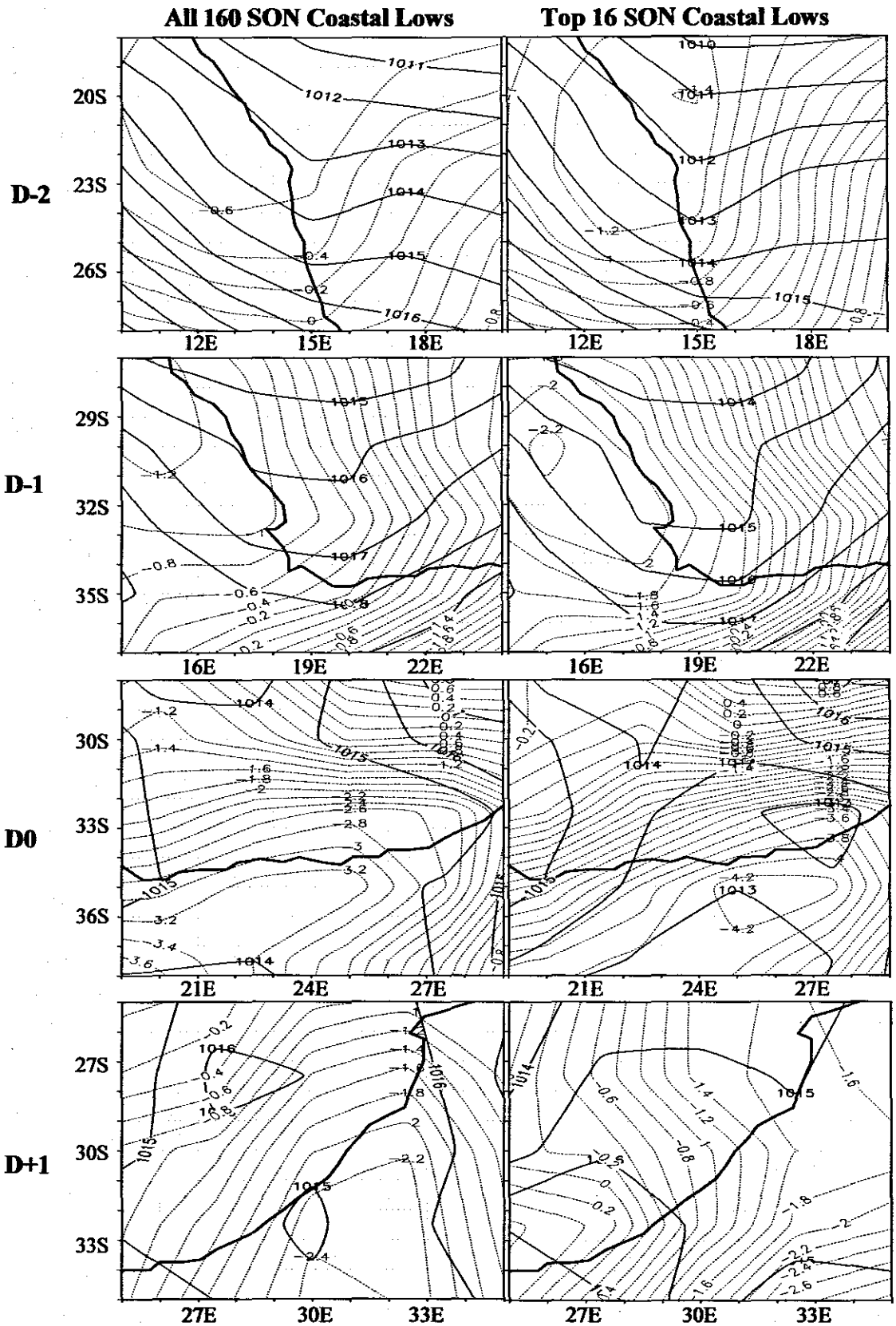

Fig. 4.19 System following composites of sea level pressure from two days before (D-2) to the day after (D+1) coastal low passage at Port Elizabeth. The solid lines represent the means of the cases, and the dotted lines show the pressure anomalies.

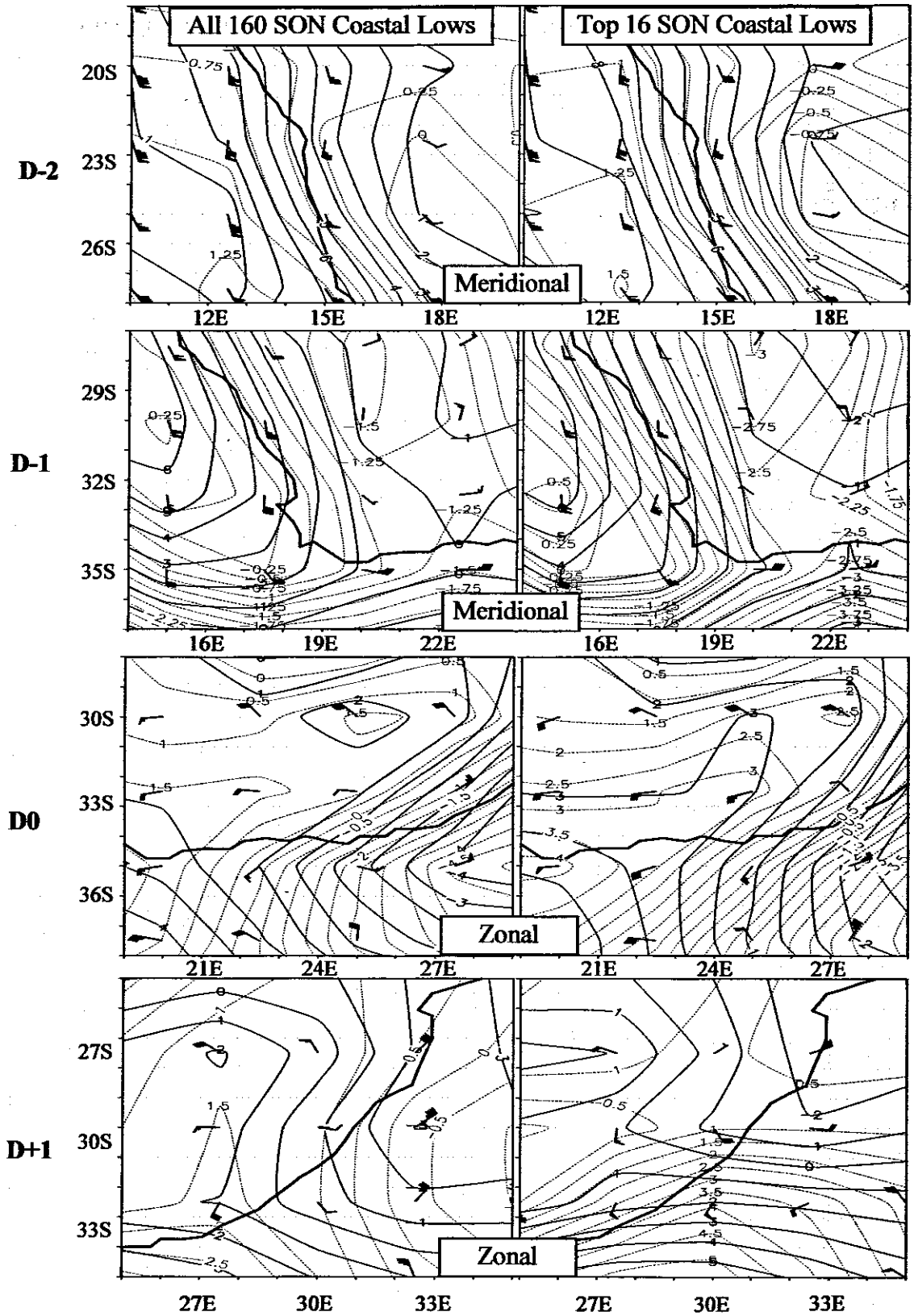

Fig. 4.20 System following composites of the surface wind (predominantly alongshore flow at the coast) from two days before (D-2) to the day after (D+1) coastal low passage at Port Elizabeth. The solid lines represent the means of the cases, and the dotted lines show the anomalies. The wind barbs show the means of the winds, with one full feather equal to 1 $m.s^{-1}$.

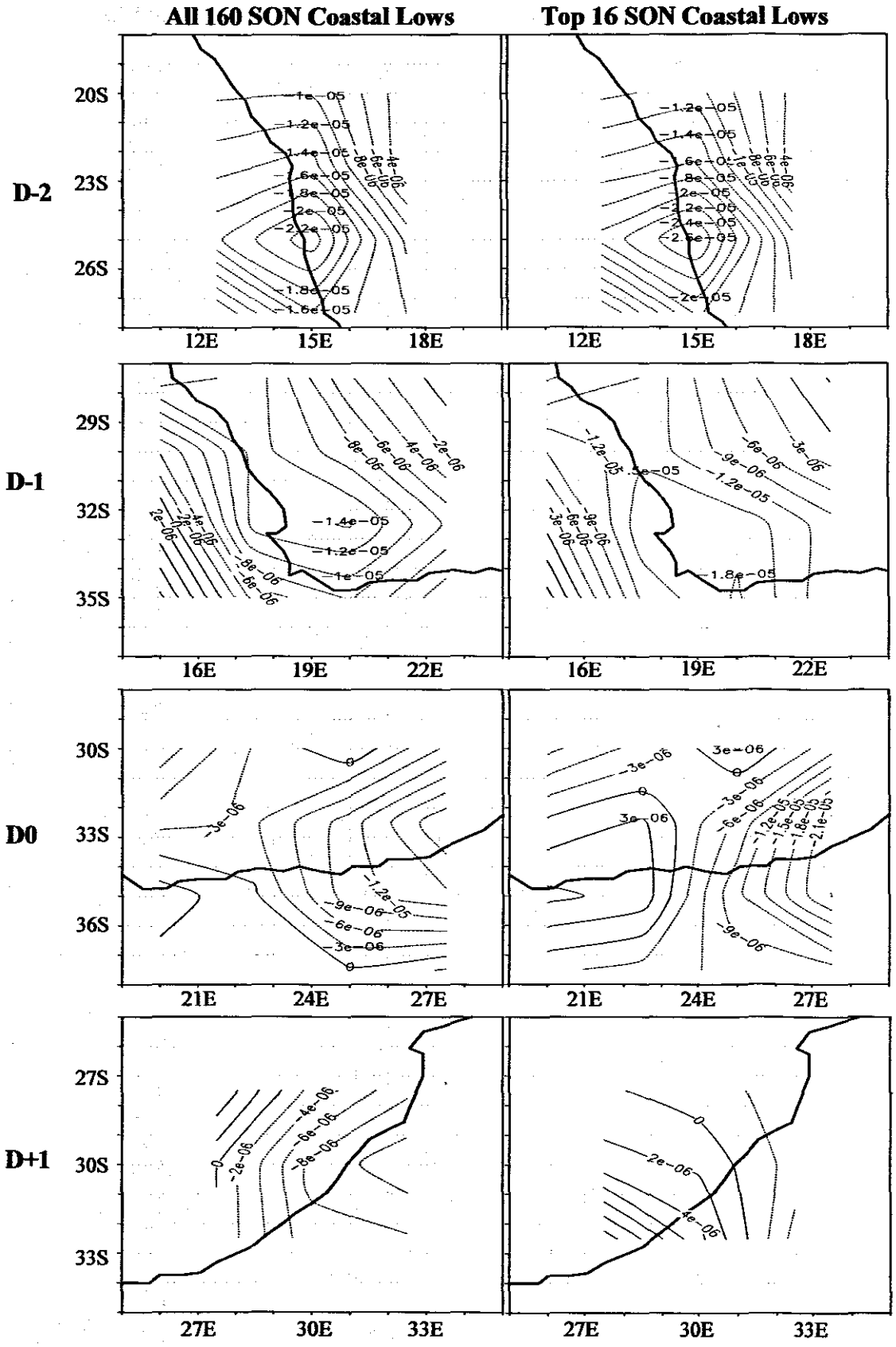

Fig. 4.21 System following composites of the mean surface vorticity from two days before (D-2) to the day after (D+1) coastal low passage at Port Elizabeth.

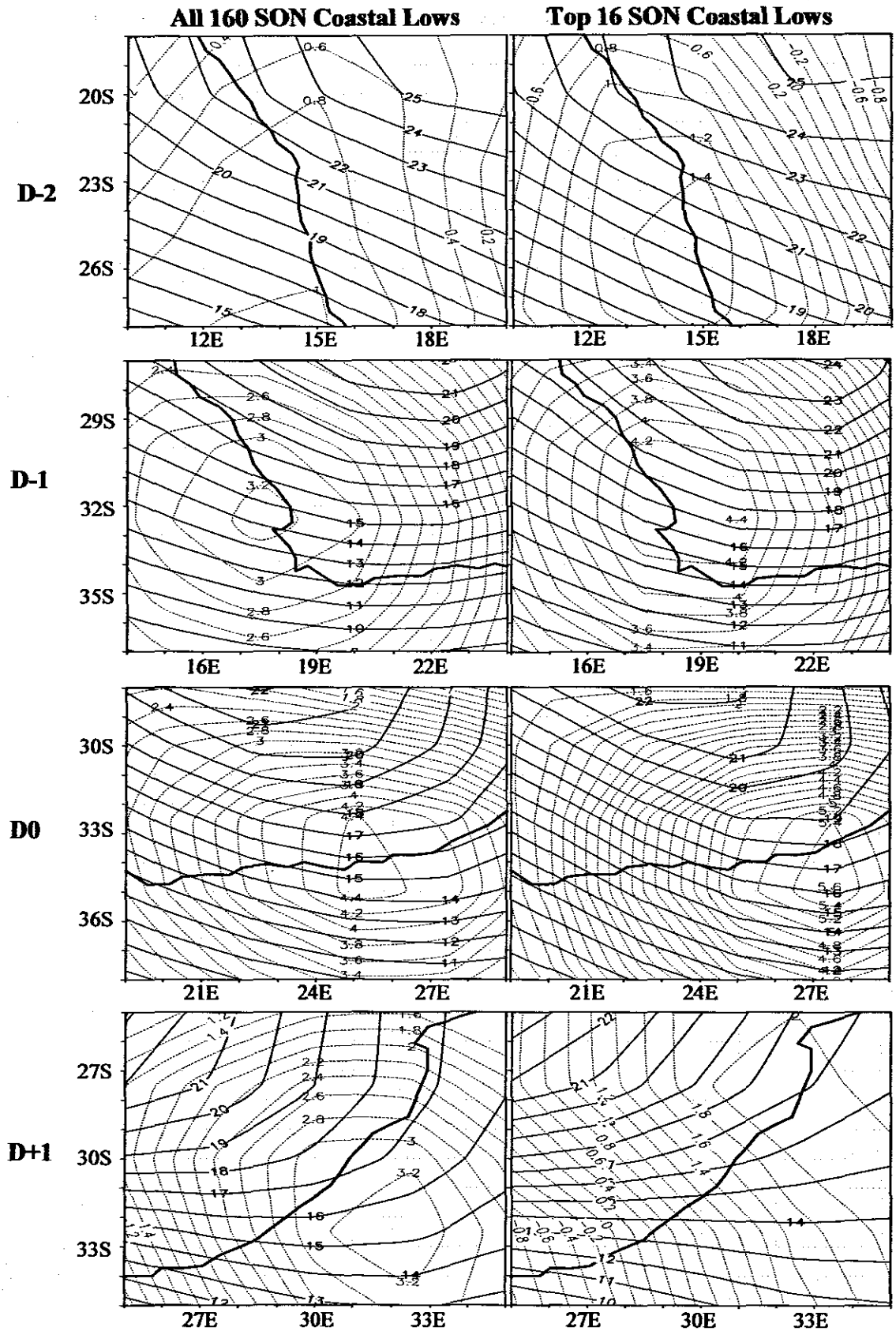

Fig. 4.22 System following composites of air temperature at 850 hPa from two days before (D-2) to the day after (D+1) coastal low passage at Port Elizabeth. The solid lines represent the means, and the dotted lines show the temperature anomalies.

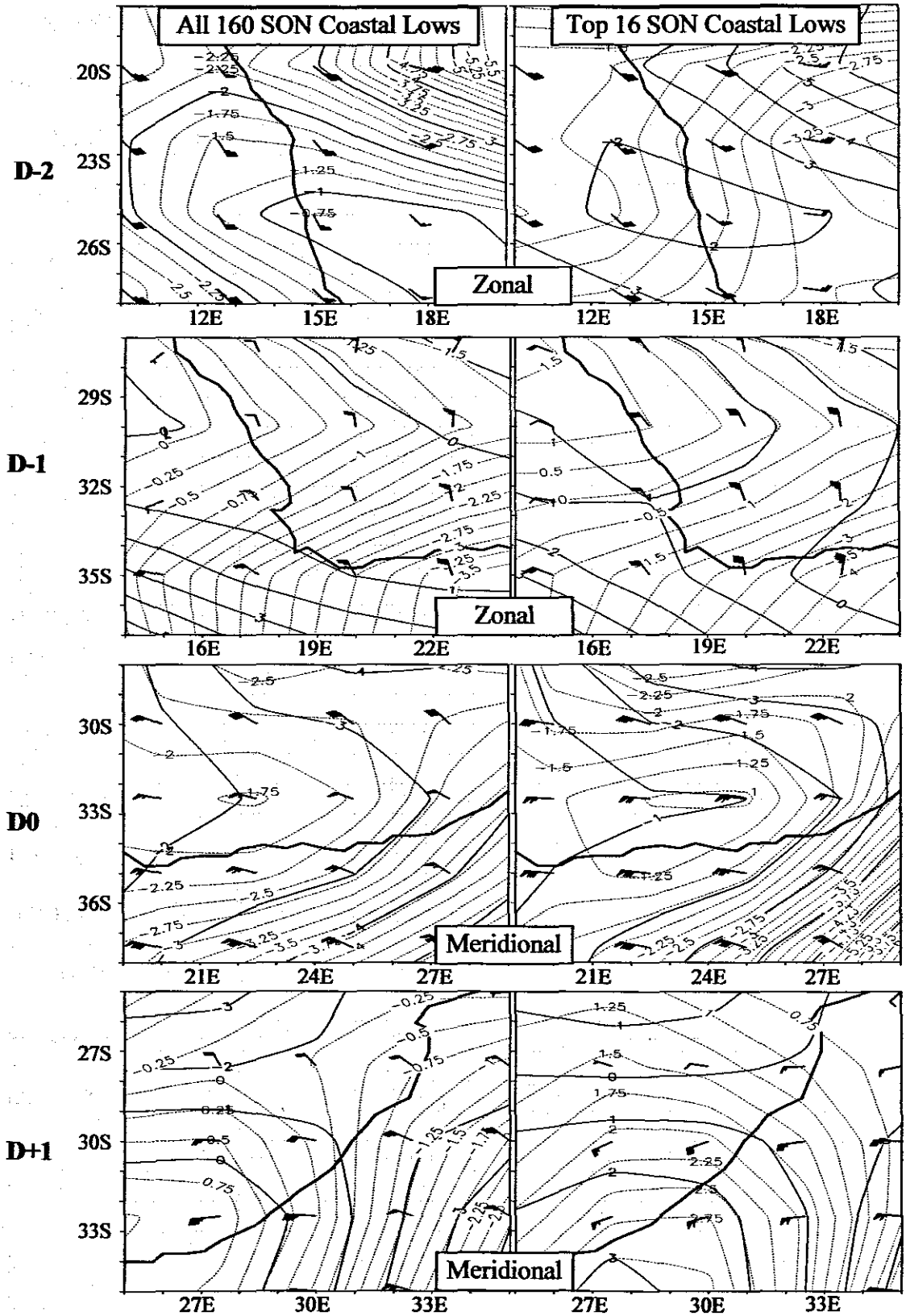

Fig. 4.23 System following composites of the 850 hPa wind (predominantly offshore flow at the coast) from two days before (D-2) to the day after (D+1) coastal low passage at Port Elizabeth. The solid lines represent the means of the cases, and the dotted lines show the anomalies. The wind barbs show the mean winds, with one full feather equal to 1 $m.s^{-1}$.

On the day of coastal low passage at Port Elizabeth (Fig. 4.21, D0), the composite zonal wind still shows a negative component to the northeast of Port Elizabeth for the mean cases, while the strong cases show a significantly stronger convergent positive zonal flow to the west and southwest of Port Elizabeth. This is reflected by the significantly stronger west to southwesterly post-coastal low vector wind flow (wind barbs) which is apparent all the way through, westwards of Port Elizabeth to 19° East and southwards of 30° South.

By the day after coastal low passage at Port Elizabeth (Fig. 4.21, D+1), the mean case composite zonal flow is still predominantly negative east of 32° East, while the strong case flow is significantly positive zonal offshore, with a region of cyclonic rotation visible to the southeast of land, at about 35° South and 34° East.

The composite of the air temperature at 850 hPa for the strong case coastal lows (Fig. 4.23, D-2) displays a positive anomalous temperature departure already, two days before coastal low passage at Port Elizabeth from that of the mean cases, and the 1.2°C difference between the anomaly of the strong case and the anomaly of the mean case coastal low is maintained up to, and including, the day of coastal low passage at Port Elizabeth (D-1, D0), even while the air temperature increases from around one degree above normal at two days before passage, to around five degrees above normal on the day of coastal low passage at Port Elizabeth.

By the day after coastal low passage (Fig. 4.23, D+1), the strong positive zonal flow (Fig. 4.24, D0 and D+1) has cooled the strong case composite air temperature field at

850 hPa so significantly that the mean case coastal low air temperature composite is warmer than that of the strong case coastal low south of 30° South.

At 850 hPa, two days before coastal low passage at Port Elizabeth (Fig. 4.24, D-2), the composite zonal wind anomaly for the strong case coastal lows maximum is further south already than that of the mean case coastal low (at about 23°S as opposed to 19°S). The wind speeds, as shown by the wind barbs, are very similar to each other, with 0.5 to 1 $m.s^{-1}$ difference between the strong and mean case coastal lows over the whole region.

By the day before coastal low passage at Port Elizabeth (Fig. 4.24, D-1), the difference between the offshore flow over the southern coast has increased significantly, with the strong case coastal lows 1.5 to 2 $m.s^{-1}$ stronger (northerly flow) than the mean case coastal lows over the whole southwestern Cape interior. There is also a slightly more negative zonal component to the wind flow over the south coast (in the region of 21 to 24° East) apparent with the strong case coastal lows, and as this flow backs, with time, to the day of coastal low passage at Port Elizabeth (D0). This also suggests that the stronger offshore flow remains perpendicular to the coast for a longer time, between the day before and the day of coastal low passage, for the strong case coastal lows.

On the day of coastal low passage at Port Elizabeth (Fig. 4.24, D0), the 850 hPa composite meridional wind components for both the strong and the mean case coastal lows are negative over the whole region, with westerly flow over the Karoo region for both the strong and the mean cases, between the coastal low and the approaching

trough system. The strong case wind speeds are stronger by 1.5 $m.s^{-1}$ over this region (post-coastal low region). By the day after coastal low passage (D+1), the strong case winds have already started to back over the southeast coast (positive meridional), while the mean case coastal low winds remain westerly over the same region. It should be noted here that the NCEP model tends to move the coastal low too slowly along the east coast.

4.5 Summary

Taking into account the scarcity of data in general over the ocean south of land and the large grid spacing (2.5°) of the reanalysis data used, the analysis of these data has yielded some significant new results. Confirmation of station data results from the previous chapter has been obtained as well.

The Indian Ocean Anticyclone (IOA) is significantly stronger during the strong coastal low case passage days, and its centre is placed 15° southeastwards of that of the mean coastal low cases. This feature is represented well from the surface to 500 hPa.

The following trough system is less intense just before strong coastal low case days; however, the centre of the low associated with that trough system is placed 5° northeastwards of that of the mean case coastal low cases, and the wind at 700 hPa is stronger and has veered more to the north over the southwestern parts of land on the

day before coastal low passage at Port Elizabeth. This feature is also represented well throughout the air column to 500 hPa.

The low associated with the following trough system for the mean coastal low cases starts off deeper to the west, but weakens as it moves southeastwards during its passage south of land.

The coastal low pressure minimum, associated with the strong coastal low cases, is deeper than that of the mean coastal low cases.

The air temperature through most of the column from the surface to 700 hPa (from two days before coastal low passage up to, and including, the day of coastal low passage at Port Elizabeth) associated with the strong coastal low cases is significantly higher than that of the mean coastal low cases. These temperatures also increase from two days before passage up to the day of passage, when it reaches a peak over the southeastern parts of the country, with the maxima stretching out over the Indian Ocean.

The maxima of the positive temperature anomaly are centered at about 850 hPa from two days before coastal low passage at Port Elizabeth (where they would be close to ground level), but stay at that level even by the day of coastal low passage at Port Elizabeth, when 850 hPa is approximately 1500 m above ground level.

It takes the strong coastal lows approximately 4 - 5 days from its birth on the west coast, to dissipation on the east coast, and back to birth on the west coast again.

The wind speed in general for the strong coastal low cases is stronger than that for the mean coastal low cases. This is true for the negative meridional (easterly) flow over the southern parts of the land ahead of the coastal low passage (due to the stronger IOA), and for the offshore flow directly ahead of, and during coastal low formation (the forcing function) as the coastal low moves along the coast. This is particularly true during the day before and for the day of coastal low passage at Port Elizabeth (along the south and southeastern coasts). This is also true for the post coastal low passage positive zonal component (westerly) flow, from surface to at least 700 hPa.

For the strong case coastal lows, the 700 hPa flow at two days before coastal low passage is positive zonal over South Africa, with the trough still well to the west of land. This flow is almost directly opposite to the negative zonal offshore flow below it at 850 hPa. By the day before coastal low passage, the coastal low has moved southwards to the southwestern Cape region, and the flow at 700 hPa has veered more to the northwest and strengthened due to the proximity of the trough, which has moved to lie just west of land. On this day there is still shear visible between the predominantly northeasterly offshore flow at 850 hPa and the northwesterly flow above it at 700 hPa. By the day of coastal low passage at Port Elizabeth, the winds at both 850 hPa and 700 hPa are both under minimum shear, with northwesterly winds at both levels over the southeastern parts of the land, above and to the north and east of the position of the coastal low. These conditions are maintained as the coastal low moves northwards along the east coast during the day after coastal low passage at Port Elizabeth.

The post coastal low positive zonal flow, for the 24 hour period after coastal low passage at Port Elizabeth, is stronger over the southern and southwestern parts of the country during the strong coastal low cases, and this is most likely due to the fact that the following trough system associated with the mean coastal low cases weakens and slips southeastwards, while the following trough of the strong coastal low cases maintains a closer track to land, and so keeps a stronger westerly flow during the post coastal low passage period as the AOA ridges over the southern parts of the land.

CHAPTER 5

COASTAL LOW CONCEPTUAL MODEL, CORRELATIONS, NUMERICAL MODEL CASE STUDY AND MATHEMATICAL FRAMEWORK

5.1 Introduction

The difficulty in not being able to forecast the strong case coastal lows is due mainly to the small size of these lows. Regional scale models have grids that are too large to sufficiently resolve small-scale features like coastal lows. Mesoscale models fare better but also have limitations where the timing of the coastal low passage and particularly the strength of the wind may not be forecast well. Data scarcity also plays a role, with very little observational data available on the ocean south of land, and limited land observation and upper air reporting stations westwards of Port Elizabeth.

An operational forecaster needs to recognize potential strong case coastal lows over the longer-term forecasting period (between 2 and 7 days lead-time). The numerical weather forecast models, which provide forecasts over this length of period, are the global scale models. Mesoscale models generally have a forecast period of up to 48 hours.

The global scale forecast models forecast the large-scale synoptic systems well. Considering that it is the offshore flow which originates with the Southern Indian

Ocean Anticyclone that creates the coastal low, and steers its movement along the coast, the position of the coastal low is forecast reasonably well along the south coast by the global models, while the intensity of coastal lows are not forecast well. Comparing the characteristics which differentiate the strong case coastal lows against the mesoscale model output should then further improve the forecasts, keeping in mind the cautions (COMET, 1999; COMET, 2003) against the efficiency of the mesoscale models themselves when forecasting mesoscale systems (in short, the actual wind forecasts by the mesoscale models for the coastal lows will not be forecast well at times).

The first section of the chapter will consist of correlations done between some of the factors which are likely to play a role in the formation, propagation and strength of the coastal low, and the intensity of the coastal lows. The second section will provide a day-by-day model of the movement of an idealized strong coastal low from the west coast through to its dissipation on the east coast, highlighting the characteristics that differentiate the strong coastal lows. This model was built from the analysis of how strong case coastal lows differ from normal coastal lows, highlighted in previous chapters. The last section will consist of analyzing a mesoscale model run of a strong case coastal low which took place during the 2003 SON season.

5.2 Correlations

The Pearson's coefficients were calculated using data from all 642 coastal lows during the 10-year period from 1987 to 1996, and also for the September, October and

November (SON) seasons during the same 10-year period. The 850 hPa and 700 hPa wind speeds and the interior surface temperature were correlated against the strength of the coastal lows. The strength of each coastal low is represented by the average of the 8-hour post coastal low southwesterly wind speed.

Table 5.1 Correlations between 850 hPa wind speed, 700 hPa wind speed and the interior surface temperature against the strength of the coastal low.

		Sample Size	8-Hour average wind speed	Standard Deviation	Variance	Mean	Pearson's correlation coefficient as measured against the 8-hour average
All 642 Coastal Lows	8-Hour average wind speed	642	6.2	2.6	6.6	6.2	-
	Interior Temperature	642	29.6	4.7	22.4	29.6	0.2
	850 hPa Wind Speed	642	8.6	4.6	21.4	8.6	0.08
	700 hPa Wind Speed	642	13.5	5.5	30.4	13.5	0.06
All 642 Hours 12:00 to 15:00 SAST	8-Hour average wind speed	132	5.9	2.3	5.1	5.9	-
	Interior Temperature	132	29.5	5.3	27.9	29.5	0.46
SON Coastal Lows	8-Hour average wind speed	160	7.0	2.5	6.1	7.0	-
	Interior Temperature	160	29.6	3.7	14	29.6	0.13
	850 hPa Wind Speed	160	8.0	3.6	13	8.0	0.21
	700 hPa Wind Speed	160	13.6	4.8	23.4	13.6	0.16
SON Hours 10:00 to 16:00 SAST	8-Hour average wind speed	44	7.2	2.3	5.2	7.2	-
	Interior Temperature	44	29.8	3.4	11.6	29.8	0.42

The interior temperature used is a mean of the maximum temperatures as measured on the day of coastal low passage at Port Elizabeth for three interior stations: Somerset

East, Graaff-Reinet and Uitenhage (Table 5.1). The data were then filtered further, in the case of the correlations calculated using the interior temperatures, to only coastal lows which passed Port Elizabeth during the middle parts of the day as that is generally when the maximum temperatures occur.

Positive correlations were found for all the variables. The wind speed at 850 hPa and 700 hPa both indicated weak positive correlation. The best correlations were found between the strength of the coastal low and the mean of the interior maximum temperatures when the middle part of the day was used.

5.3 Conceptual model

A basic model is presented of the synoptic evolution and progression of a stereotypical strong case coastal low around the coast of South Africa, in the form of a daily sequence of events. The characteristics which mark strong case coastal lows during the SON period are discussed, based on previous findings within this study.

Along the south coast the basic wind flow pattern associated with the coastal low consists firstly of the forcing function, which is the north to northwesterly flow just above the ground level of the interior plateau, moving overhead perpendicular to the coast. In the schematic drawing (Fig. 5.1) this flow is indicated by the red arrow at 850 hPa. This flow originates with the IOA (Southern Indian Ocean Anticyclone), but it has been modified by its track around the continental high pressure cell over the western parts of Southern Africa.

The air has warmed dynamically on its overland track, and as it moves from the interior plateau over the coast, further buoyancy is added due to adiabatic warming on the descent. At the same time, stretching takes place within the column, and the resultant lee side troughing essentially brings about the formation of the low pressure on the coast.

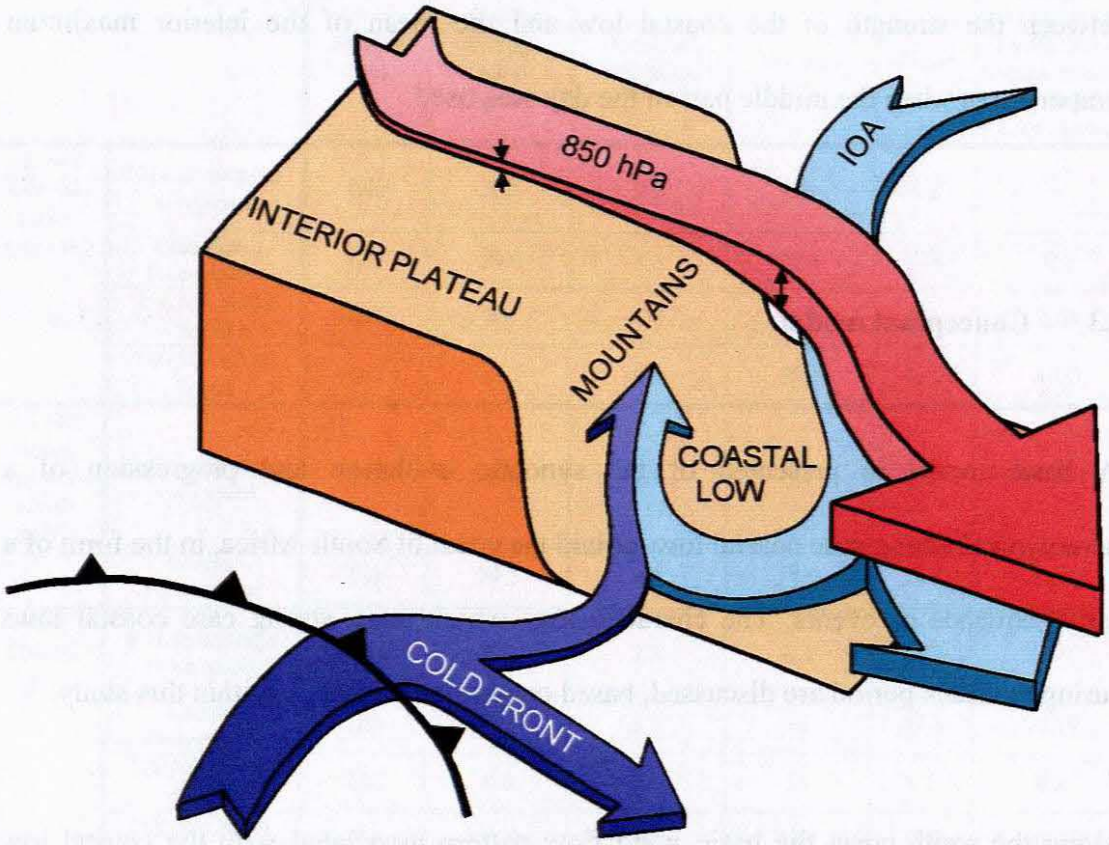

Fig. 5.1 Schematic drawing of the major wind flow associated with the coastal low.

At surface level, the coastal low is preceded by easterly flow along the south coast, originating with the IOA. The coastal low propagates along the coast, dragged along by the eastwards movement of the forcing function overhead. Recurved easterly flow

at surface level joins up with westerly flow originating with the approaching frontal system to make up the post coastal low passage onshore southwesterly wind.

Day 1

The subtropical high-pressure belt dominates the region between 20°S and 40°S with the belt disrupted by the remains of a cold front wave southeast of the continent. The next approaching wave is apparent at about 5°W (Fig. 5.2). The South Atlantic Ocean Anticyclone (AOA) ridges eastwards during this period, just to the south of land. The coastal low is starting to form on the Namibian coast, underneath the tongue of warm offshore flow at about 850 hPa. The flow at 700 hPa is westerly and at 850 hPa it is easterly.

Air temperatures on the northern west coast, east of 18° E (Namibian coastal region), are higher than the climatic norm, with positive temperature anomalies of 0.5°C for the mean cases and 0.8°C for the strong case coastal lows (Fig. 4.7). The offshore flow at 850 hPa is also stronger for the strong case coastal lows than that of the mean cases over this region (Figs. 4.11; 4.24).

The offshore flow from the high interior plateau leads to stretching of the air mass, at around 24°S on the west coast, creating cyclonic vorticity at the surface and leads to the formation of the coastal low. The stronger the offshore wind (negative zonal component), as is the case during strong case coastal lows, the stronger the vorticity (Fig. 4.22) and the deeper the coastal low should be. This is confirmed by the pressure

minima associated with the strong case coastal lows that are twice as deep as those of mean case coastal lows (Figs. 4.8; 4.20).

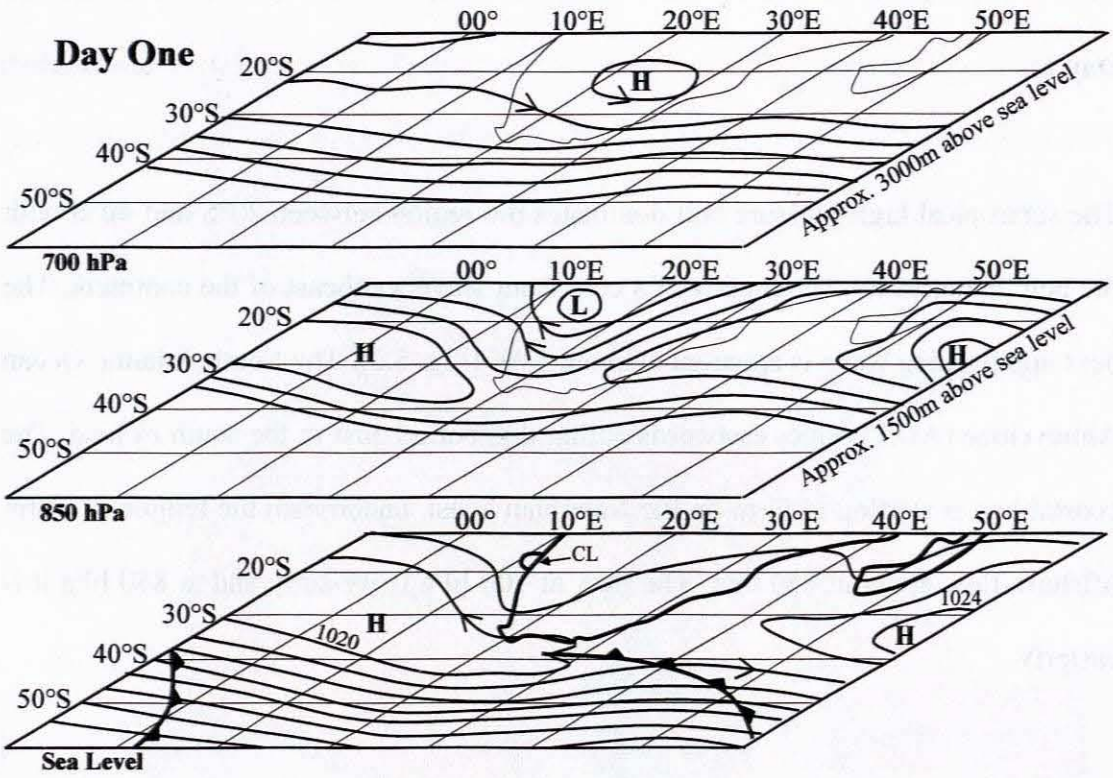

Fig. 5.2 Schematic presentation of day 1 for the strong case coastal lows at sea level, 850 hPa and 700 hPa showing the isobars and contours in the conventional manner. The positions of the trough at 700 hPa, the front, and the coastal low at sea level are indicated roughly.

Day 2

The most significant synoptic feature is the position and strength of the IOA. This is brought about by a bud off cell of the AOA, which passes south of land during the preceding 24 hours, and which has now amalgamated with the IOA (Fig. 5.3). For the strong case coastal lows, the IOA is centered well south of the land and around 3 hPa

stronger than that of the mean (Fig. 4.8). The coastal low has propagated southwards to lie close to the southwest tip of Africa.

An approaching frontal system is now apparent at about 5°E for both the strong and mean case coastal lows (Fig. 5.3). The coastal low has propagated southwards during the preceding 24 hours. In the case of the strong coastal low it is already a closed anomalous region, twice as deep and slightly further southwards of the mean case coastal lows position (Fig. 4.8). The coastal low has deepened, with the pressure anomaly for the mean cases showing a negative anomaly of 1 hPa and that of the strong cases, 2 hPa below climatic norm (Figs. 4.8; 4.20).

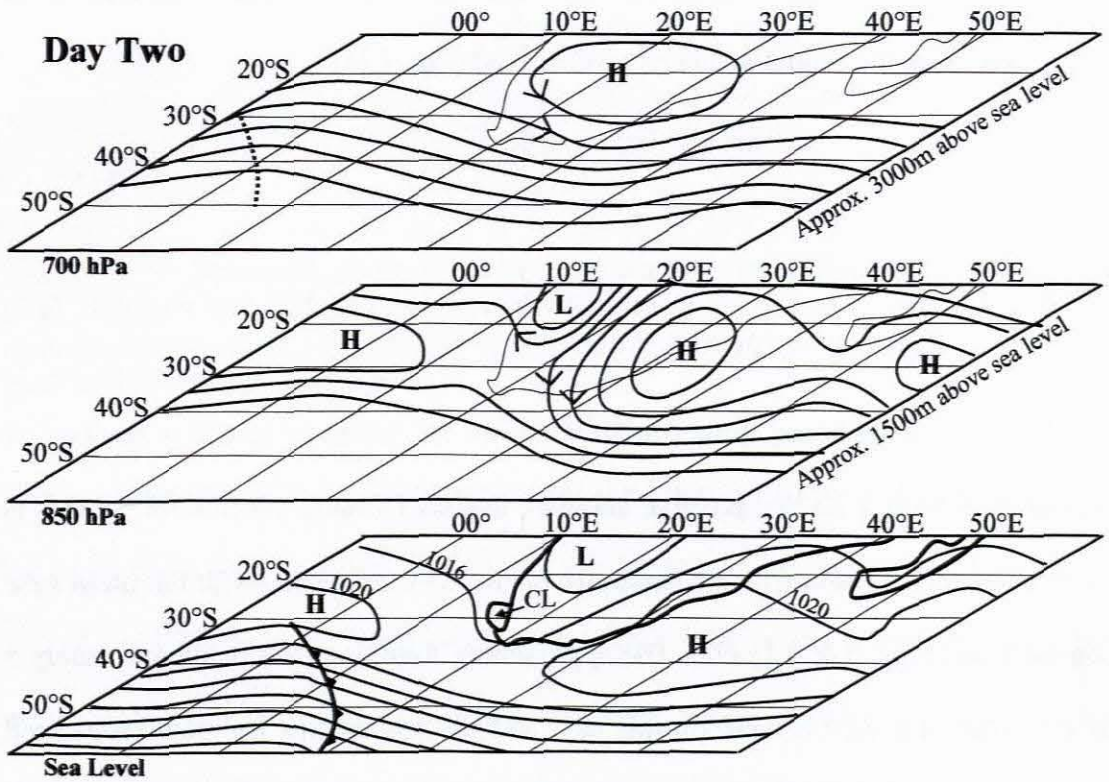

Fig. 5.3 Schematic presentation of day 2 for the strong case coastal lows at sea level, 850 hPa and 700 hPa showing the isobars and contours in the conventional manner. The positions of the trough at 700 hPa, the front, and the coastal low at sea level are indicated roughly.

On day 2 the air temperatures over the western half of the country for the mean coastal lows are higher than climatic norm by approximately 2 – 3°C over the western half of the country, stretching southwards of the land over the sea, and they are significantly higher still at 3 – 4°C for the strong case coastal lows over the same general area (Fig. 4.17). This flow along the eastern side of the interior thermal trough originates from the east-northeast and has been dynamically warmed under clear skies. The maximum temperatures are found between about 850 and 875hPa (Figs. 4.16; 4.18).

The flow at 700 hPa is northwesterly while that at 850 hPa is northerly. The gradient along the eastern side of the interior trough has steepened; with the northerly flow at 850 hPa for the strong cases 1.5 $m.s^{-1}$ stronger than the winds associated with the mean cases over the central southern parts of land (Fig. 4.11).

Day 3

The IOA has strengthened further to 1024hPa for the strong cases and is centered at almost 40°S with a 10 hPa positive anomaly against climatic norm at 48°S. This is more than twice as strong as the departure of the IOA associated with the mean case coastal lows (Figs. 5.4; 4.1; 4.2). The approaching frontal system is approximately 5 to 10° south and west of land on this day, and the coastal low has now propagated eastwards along the south coast to Port Elizabeth (Fig. 5.4). Propagation speeds during the passage from Cape Town to Port Elizabeth also show that the strong

coastal lows have propagated faster than the mean (Tables A1; A2) with speeds of 9 $m.s^{-1}$ and 6.1 $m.s^{-1}$, respectively.

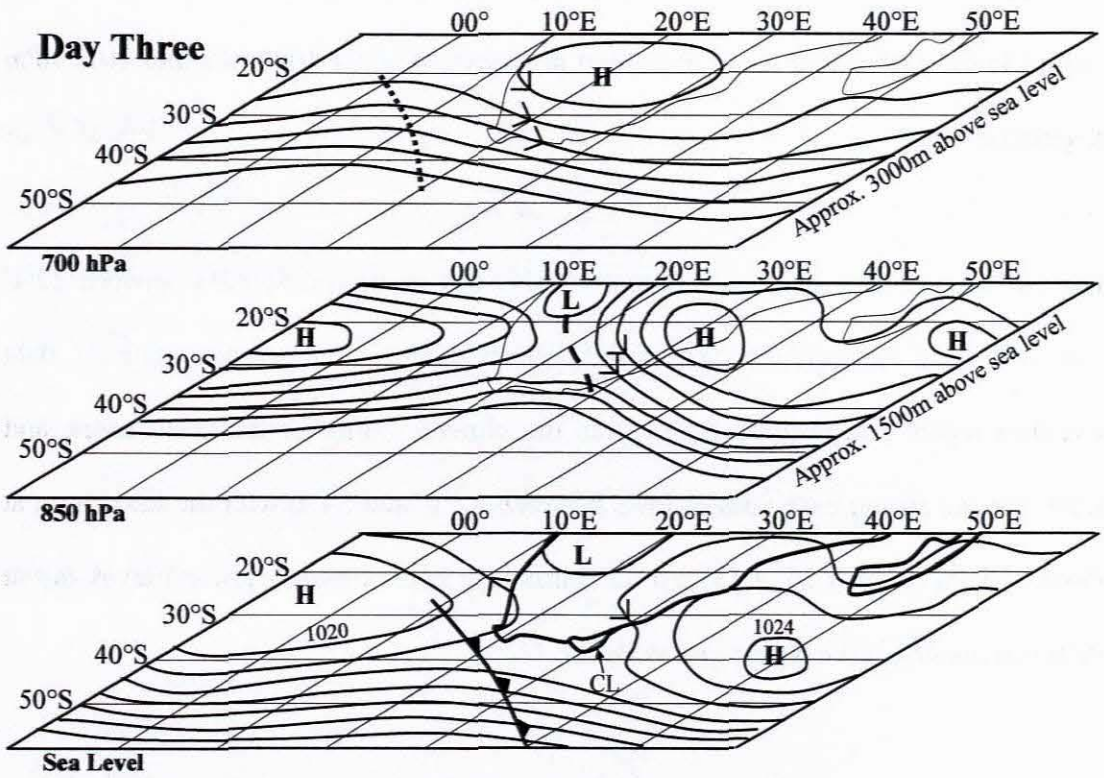

Fig. 5.4 Schematic presentation of day 3 for the strong case coastal lows at sea level, 850 hPa and 700 hPa showing the isobars and contours in the conventional manner. The positions of the trough at 700 hPa, the front, and the coastal low at sea level are indicated roughly.

The northwesterly offshore flow coming off the interior plateau and extending over the south coast is still stronger during this day for the strong case coastal lows (Figs. 4.11; 4.17; 4.24) by about 1 $m.s^{-1}$ over the southeast interior and coast than that of the mean cases. This stronger flow in the confluent region between the approaching trough and the IOA is apparent from surface to 700 hPa. This maintains the stronger forcing function, and hence, the more intense coastal lows (Figs. 5.4).

The coastal low has deepened further, with negative departures from the climatic norm of 3.2 hPa for the mean cases, and 4.2 hPa for the strong cases according to the reanalysis data (Figs. 4.8; 4.20). In reality, the strong case coastal lows are about 4 hPa deeper than the mean cases (Fig. 3.4) according to the station data for all 642 coastal lows, with actual mean minimum pressures of about 1008 hPa and 1012 hPa, respectively.

The air temperatures also reach a peak on this day at around 850hPa between 22°E and 28°E over the southern part of the country. The air temperature anomaly data reveals a positive departure of 4°C from the climatic norm for the mean cases, and 5.2°C for the strong case coastal lows between 32°C and 34°S with the maximum at about 850hPa (Figs. 4.16; 4.18). At 32°S this is at approximately ground level, but at 34°S it is about 1500m above ground level.

Sonde data shows a significant strengthening of the temperature inversion at a mean level of 925 hPa at 24-hours and 12-hours before the passage of a coastal low at Port Elizabeth (Tables A3; A4). The average increase is about 5°C for the mean coastal low cases and 7°C for the strong cases.

The sounding data also show that the northwesterly wind at 12 hours before coastal low passage is about 25% stronger between 900 and 700hPa during strong coastal lows (Fig. 3.9). The origin of this air is from the northwest, having been warmed dynamically under relatively clear skies over the continent (on the western reaches of the interior trough), and this warm air is now further heated adiabatically as it is advected southwards from the high interior plateau over the escarpment and down

over the coastal belt. It is also the 24-hour period during which the flow at 850 hPa and 700 hPa has both aligned from the northwest, with the least shear apparent (Figs. 4.13; 5.4) allowing for the possibility of downwards momentum transfer to take place.

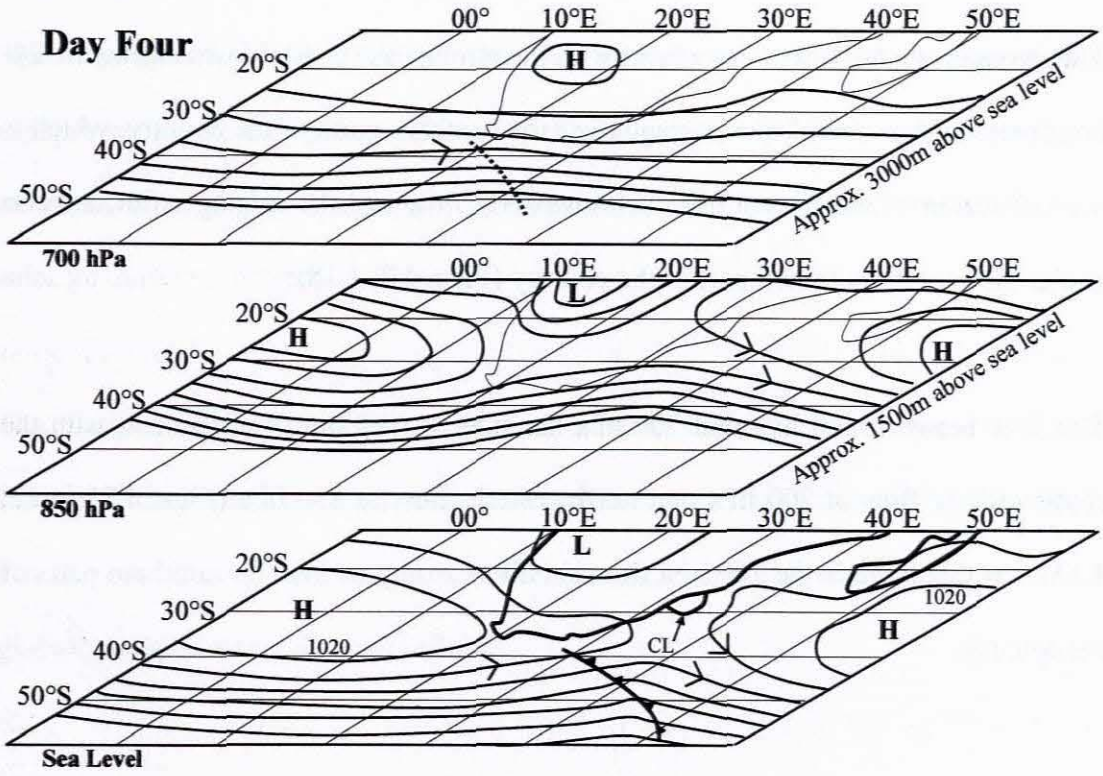

Fig. 5.5 Schematic presentation of day 4 for the strong case coastal lows at sea level, 850 hPa and 700 hPa showing the isobars and contours in the conventional manner. The positions of the trough at 700 hPa, the front, and the coastal low at sea level are indicated roughly.

Day 4

The AOA starts to ridge over the southern parts of the land, and the IOA has weakened and moved significantly further eastwards in the case of the strong case coastal lows (Fig. 5.5). The forcing function in the case of the strong coastal lows is already in the process of dissipating (Fig. 4.11), leading to the earlier decay of the strong coastal lows on the northern parts of the east coast.

The strong case coastal low is now located at 28°S on the east coast and the mean case low is situated at 31°S (Figs. 4.20; 5.5). The propagation speed for the strong cases is 13.5 $m.s^{-1}$ between Port Elizabeth and Durban, considerably faster than that of the mean case coastal lows at 10.5 $m.s^{-1}$.

The stronger westerly flow associated with the strong case coastal lows during the 24-hour period after coastal low passage over the southern parts of the country, which is a combination of the coastal lows southwesterly flow and the ridging AOA, advects cooler air over the southern part of the country (Figs. 4.7; 4.18).

The flow between 850 hPa and 700 hPa has now moved out of alignment, with the southwesterly flow at 700 hPa and northwesterly flow at 850 hPa (Figs. 4.11; 4.12; 4.13). At this latitude the 700 hPa flow is half as strong as over the southern parts of the country.

Day 5

The synoptic picture returns to that of day 1, where the Atlantic Ocean Anticyclone (AOA) has ridged eastwards, south of the land, with the remainder of the frontal system off to the southeast of the land (Figs. 5.2). The next approaching Rossby wave is again visible at about 5°W. The subtropical high-pressure belt again dominates the region between 20° and 40° S.

5.4 A numerical model case study of a strong coastal low on the 14th of November 2003

5.4.1 Introduction

The input files for the 2003 SON season, as used for operational forecasting model runs, were saved and used to find a classic strong coastal low case. From the 3 strongest cases during this season, the coastal low of the 14th November 2003 was selected as the most representative.

The Eta workstation mesoscale model was used for the study, in the same way as a forecast office might use it. The attributes of the model are presented in Chapter 2. For the case study, winds are presented in knots in the conventional form as used globally in operational forecast offices.

5.4.2 Case study

The coastal low passed Port Elizabeth at 07:00 SAST (05:00Z) with the backing of the surface wind to the southwest, after having been light and varying between westerly and northerly from midnight onwards. The wind gusted up to 35 knots within the hour at the airport between 07:00 and 08:00 local time with an average wind recorded of 24 knots.

The surface pressure minimum recorded before the coastal low passage averaged 1005 hPa between 02:00 and 07:00 hours. Actual surface temperature, after coastal low passage, averaged 22°C from 07:00 up to 13:00 hours. At 13:00 and 14:00 the average wind speeds recorded were 32 knots and the hourly observed maximum wind gust of the day, at 51 knots, occurred within the next hour.

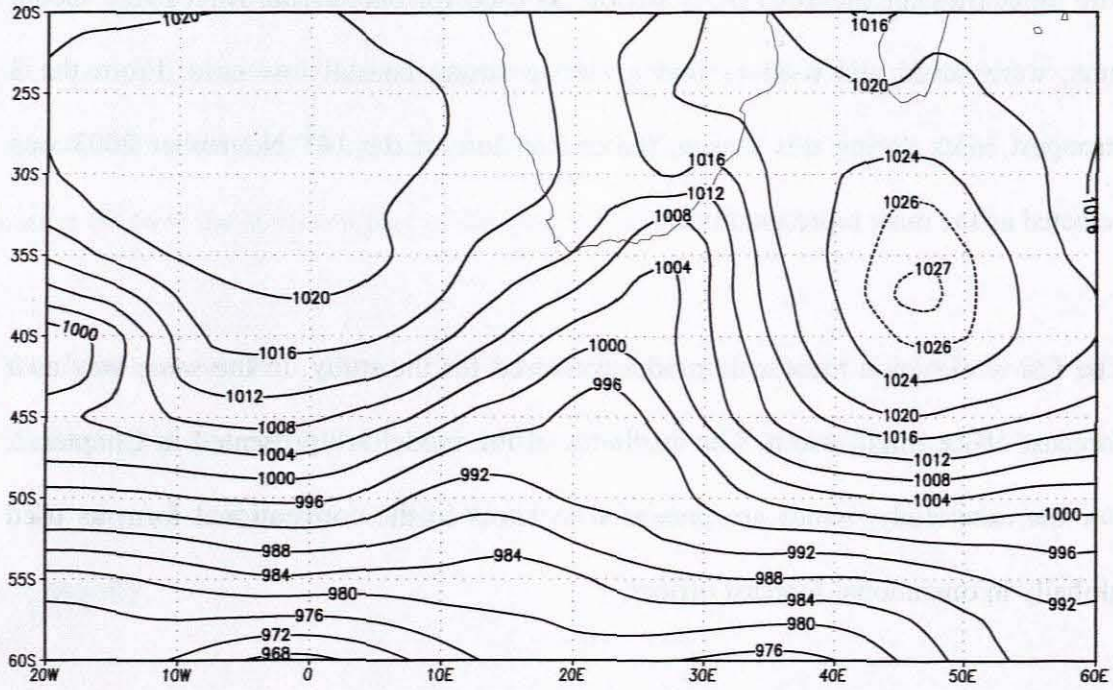

Fig. 5.6 Sea level pressure (hPa) at 06:00 UTC on the 14th November 2003 (CDC NCEP Reanalysis data). The center of the IOA is highlighted with dotted lines.

The IOA is strong on the day of coastal low passage, with a core of about 1027 hPa well to the southeast of land at 37°S and 47°E (Figs. 5.6; 5.7). The position and intensity of the IOA agrees well with the findings on strong case coastal lows in Chapter 4. The AOA is relatively weak at 1020 hPa, and is centered west of land. The frontal system is approaching land, with the front itself approximately 5° west of the land.

In the upper air, the upper ridge just east of the land is strong and extends well to the south. The approaching upper trough, associated with the frontal system, is visible at about 11°E. The implied coastal low minimum pressure is around 1006 hPa. A strong pressure gradient exists over the southeastern parts of the land, from surface level through to 500 hPa, driving the offshore flow which in turn creates and steers the coastal low eastwards along the south and southeast coasts (Figs. 5.6; 5.7).

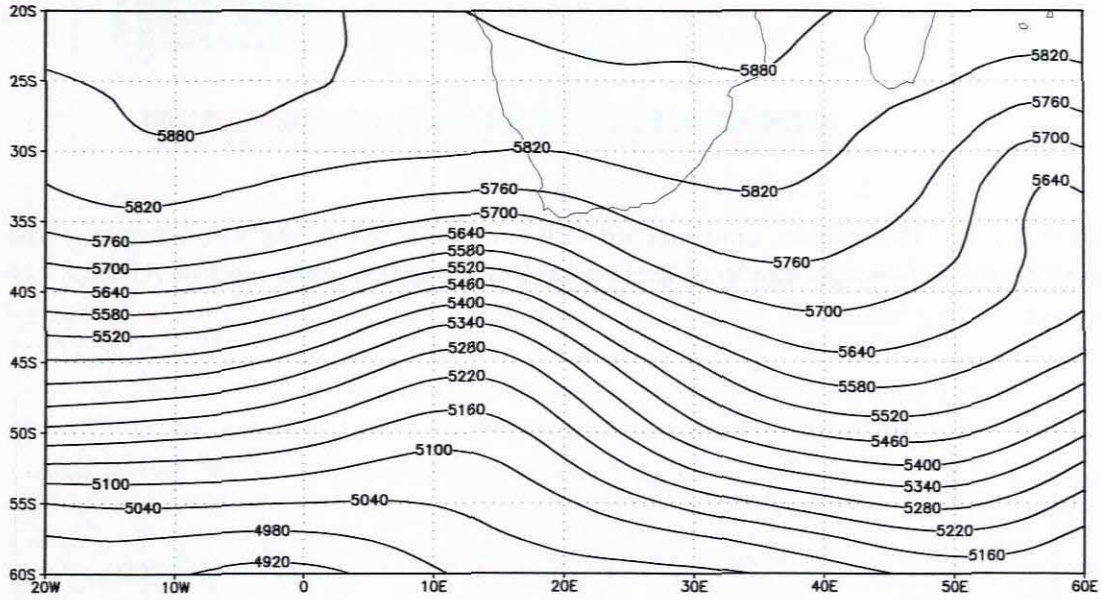

Fig. 5.7 500 hPa contours (gpm) at 06:00 UTC on the 14th November 2003 (CDC NCEP Reanalysis data).

The coastal low weakens slightly as it moves eastwards from Cape Town along the south coast and then intensifies as it moves east of 25°E (Fig. 5.8). This intensification is visible in the deepening coastal low and in the strengthening of the post-coastal low winds along the southeast coast (Figs. 5.8; 5.11; 5.12). The coastal low passes Port Elizabeth just after the tongue of warmest offshore air, at about 925 hPa in this case, and the strongest northwesterly offshore flow, between 925 and 800 hPa, passes eastwards overhead (Figs. 5.9; 5.17; 5.18).

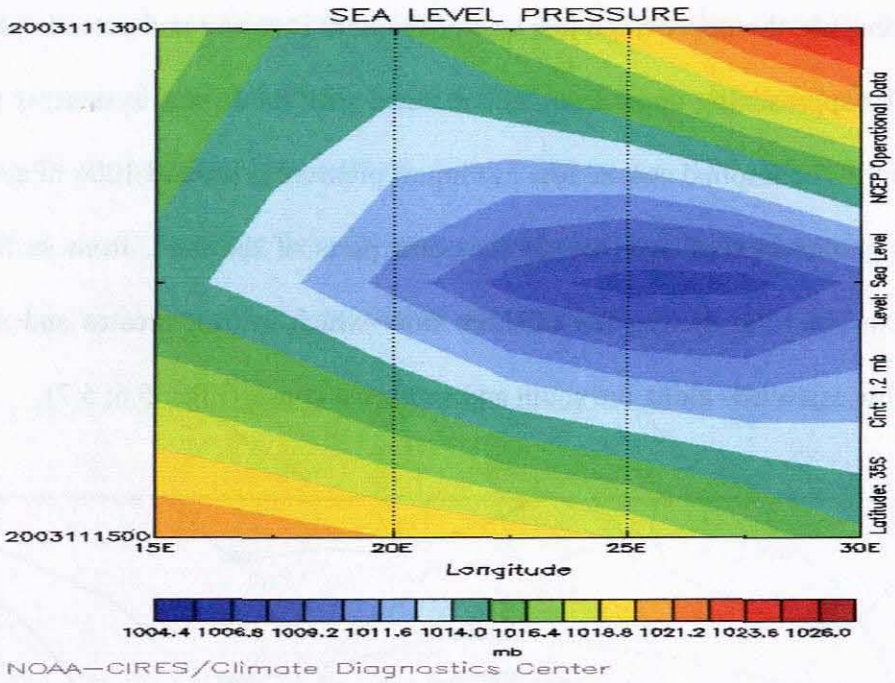

Fig. 5.8 Horizontal time section plot of sea level pressure showing the progression and intensification of the coastal low along the south coast of Africa.

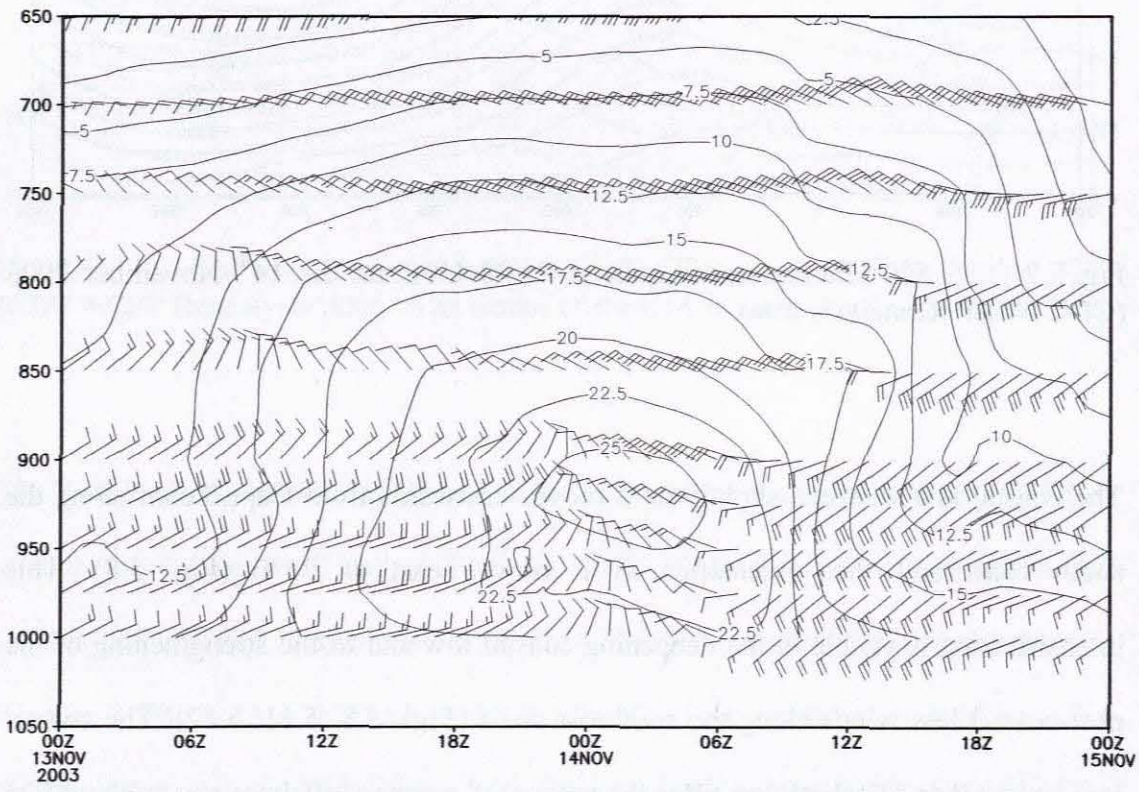

Fig. 5.9 Vertical time section plot at Port Elizabeth with wind barbs (each feather is 10 knots) and temperature (°C), from the Eta 32 km horizontal grid initialized at 00Z on the 13th. Vertical levels indicate height in hPa.

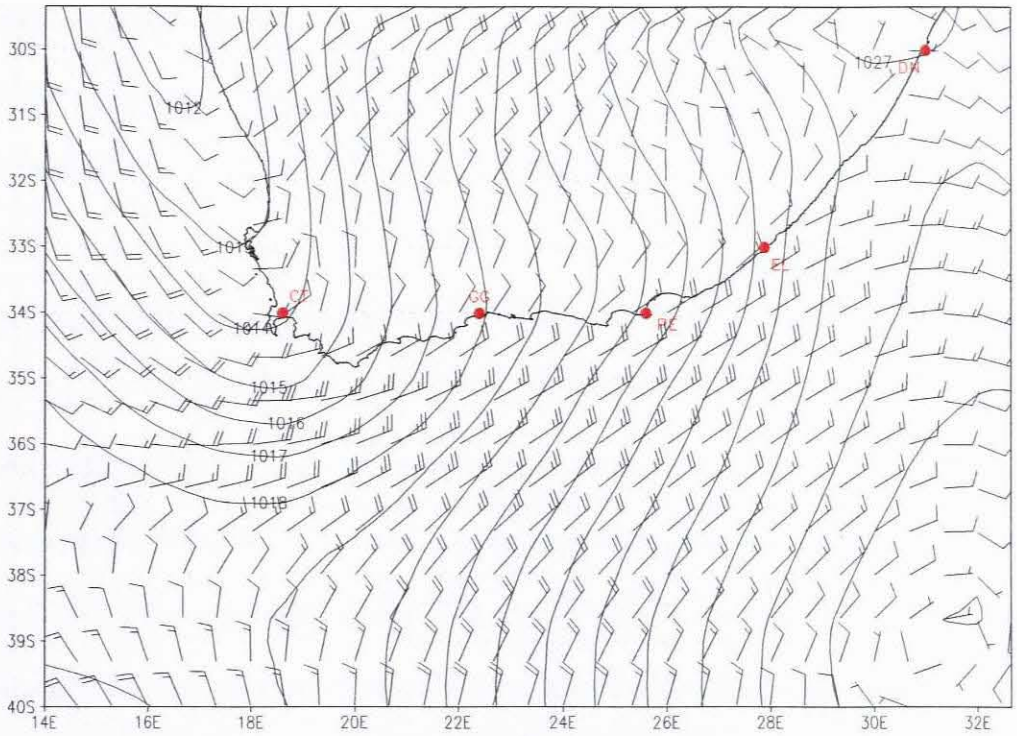

Fig. 5.10 10m wind barbs (each feather is 10 knots) and sea level pressure (hPa) for 06Z on the 13th of November 2003 from the Eta 32 km horizontal grid initialized at 00Z on the 13th.

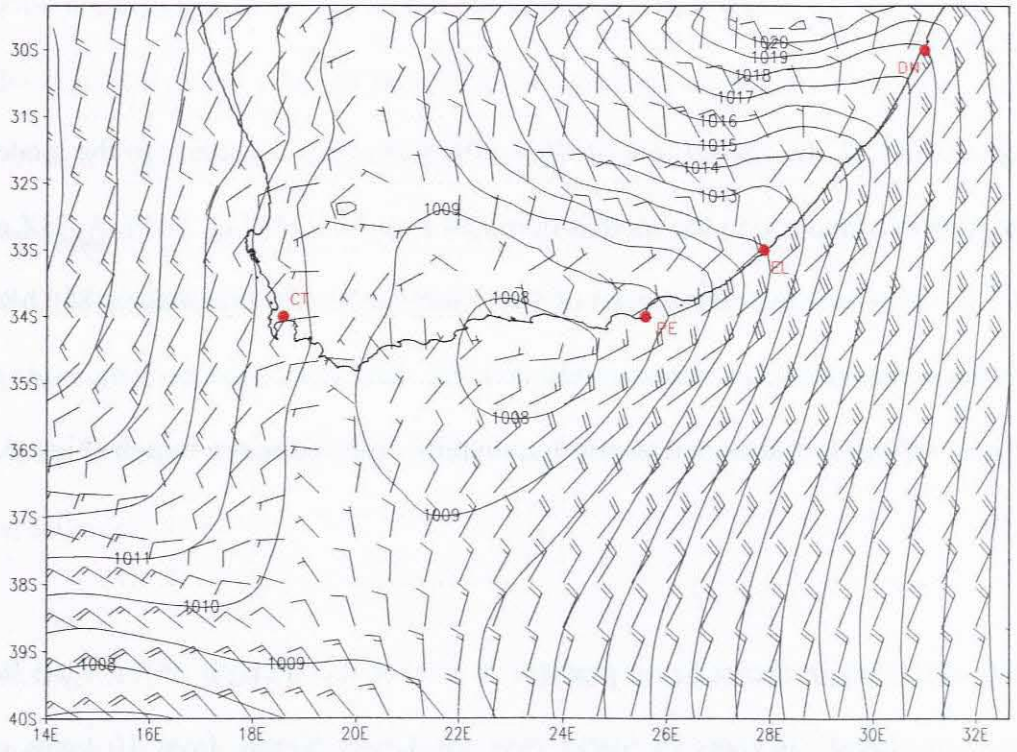

Fig. 5.11 10m wind barbs (each feather is 10 knots) and sea level pressure (hPa) for 21Z on the 13th of November 2003, from the Eta 32 km horizontal grid initialized at 00Z on the 13th.

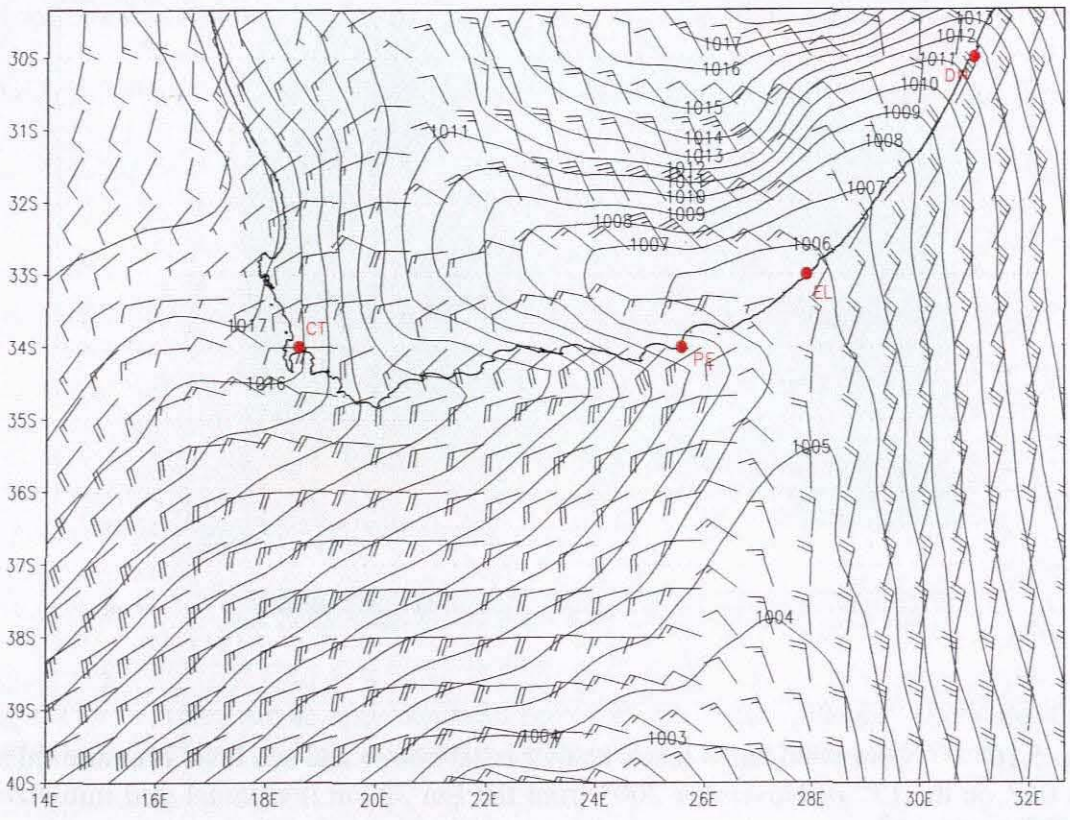

Fig. 5.12 10m wind barbs (each feather is 10 knots) and sea level pressure (hPa) for 09Z on the 14th of November 2003, from the Eta 32 km horizontal grid initialized 00Z on the 13th.

At 06Z on the 13th, the coastal low is still on the west coast according to the model, and the flow overland and to the south is dominated by the IOA (Fig. 5.10). At 21Z on the 13th, the flow over the central parts of the country at 10m (approximately 850 hPa) is from the north (Fig. 5.11). Between 00Z and 09Z, this flow on the eastwards side of the interior trough becomes northwesterly, aligning with the upper trough (Figs. 5.7 and 5.9).

By 09Z, even though the pressure gradient is weaker the strength of the wind has increased to almost 30 knots in places over the Upper Karoo, from 10 knots on average at 21Z (Figs. 5.9; 5.11; 5.12). The model shows that the pressure minima associated with the coastal low has deepened from 1012 hPa on the west coast, to

1006 hPa on the southeast coast in 24 hours (Figs. 5.10; 5.12). Post- coastal low wind speeds have strengthened from 5 knots to as high as 30 knots within the 12-hour period from Mosselbay at 21Z to Cape St. Francis at 09Z (Figs 5.11 and 5.12).

The Eta workstation model, run at a 32 km grid, gave a fairly accurate forecast of up to 30 knots southwesterly surface coastal low winds at Port Elizabeth, and the forecasted timing of the coastal low passage was only 2 hours later than the time of actual passage (Fig. 5.9). The depth of the coastal low was also forecast well, with the model showing 1006 hPa at 09Z just east of Port Alfred, and the actual surface pressure recorded at Port Elizabeth was 1005 hPa between 02:00 and 07:00 SAST (Fig. 5.12).

At Cape Town, the passage of the low at 22:00 local time on the 13th occurred 5 hours later than the model forecast time, but the wind speed forecast evaluated well. At Durban a thunderstorm occurred right during the time of passage and obfuscated the readings, but the time of coastal low passage appeared to occur at 23:00 SAST, two hours earlier than the model forecast. The wind speeds evaluated well with the model forecast, at 20 knots. The coastal low minimum pressure evaluated well with the models forecast for both Cape Town and Durban, at 1010 hPa and 1008 hPa respectively.

Running the forecast model at a 15 or 10 km horizontal grid allows for a better resolution of the mesoscale properties of the coastal low upon initialization; and according to the theory, the model should then forecast the evolution of the low better throughout the forecast period as the orography is defined at better resolution as well

(Jascourt *et al.*, 2001; COMET, 1999). The SST input files used by the model are at a relatively coarse grid of 40 km by 40 km, and the Agulhas heat fluxes and boundary layer height may not see significant improvement when model itself is run at resolutions lower than that.

The first 10 km and 15 km run were also initialized on 00Z on the 13th, in order to compare with the 32 km model run. Significantly, increasing the grid to 10 km brought about a better forecast of the intensity of the coastal low as the winds in the Port Elizabeth region show a peak of 35 knots at 11Z just to the west of the airport at Port Elizabeth (Fig. 5.15). The passage of the low takes place at 07Z (Figs. 5.13; 5.14; 5.16). The implied strong temperature gradient of 9 °C over approximately 50 km in distance from the coast to north of Addo is visible in Figure 5.15.

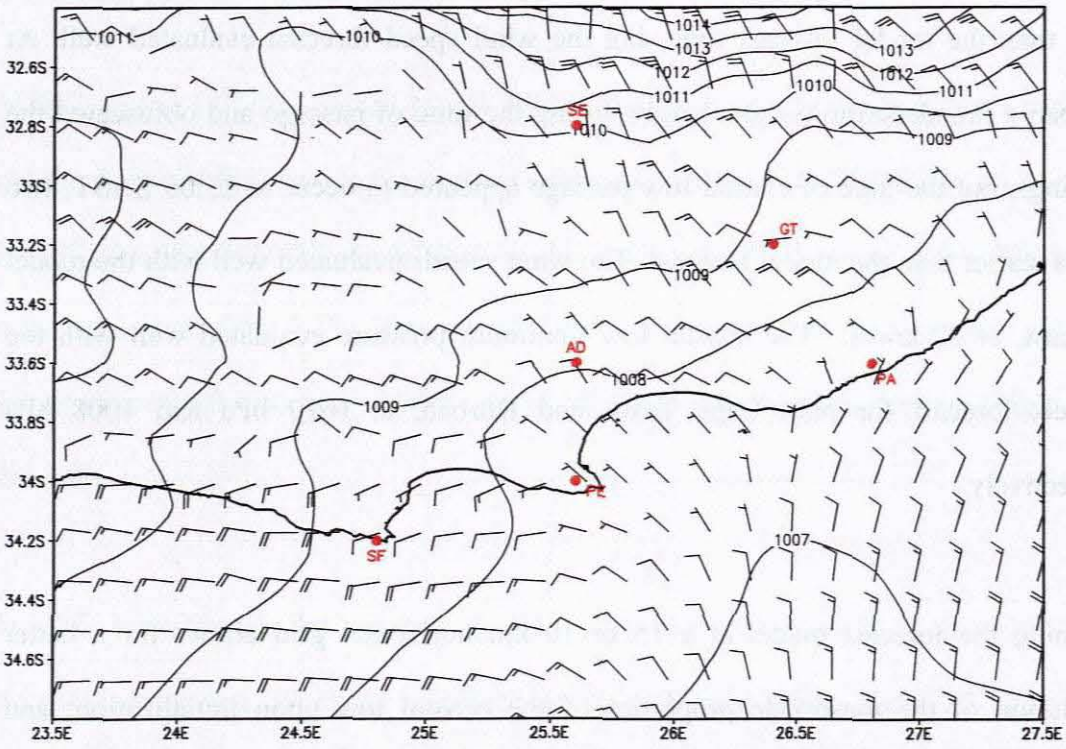

Fig. 5.13 10m wind barbs (each feather is 10 knots) and sea level pressure (hPa) for 06Z on the 14th of November 2003, from the Eta 10 km horizontal grid run initialized at 00Z on the 13th.

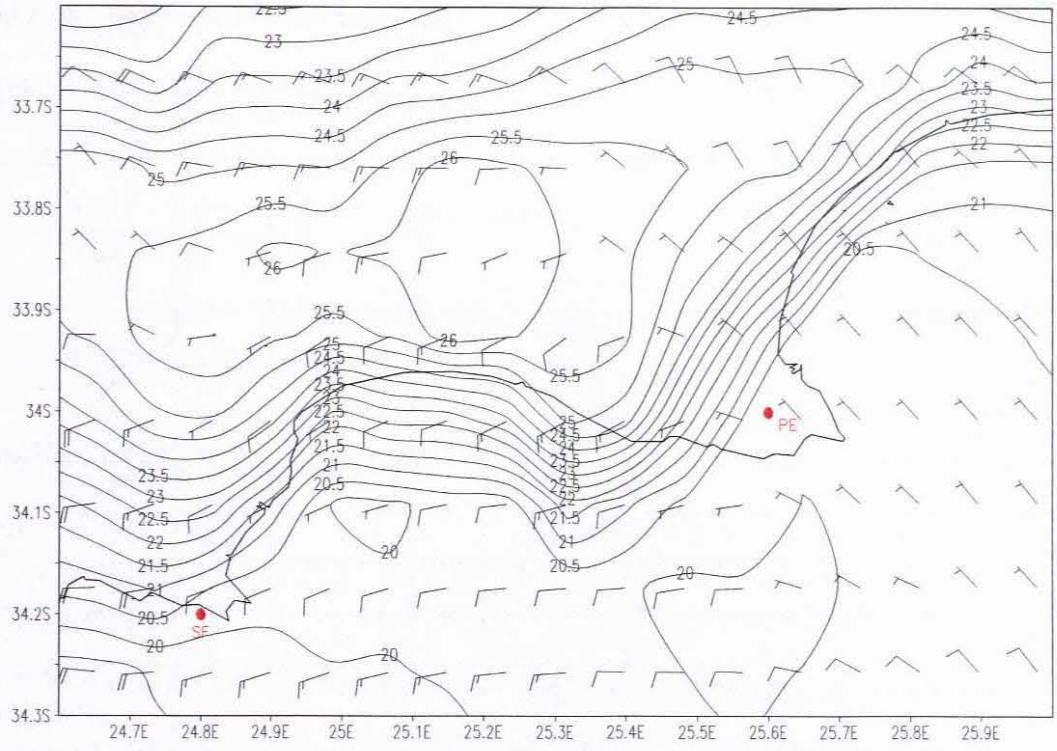

Fig. 5.14 10m wind barbs (each feather is 10 knots) and 1000 hPa temperature (°C) for 06Z on the 14th of November 2003, from the Eta 10 km horizontal grid run initialized at 00Z on the 13th.

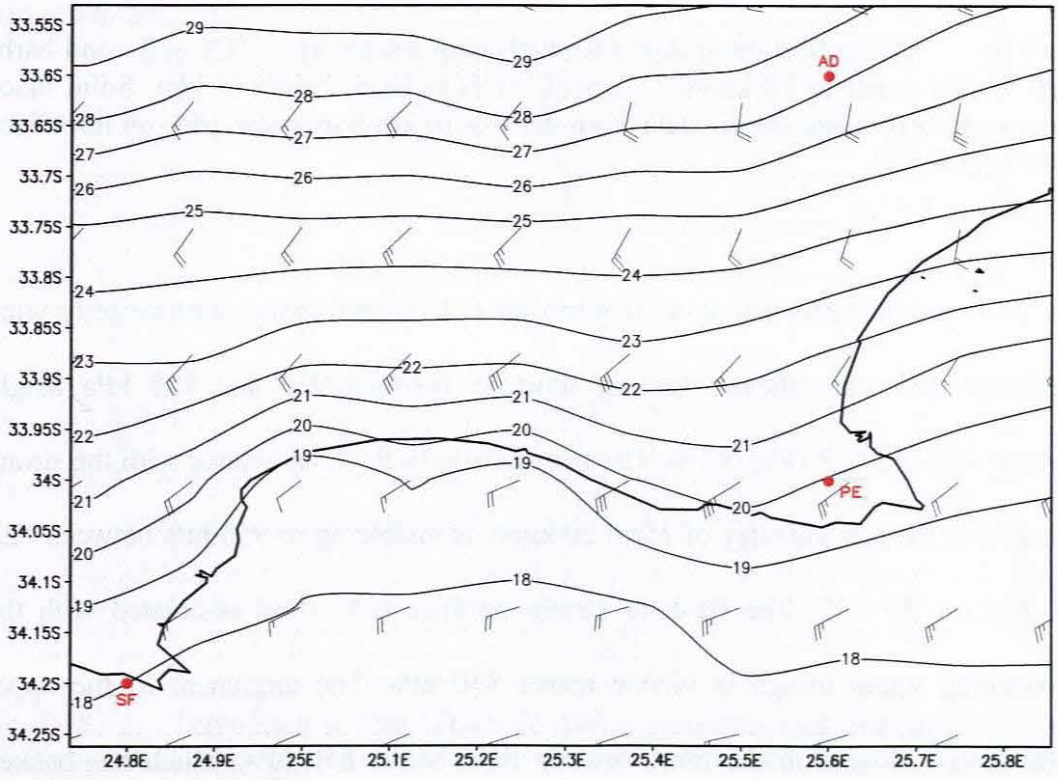

Fig. 5.15 10m wind barbs (each feather is 10 knots) and 1000 hPa temperature (°C) for 11Z on the 14th of November 2003, from the Eta 15 km horizontal grid run initialized at 00Z on the 13th.

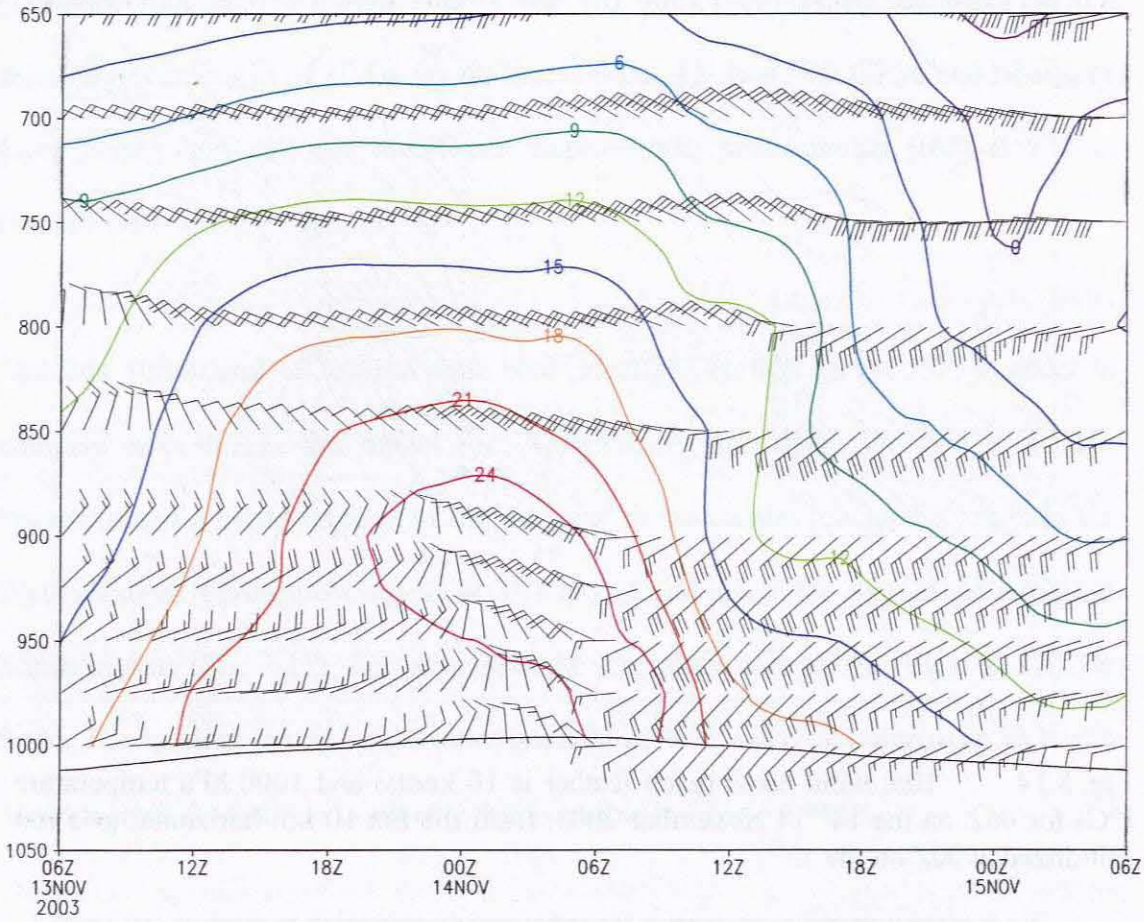

Fig. 5.16 Time Section at Port Elizabeth with temperature (°C), and wind barbs (each feather equal to 10 knots). Vertical levels indicate height in hPa. Solid black line is surface pressure (hPa). Data from the Eta 10 km horizontal grid run initialized at 06Z on the 13th.

The time section shows a tongue of warm air (24°C) and strong northwesterly wind associated with the offshore forcing function between 925 and 850 hPa height between 01Z and 07Z (Fig. 5.16). The strong easterly flow, associated with the strong IOA during the previous day of 15 to 20 knots is visible up to 950 hPa between 12Z and 23Z on the 13th. The fresh to strong northwesterly flow associated with the approaching upper trough is visible above 850 hPa. The alignment of the upper northwesterly flow with the northwesterly flow below 850 hPa, which has backed

from the northeast is clear from 12Z on the 13th, steadily advancing downwards to 925 hPa by 02Z on the 13th (Fig. 5.16).

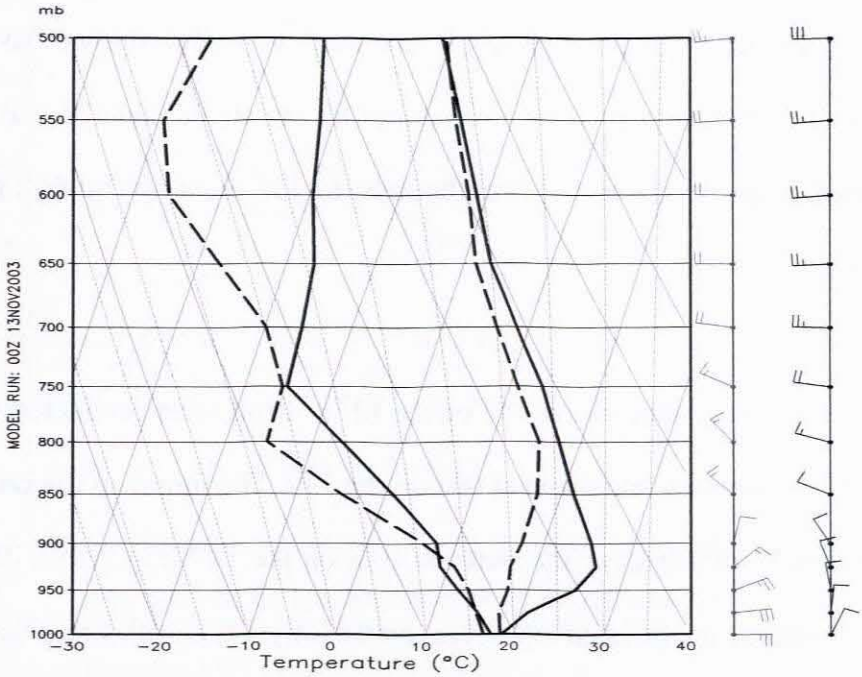

Fig. 5.17 Tephigram at Port Elizabeth with temperature and dew point (°C) and wind (each feather is 10 knots) for 00Z on the 14th (solid black lines and black barbs) and for 12Z on the 13th (dotted lines and gray barbs), from the Eta 10 km horizontal grid run initialized at 06Z on the 13th.

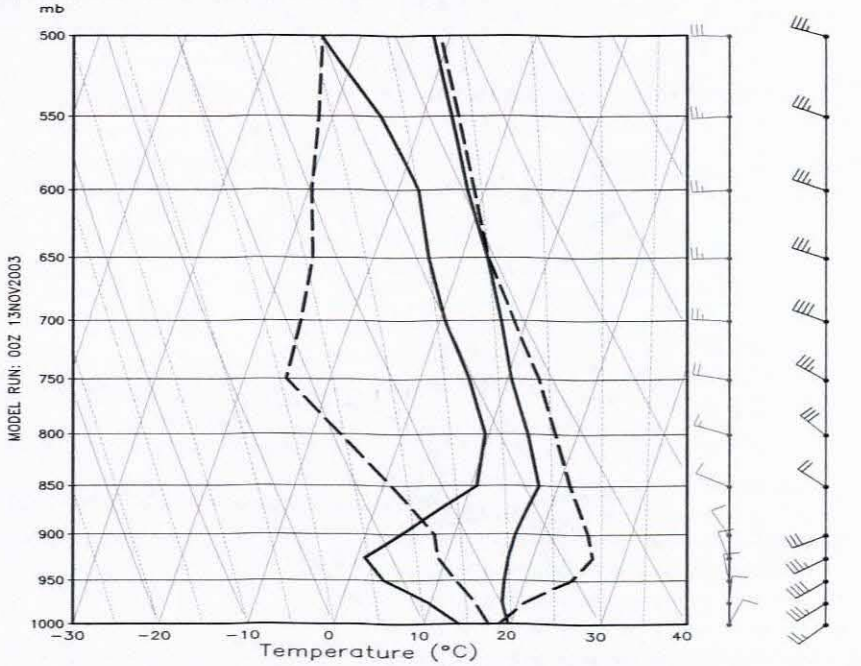

Fig. 5.18 Tephigram at Port Elizabeth with temperature and dew point (°C) and wind (each feather is 10 knots) for 12Z on the 14th (solid black lines and black barbs) and for 00Z on the 14th (dotted lines and gray barbs), from the Eta 10 km horizontal grid run initialized at 06Z on the 13th.

From the easterly low-level flow at 12Z on the 13th up to 00Z on the 14th, strong low level warming of up to 8°C is apparent at 925 hPa (Fig 5.17), caused by the previously dynamically and adiabatically heated north to northwesterly offshore flow. This tongue of heated air then cools down almost by exactly the same degree after the post-low southwesterly flow moves over the coast by 12Z on the 14th at Port Elizabeth (Fig. 5.18).

The final 10 km run is initialized at 18Z on the 13th with all other parameters the same as the 10 and 15 km runs initialized at 00z on the 13th. The timing of the coastal low passage at Port Elizabeth stays the same, at 07Z on the 14th (Fig. 5.19). There is a further improvement on the intensity of the coastal low, winds with a maximum of 40 knots forecast within 20 km westwards of the airport at 13Z (Fig. 5.20).

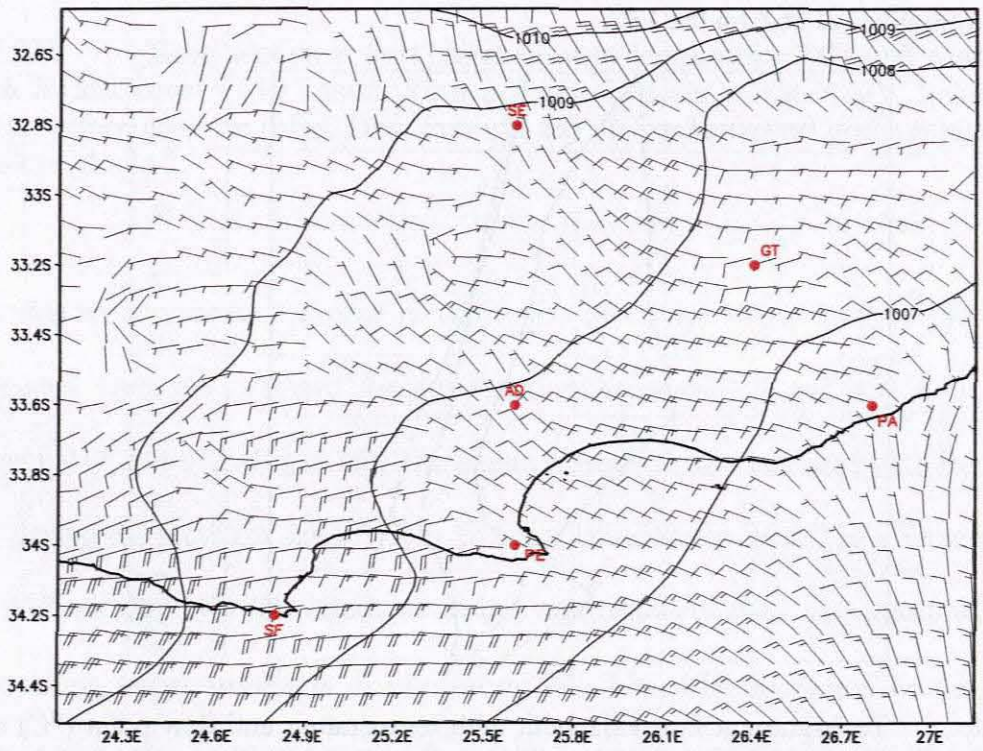

Fig. 5.19 10m wind barbs (each feather is 10 knots) and sea level pressure (hPa) at 06Z on the 14th of November 2003, from the Eta 10 km horizontal grid run initialized at 18Z on the 13th.

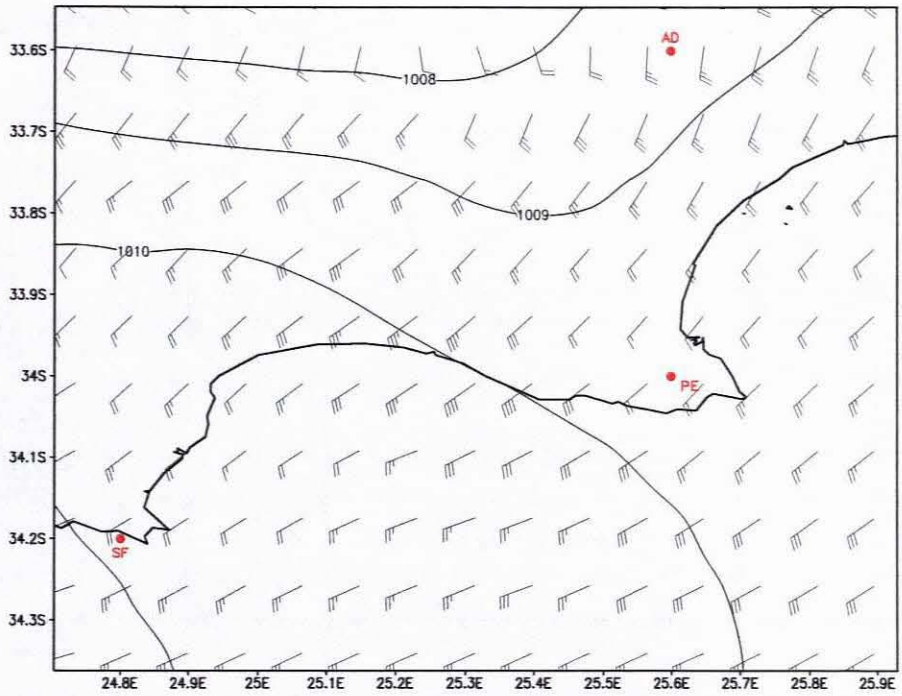

Fig. 5.20 10m wind barbs (each feather is 10 knots) and sea level pressure (hPa) at 13Z on the 14th of November 2003, from the Eta 10 km horizontal grid run initialized at 18Z on the 13th.

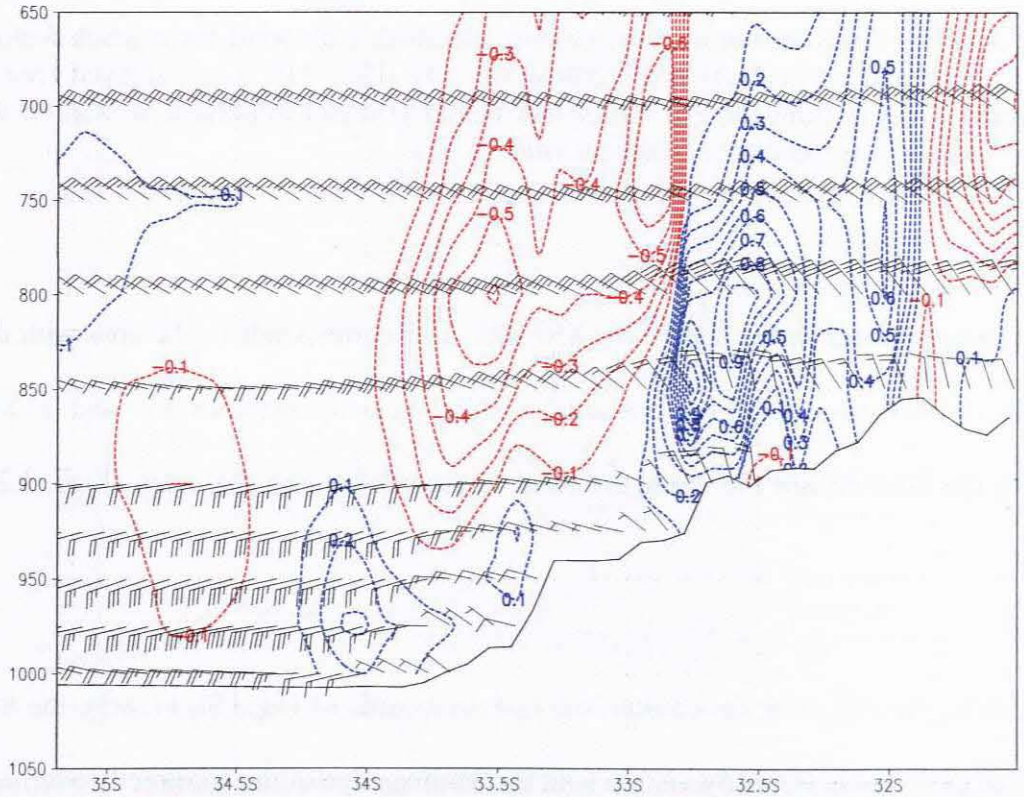

Fig. 5.21 Cross section display at 25.6°E for 06Z on the 14th of November 2003. Wind barbs (each feather is 10 knots) and vertical velocity ($Pa.s^{-1}*10^{-3}$) is displayed (red is upwards). Ground level is approximated by the surface pressure (hPa). Data is from the Eta 10 km horizontal grid run initialized at 18Z on the 13th.

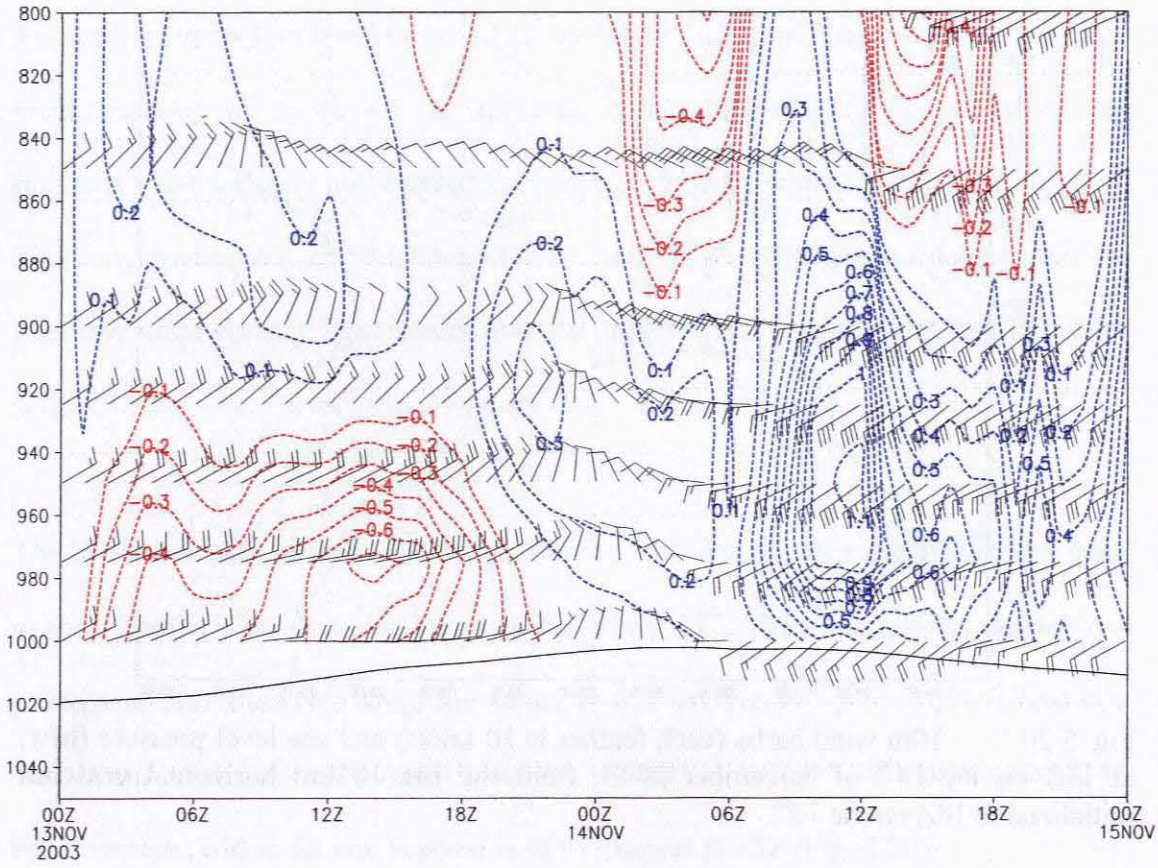

Fig. 5.22 Time section display for Port Elizabeth with wind barbs (each feather is 10 knots) and vertical velocity vertical velocity ($Pa.s^{-1}*10^{-3}$) is displayed (red is upwards). Data is from the Eta 10 km horizontal grid run initialized at 00Z on the 13th. The solid line indicates surface pressure in hPa.

The strongest wind shear, just below 850 hPa, also corresponds to the area with the region of maximum negative (upwards) vertical velocity between 33° and 33.8°S during the hour before the strongest wind is recorded along the coast (Figs. 5.21; 5.22).

At 03Z on the 14th, with the coastal low just westwards of Cape St. Francis, the low level jet of 40 knots is clearly visible with the leading edge of the jet directly overhead at Cape St. Francis and extending backwards to 32°S (Fig. 5.23). The increase in 700 hPa wind speed is also visible overhead and to the west of the jet from 20 to 25 knots.

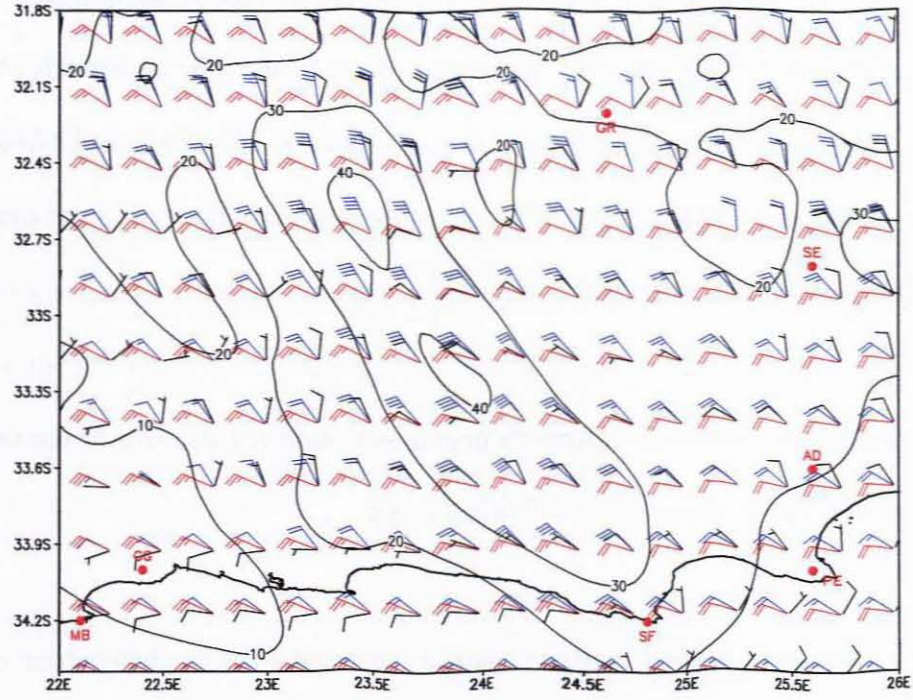

Fig. 5.23 Wind at 10m (black), 850 hPa (blue) and 700 hPa (red) in knots with the 10 knot isotachs at 850 hPa. This is at 03Z on the 14th from the Eta 10 km horizontal grid run initialized at 18Z on the 13th. Each full feather is 10 knots.

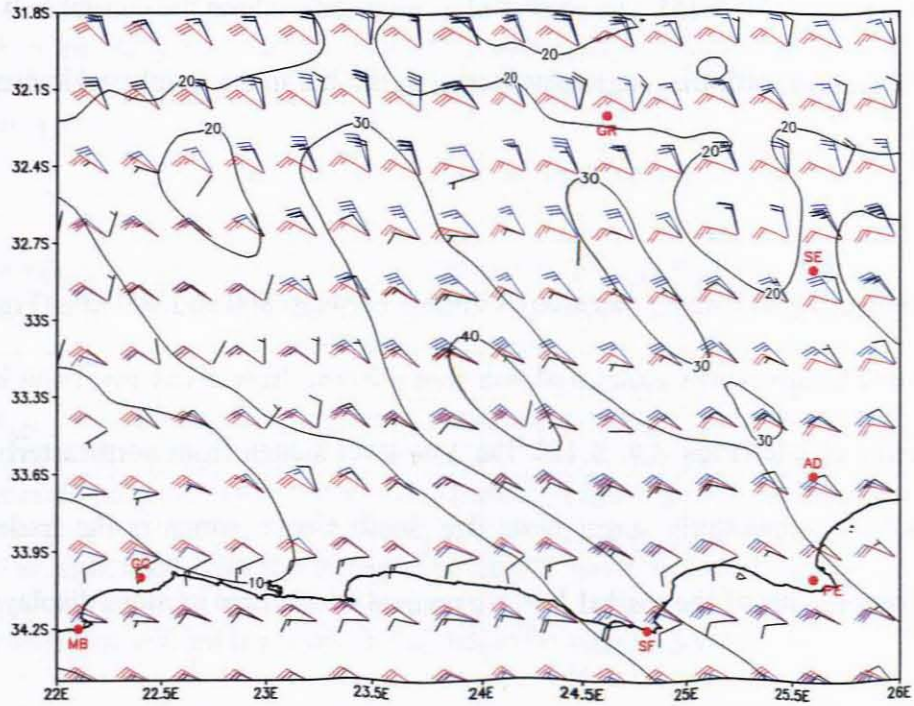

Fig. 5.24 Wind at 10m (black), 850 hPa (blue) and 700 hPa (red) in knots with the 10 knot isotachs at 850 hPa. This is at 06Z on the 14th from the Eta 10 km horizontal grid run initialized at 18Z on the 13th. Each full feather is 10 knots.

By 06Z on the 14th, the low level jet at 850 hPa has moved eastwards with its eastern edge overhead at Port Elizabeth, and the coastal low is visible just westwards of Port Elizabeth, underneath the jet. The increase in wind speed at 700 hPa from 20 knots on the eastern side of the 850 hPa jet to 30 knots on the western side is apparent over the coastal belt region (Fig. 5.24).

The numerical model simulation supports previously accepted theories of the coastal low as a trapped phenomenon in the following ways.

Firstly, it a mesoscale system, trapped against the coastal orographic barrier in the horizontal (Fig. 5.21) and against the inversion in the horizontal (Figs. 5.17, 5.18), decaying in intensity away from the coast (implied by the surface wind maximum speeds on Figures 5.14, 5.15). The system also propagates along the coastal belt in an eastwards direction, with the orographic barrier to the left in the Southern Hemisphere (Fig. 5.8).

The offshore flow (the forcing function) is visible between 800 and 900 hPa (Fig. 5.9) and the higher temperatures associated with that offshore flow above inversion height is also clearly visible (Figs. 5.9, 5.16). The low-level switch from northeasterly to a strong, cooler southwesterly surge along the South Coast, which is the trademark sensible characteristic of the coastal low, is apparent on the time sections displays.

The upper trough, associated with the following frontal system at 500 hPa, is placed around 10° westwards of the position of the coastal low (Fig. 5.7), showing that there is no direct link between the upper trough itself and the coastal low system.

5.5 Mathematical framework

Given the hypothesis that a warmer and stronger forcing function to the coastal low (which is the offshore flow originating over the interior plateau) leads to more intense coastal lows, with stronger than normal southwesterly surges along the south coast of Africa, the following basic mathematical framework is used.

From the equation of state;

$$\rho = \frac{p}{RT} \qquad (1)$$

where ρ is the density of dry air, p is pressure, R is the gas constant for dry air (287 J $kg^{-1}K^{-1}$) and T is temperature (K); it follows that the higher the temperature of a parcel of air, the lower will be its density and consequently the greater its buoyancy (and vice versa).

The temperature of the offshore flow is shown by the findings of this study to be warmer in the case of the more intense coastal lows than that which occurs during 'average' coastal lows, having being heated dynamically over the interior and then also adiabatically on descent from the interior plateau. This causes the lower pressure, which is associated with the strong case coastal lows, to lead to a stronger pressure gradient response from the low-level winds in the marine layer.

From the conservation of absolute vorticity (given that the latitude Φ does not change);

$$\frac{\zeta + f}{D} = \text{constant} \qquad (2)$$

where **D** is the depth of the system, ζ is the relative vorticity, **f** is the earths vorticity (Coriolis parameter) and the term $\zeta + f$ is the absolute vorticity; it follows that when air descends on the lee side of a mountain, **D** increases, ζ increases and the flow acquires cyclonic vorticity and curvature, facilitating the formation of a lee-side trough.

Using the formula for the Coriolis parameter;

$$f = 2\omega \sin\Phi \qquad (3)$$

where ω is the angular velocity of the earth's rotation, it follows that when the latitude Φ increases, the Coriolis parameter **f** also increases, adding a further amount of vorticity to the absolute vorticity term within **(2).**

This is relevant to the coastal lows moving along the south coast of South Africa as this coast is situated at around 34°S, almost 10° further south than the west coast of Namibia where coastal lows are generally first spawned.

From the usual form of the equation of continuity;

$$\frac{\partial u}{\partial x} + \frac{\partial v}{\partial y} + \frac{\partial w}{\partial z} = 0 \qquad (4)$$

local changes in the horizontal **u** and **v** components of the wind in the **x** and **y** directions, must be balanced by an equal and opposite local change in the vertical **w** component in the **z** direction. Or, in other words, horizontal divergence such as the strong offshore flow moving overhead over the coast, is accompanied by vertical

stretching and positive (upward) vertical velocities coupled with horizontal convergence at surface level. In order for continuity to be preserved, the stronger the upper divergence flow, the stronger the convergence will be at surface level.

These processes show why a stronger coastal low should occur, if the offshore flow is stronger and warmer than normal.

The coastal low then propagates at the theoretical Kelvin wave phase speed;

$$c = (g'H)^{0.5} \quad (5)$$

where **g'** is related to the inversion strength and **H** is the height of the inversion (Reason and Jury, 1990). An important consideration is that the inversion strength should weaken as the coastal low moves eastwards, due to the higher sea surface temperatures caused by the warm current, thereby theoretically slowing the propagation speed of the coastal low as **g'** decreases.

5.6 Summary

A positive relationship is found between warmer than normal pre-coastal low passage periods and the strong coastal low surface wind surge using the maximum temperatures recorded during the period around midday.

An idealized model is presented which shows the synoptic progression and mesoscale evolution of a strong case coastal low along the coastal belt as a daily sequence of events, highlighting the significant data results and findings from Chapter 4.

The improvement in numerical model forecast ability, by using a smaller resolution horizontal grid mesoscale model, is clearly shown in the strong coastal low case study of 14th November 2003. The forecasted 30 knot southwesterly wind in the Port Elizabeth region becomes 35 knots as the resolution is increased from a 32 km grid to a 10 km grid for a 30-hour forecast. Shortening the forecast period leading up to coastal low passage to a 12-hour forecast improves the model wind forecast further to 40 knots.

The previous finding from Chapter 4, that a strong IOA with its center well to the south is a good indicator of strong case coastal lows on the synoptic scale, and a stronger and warmer than normal offshore flow off the interior plateau corresponds with the passage of the strong coastal low is confirmed by the case study.

The intensification of the coastal low, as it moves eastwards along the south coast, is highlighted by the case study. It is likely that the coastal low intensity increases are due to marine boundary layer characteristics, in addition to changes in offshore flow and escarpment profiles. The marine boundary conditions change significantly along the east coast, where the Agulhas Current sometimes comes within 10 km of the coast.

The alignment of the warm tongue of northwesterly flow on the eastwards side of the interior trough at around 850 hPa, during the period just before coastal low passage, is highlighted by the case study. The stronger northwesterly flow associated with the leading side of the approaching upper trough above that at 700 hPa is also shown.

The position of the coastal low below the tongue of warm offshore flow is highlighted by the case study. The eastwards movement of the offshore low level jet at 850 hPa and the corresponding movement of the coastal low underneath the jet is shown.

The model evaluation agreed well with actual observations on the wind speeds and the pressure minimums of the low from Cape Town to Durban, but the timing of the passage of the low was less well resolved at Cape Town. The manned coastal observing stations of the South African Weather Service are primarily sited at the airfields and, therefore, are not always representative of the marine environment itself. Local effects, such as the varied orography in the Cape Town Weather Office region play a big role in the representivity of the observations. The propagation of the coastal low along the east coast was handled well by the model, with the actual passage timings two hours earlier than the model forecast for both Port Elizabeth and Durban.

CHAPTER 6

Summary and Conclusions

6.1 Summary

6.1.1 General overview

Coastal lows are a dominant weather feature along the South African coast. They are shallow, mesoscale systems that are characterized by a marked change in weather from warm, dry and light wind offshore conditions to cooler, moist and breezy onshore weather. At times, this change can be rapid with a jump to strong southwesterly winds along the southeast and east coasts. The coastal low is termed a "buster" when the wind increases to more than 10 $m.s^{-1}$ (Hunter, 1987).

In order to try to improve the ability to forecast strong coastal lows, a climate profile was built of an average or mean coastal low, using 642 coastal lows out of a 10-year population of station data in Chapter 3. Comparison was made against the top 5% of all the coastal lows using the mean of the 8-hour post coastal low passage wind speed as grading criteria for coastal low intensity.

This general profile was then further refined into a climate study of station data for the season when strong coastal lows occurred more frequently, the September, October and November (SON) season. The SON season also contains the strongest average hourly surface wind speeds at Port Elizabeth. For comparative purposes, a

10% sample was taken from the middle and from the top of the population. Upper air and surface station data were used along the coast from Cape Town to Durban.

The temporal and spatial evolution of the mean of all 160 coastal lows was compared against the top 10% sample of coastal lows in the SON season using various composite analysis techniques with NCEP reanalysis data in Chapter 4, in order to find the characteristics which set the strong coastal lows apart from the mean.

The operational forecasters notion that higher than normal pre-coastal low maximum temperatures go hand-in-hand with intense coastal lows was tested in Chapter 5, followed by a summary of a conceptual model of a strong coastal low. The value of using a numerical forecast model with a small horizontal resolution on a mesoscale system like the coastal low was demonstrated in the last section of this chapter by doing a case study of a strong coastal low in the 2003 SON season using the Workstation Eta mesoscale model.

6.1.2 Summary of most significant findings

A coastal low passes Port Elizabeth every 5.7 days on average in the period 1987 – 1996. Coastal lows occur more frequently from December to February; however, the strongest coastal lows, in terms of wind surge, occur more often during the September to November (SON) season. Strong coastal lows during the SON season propagate faster along the coast than the mean, at a period of 4 – 5 days.

The easterly surface (10 m) wind preceding coastal low passage at Port Elizabeth is 2 – 3 $m.s^{-1}$ stronger during strong coastal low events. The core minimum surface pressure associated with the top 5% of coastal lows is almost 4 hPa deeper than that of the average coastal low. The surface pressure at 24 hours before coastal low passage at Port Elizabeth, associated with the IOA, and at about 40 hours after coastal low passage, associated with the ridging AOA, are 1 and 2 hPa stronger respectively than that of the average coastal low. The peak southwesterly wind after coastal low passage is about 6 $m.s^{-1}$ stronger during strong coastal low events with the wind also gusting about 10 $m.s^{-1}$ higher at 26.8 $m.s^{-1}$.

For the strong coastal low cases the northwesterly winds above 925 hPa are already stronger at Cape Town on coastal low passage there, and this becomes even stronger throughout the column up to 700 hPa by the time the coastal lows reaches Port Elizabeth.

While the surface wind backs quickly from easterly to northwesterly during the 6 hours prior to coastal low passage for the average coastal lows, a more gradual change over 12 hours takes place during strong coastal low events.

The strong coastal lows propagate 28% faster than the mean cases from Cape Town to Durban with the top 10% of SON coastal lows moving along the coast 3 $m.s^{-1}$ faster than the mean 10% at 10.7 $m.s^{-1}$. The fastest propagation speed takes place between Port Elizabeth and East London, with 18.5 $m.s^{-1}$ for the strong cases, almost 8 $m.s^{-1}$ faster than the mean 10%. The slowest propagation speeds are recorded from Cape Town and George. The coastal segments from George to Port Elizabeth, and again

from East London to Durban, produces similar propagation speeds for the strong and for the mean cases respectively.

The observations show a good chance (50% for this sample) of one strong coastal low being followed by another within the same month; suggesting that the Southern hemisphere circumpolar Rossby wave trains maintain a configuration for some time.

Using composite analysis of the NCEP reanalysis data, it was found that the temperature in the region of the forcing function's near surface flow over the interior is already warmer two days before the coastal low reaches Port Elizabeth during strong coastal low events, and that the wind strength of the forcing function is also higher during strong coastal low events. The composite analysis also highlights the significantly stronger and more southeastwards placement of the Indian Ocean Anticyclone during strong coastal low events.

A positive correlation is found between warmer than normal pre-coastal low conditions at surface level over the southeastern interior and intense coastal lows. The relationship between 700 hPa and 850 hPa winds is not clear, with very weak positive correlation, likely due to the fact that the data used is the daily averaged NCEP coarse resolution reanalysis data, which cannot define the mesoscale and short-lived significant changes in wind speed at 700 hPa and 850 hPa.

A numerical model simulation case study is presented to highlight the improvement brought about in forecast ability by using a low-resolution mesoscale numerical forecast model. The forecast model shows an improved forecast of the strength of the

coastal low as the resolution is increased, and propagation of the coastal low along the coast to Port Elizabeth and further onwards through to Durban is forecast well. The northwesterly offshore jet at 850 hPa is clearly shown, with the coastal low apparent just below the point where the jet crossed over the coast. The increase in the 700 hPa wind speed and the alignment in direction of this wind with the 850 hPa jet is highlighted over the South Coast.

6.2 Conclusions and discussion

Taking into consideration the temporal and spatial limitations of the available data used in the study, as mentioned in the methods section in Chapter 2, the following conclusions can be drawn.

The steeper the pressure gradient, or the stronger the flow, the larger the forcing function and the resulting disturbance (de Wet, 1983). The mid-level offshore flow, at around 850 hPa and just below that, is the forcing function for the coastal low. The composite study shows the link between a stronger forcing function and intense coastal lows.

The stronger Indian Ocean anticyclone on strong coastal low days combined with the closer proximity of the approaching frontal system and the position and depth of the interior thermal trough over the high interior plateau creates a stronger than normal pre-coastal low passage offshore northwesterly flow overhead over the South and Southeastern Coasts of Southern Africa. The stronger offshore flow causes a stronger

than normal surface coastal convergence response underneath the region of the strongest offshore jet axis.

The offshore flow is warmer during strong coastal low events, having been dynamically warmed over the interior plateau by up to 2 days before coastal low passage, leading to a reduced pressure along the coast due to buoyancy advection as this flow moves out over the coast. This flow is also warmed further adiabatically upon descent down the escarpment to the coast. The response from the winds within the marine layer around the low pressure is a stronger southwesterly wind surge on coastal low passage due to the tighter pressure gradient.

This influence by the mainly synoptic-scale offshore flow is possibly also augmented by the alignment of the stronger upper air northwesterly flow at about 700 hPa (caused by the convergence between the approaching upper wave and the strong upper ridge) and the mid-level northwesterly offshore flow at about 850 hPa associated with the interior surface trough. This alignment allows for downwards momentum transfer to take place into the mid-level flow, which should result in an even stronger forcing function.

This notion, that the mid- and high-level winds align in direction, allowing for downwards momentum transfer, would also explain why the coastal low does not become as strong along the west coast, as the upper northwesterly flow opposes the mid-level easterly offshore flow which creates and propagates the coastal low in that region. So instead of the offshore flow being enhanced by downward momentum

transfer, this flow could only be weakened (or have little effect at all) along the west coast.

Another factor which plays a role in the stronger coastal low events, is the fact that the Coriolis parameter is stronger along the south coast (Port Elizabeth is at about the same latitude as Cape Town at about 34°S) than along the west and east coasts and it is the Coriolis force which traps the coastal low against the vertical mountain barrier. If the earth's vorticity is increased, then the absolute vorticity term is also increased, leading to stronger cyclonic vorticity and curvature.

The warmer offshore flow during strong coastal low events would lead to a more pronounced inversion as the flow moves over the marine layer, and this would increase the propagation speed as the phase speed of the coastal low is dependent on the height and the strength of the inversion. The IOA is stronger during strong case coastal lows, which causes the pre- coastal low easterly flow to be stronger, with the effect that the marine boundary layer inversion height is lifted above the norm before the arrival of the coastal low.

This study concentrates on the coastal low intensity response to the synoptic scale offshore flow and does not take into considerations other effects which also play roles in the propagation and characteristics of the coastal low such as variations in the marine layer, changes in sea surface temperatures or local diurnal flow variations such as land and sea breezes.

The advantage of using a mesoscale forecast model for a small-scale system like the coastal low is highlighted by the case study in Chapter 5. The position of the coastal low is generally forecast well by the global scale models along the south coast because they forecast the eastwards progression of the synoptic scale systems along the south coast well, and it is the flow associated with the synoptic scale systems which steers the coastal low.

The intensity of the coastal low itself is not forecast as well by the global scale models, mainly because the large grid resolution of these models cannot resolve features that are smaller than four grid lengths; these smaller features will be 'aliased', meaning that they will be misinterpreted as having longer wavelength than they actually do.

This can be improved by increasing the horizontal resolution to the point where the features' smallest orientation size spans at least 8 to 10 grid points (Jascourt *et al.*, 2001; COMET, 1999). With the coastal low trapped to within a Rossby radius (approximately 100 and 200 km) of the escarpment or blocking mountains (Anh and Gill, 1981; Reason and Jury, 1990) a horizontal grid resolution of 10 to 15 km would be necessary to resolve, and to forecast coastal lows well over the 1 to 2 day period.

6.3 Recommendations for operational practice

It is recommended that the South African Weather Service reduce the horizontal resolution of their operational forecast model to a 10 - 15 km horizontal grid,

depending on whether it is cost-effective relative to the impacts. This will improve the shorter-term, one to two days lead time, coastal low forecasts and would give the operational forecasters, who are tasked with forecasts for the south and southeastern coastline, a better tool with which to give timely warning of strong coastal lows. It is also suggested that the SST data ingested by the model is of vital importance to marine boundary layer characteristics, and the lowest possible resolution of SST data should be used.

In personal communication with Dr. Warren Tennant of the SAWS, he stated that they are planning to develop the UK Meteorological Office UM system as the new operational forecast model and to start using this model at a 12 km horizontal grid by mid-2006. This promises to have an exciting effect on forecasting coastal lows and for other mesoscale systems.

A concise summary of this study's findings is provided in Appendix B for operational forecasters' use.

6.4 Further research

Comparison of the SON findings could be done for other seasons to confirm that the arguments in this study hold true for strong coastal lows throughout the year.

An expanded version of this study along the South African coast would be of value if the more recent 5-minute data is used from the SAWS coastal AWS's because these

data would be more representative of the marine environment. The relatively new Meteosat 8 also provides an opportunity to do daily SST analysis, providing cloud conditions are not overcast.

The notion that downwards momentum transfer is a significant factor in the development of stronger coastal lows along the south and southeast coasts could be investigated in more detail. The effects of SST and other marine influences should also receive further attention, as they play a significant role in coastal low dynamics.

REFERENCES

Anh, N. N. and Gill, A. E., 1981: Generation of coastal lows by synoptic-scale waves. *Quart. J. Roy. Meteor. Soc.*, **107**; 521 – 531.

Baines, P. G., 1980: The dynamics of the southerly buster. *Aust. Meteor. Mag.*, **28**; 175 – 200.

Bosart, L. F., V. Pagnotti, and B. Lettau, 1973: Climatological aspects of Eastern United States backdoor frontal passages. *Mon. Wea. Rev.*, **101**; 627 – 635.

Carr, J. A., 1951: The East Coast "backdoor" front of May 16th – 20th, 1951. *Mon. Wea. Rev.*, **79**; 100 – 110.

Chang, C. P., Erickson, J. E. and Lau, K. M., 1979: Northeasterly cold surges and near-equatorial disturbances over the Winter MONEX area during December 1974. Part I: Synoptic aspects. *Mon Wea. Rev.*, **107**; 293 – 307.

CLW, 1984: Summary and Recommendations, *Abstracts and Summary of the coastal low workshop*. Institute of Maritime Technology, Simonstown. 56 - 62.

Colquhoun, J. R., 1981: The origin, evolution and structure of some southerly bursters. Bureau of Meteorology, *Technical Paper No.* 40.

The COMET Program, 1999: The Impact of Model Structure and Dynamics, http://meted.ucar.edu/nwp/pcul/ic2/index.htm.

The COMET Program, 2003: Coastally Trapped Wind Reversals, http://meted.ucar.edu/mesoprim/ctwr/index.htm.

de Wet, L. W., 1983: The influence of the South African orography on the development and propagation of atmospheric disturbances. First international conference on Southern Hemisphere Meteorology. *In proceedings*, pp. 367.

Dorman, C. E., 1985: Evidence of Kelvin waves in California's marine layer and related eddy generation. *Mon. Wea. Rev.*, **113**; 827 – 839.

Dorman, C. E., 1987: Possible role of gravity currents in Northern California's coastal summer wind reversals. *J. Geophys.* Res., **92**; 1497 – 1506.

Estie, K. E., 1984: Forecasting the formation and movement of coastal lows, *Abstracts and Summary of the Coastal Low Workshop*, Institute of Maritime Technology, Simonstown, 17 - 27.

Estie, K. E., 1990: The Coastal Low - a Potential Hazard to Aviators. *Proceedings Conference on Weather Radar and Flight Safety.* May 10 - 11, Taipei.

Gill, A.E, 1977: Coastally trapped waves in the atmosphere. *Quart. J. R. Met. Soc.*, **103**; 430 - 440.

Gill, A. E., 1982: *Atmosphere-Ocean Dynamics*. London: Academic Press, 662 pp.

Goschen, W. S. and E. H. Schumann, 1995: Upwelling and the occurrence of cold water around Cape Recife, Algoa Bay, South Africa. *S. Afr. J. Mar. Sci.* 16; 57 - 67.

Heydenrych, C.M., 1987: A Climatology of the coastal low in the S.W. Cape. *MSc. Thesis*, University of Cape Town.

Holland G.J. and Leslie L. M., 1986: Ducted Coastal Ridging over S.E. Australia, *Quart. J. R. Met. Soc.* (1986), 112; 731 - 748.

Hunter, I.T., 1984: Coastal lows from a synoptic point of view, *Abstracts and Summary of the Coastal Low Workshop*, Institute of Maritime Technology, Simonstown, 12 – 15.

Hunter, I.T., 1987: The weather of the Agulhas Bank and the Cape south coast. *CSIR Research Report* 634.

ICAO, 1987: Wind Shear. *Circular 186-AN/122*; 1.

Jascourt, Stephen and William Bua (UCAR/COMET), 2001: Top ten misconceptions about numerical weather prediction (NWP) models. *Numerical Weather Prediction (NWP) Professional Development Series,* http://www.cira.colostate.edu/ramm/visit/nwptop10.html.

Jury, Mark, 1984: Case studies of wind shear and temperature inversions associated with coastal lows. *Abstracts and Summary of the Coastal Low Workshop,* Institute of Maritime Technology, Simonstown, 28 – 36.

Jury, M. R., 1996: South-east Atlantic warm events: composite evolution and consequences for southern African climate. *S. Afr. Journal of Mar. Sci.*, 17; 241 – 252.

Jury, M. R., C.I. MacArthur and G. B. Brundrit, 1990: Pulsing of the Benguela upwelling region: large-scale atmospheric controls. *S. Afr. Journal of Mar. Sci.*, 9; 27 - 41.

Jury, Mark, Craig MacArthur and Chris Reason, 1990: Observations of trapped waves in the atmosphere and ocean along the coast of Southern Africa. *South African Geographical Journal* 72; 33 - 46.

Jury, M. R. and B. M. R Pathack, 1993: Composite climatic patterns associated with extreme modes of summer rainfall over Southern Africa: 1975 – 1984. *Theoretical and Applied Climatology, New York, NY,* Vol. 47, No. 3; 137 – 145.

Kalnay, E. and Coauthors, 1996: The NCEP/NCAR Reanalysis 40-year Project. *Bull. Amer. Meteor. Soc.*, 77; 437 - 471.

Levey, Kevin M. and Mark R. Jury, 1996: Composite intraseasonal oscillations of convection over southern Africa. *Journal of Climate, Boston, MA.* Vol. 9, No. 8; 1910 – 1920.

Lilly, D. K., 1981: Doppler radar observations of upslope snowstorms. *Preprints, 20th Conf. On Radar Meteor.*, Amer. Meteor. Soc.

van Lingen, M.S., 1944: The coastal low of the south and southeast coasts of the Union of South Africa. S.A.A.F. Meteorological Section. *Technical notes*. No. 33.

Majodina M. and M. R. Jury, 1996: Composite winter cyclones south of Africa: Evolution during eastward transit over the Agulhas warm pool. *S. Afr. Journal of Mar. Sci.*, 17; 241 – 252.

Matarira, C. H. and M. R. Jury, 1992: Contrasting meteorological structure of intra-seasonal wet and dry spells in Zimbabwe. *International Journal of Climatology, New York, NY,* Vol. 12, No. 2; 165 – 176.

McInnes, K. L., 1993: Australian southerly busters. Part 3: The Physical Mechanism and synoptic conditions contributing to development. *Monthly Weather Review*, 121; 3261 – 3281.

Mass, Clifford F. and Mark D. Albright, 1987: Coastal southerlies and alongshore surges of the west coast of North America: Evidence of mesoscale topographically trapped response to synoptic forcing. *Monthly Weather Review*, 115; 1707 – 1783.

Mass, Clifford F. and Nicholas A. Bond, 1996: Coastally Trapped Wind Reversals along the United States West Coast during the Warm Season. Part II: Synoptic Evolution. *Monthly Weather Review*, 124; 446 – 461.

Meteorological Reports, 1948: Aviation meteorology of South America. Meteorological Office Reports, Vol. 1; 1 – 50.

Naeraa, M. and M. R. Jury, 1998: Tropical cyclone composite structure and impacts over eastern Madagascar during January – March 1994. *Meteorology and Atmospheric Physics, Vienna, Austria.* Vol. 65, No. 1 – 2; 43 – 53.

Nassor, A. and M. R. Jury, 1997: Intra-seasonal climate variability of Madagascar. Part 2: Evolution of flood events. *Meteorology and Atmospheric Physics, Vienna, Austria.* Vol. 64, No 3 – 4; 243 – 254.

Nguyen Ngoc Anh and A. E. Gill, 1980: Generation of coastal lows by synoptic-scale waves. *Quart. J. R. Met. Soc.* (1981), 107; 521 - 530.

Nuss, Wendell A., John M. Bane, William T. Thompson, Teddy Holt, Clive E. Dorman, F. Martin Ralph, Richard Rotunno, Joseph B. Klemp, William

C. Skamarock, Roger M. Samelson, Audrey M. Rogerson, Chris Reason and Peter Jackson, 2000: Coastally Trapped Wind Reversals: Progress toward Understanding. *Bulletin of the American Met. Soc.* Vol. 81, No. 4; 719 – 743.

Overland, J. E. and Bond, N., 1993: The influence of coastal orography: the Yakutat storm. *Mon. Wea. Rev.*, 121; 1388 – 1397.

Parker, B. A. and M. R. Jury, 1999: Synoptic environment of composite tropical cyclones in the south-west Indian Ocean. *S. Afr. J. Mar. Sci.*, 21; 99 – 115.

Preston-Whyte, R. A., 1975: A note on some bio-climatic consequences of coastal lows. *S. Afr. Geog. Journal*, Vol. 57, No. 1; 17 - 25.

Preston-Whyte, R. A., R. D. Diab and P. D. Tyson, 1977: Towards an inversion climatology of Southern Africa: Part II, Non-surface inversions in the lower atmosphere. *S. Afr. Geog. Journal*, Vol. 59, No. 1; 45 – 59.

Preston-Whyte, R. A. and P. D. Tyson, 1973: Note on pressure oscillations over South Africa. *Monthly Weather Review*, 101(8); 650 – 661.

Preston-Whyte, R. A. and P. D. Tyson, 1988: The Atmosphere and Weather of Southern Africa. *Oxford University Press*; 145 – 155; 198; 219 - 222.

Pyle, Matthew, 2002: Personal correspondence about Eta Workstation configuration. Matthew.Pyle@noaa.gov

Ralph, F. M., P. J. Neiman, P. O. G. Persson, J. M. Bane, M. L. Cancillo, J. M. Wilczak and W. Nuss, 2000: Kelvin Waves and Internal Bores in the Marine Boundary Layer Inversion and Their Relationship to Coastally Trapped Wind Reversals. *Monthly Weather Review*, 128; 283 – 300.

Reason, C. J. C., 1993: Orographically trapped disturbances in the lower atmosphere: Scale analysis and simple models. *Meteorol. Atmos. Phys.* 53; 131 - 136.

Reason, C. J. C. and Dunkley, R., 1993: Coastally trapped stratus events in British Columbia. *Atmosphere-Ocean*, 31; 235 – 258.

Reason, C. J. C. and D. G. Steyn, 1990: Coastally trapped disturbances in the lower atmosphere: Dynamic commonalities and geographic diversity. *Prog. in Phys. Geogr.* 14(2); 178 - 198.

Reason, C. J. C. and M. R. Jury, 1990: On the generation and propagation of the southern African coastal low. *Q. J. R. Meteorol. Soc.* 116, 1133 - 1151.

Reason, Jackson and Hai Fu, 2000: Dynamical influence of large valleys on the propagation of coastally trapped disturbances. *Meteorol. Appl.*, 7; 247 – 259.

Rogers, E., T. L. Black, D. G. Deaven, G. J. DiMego, Qingyun Zhao, M. Baldwin, N. W. Junker, Ying Lin, 1996: Changes to the Operational "Early" Eta Analysis/Forecast System at the National Centers for Environmental Prediction. *Weather and Forecasting,* Vol. 11, No. 3; 391 – 413.

Rui, Hualan and Bin Wang, 1990: Development characteristics and dynamic structure of tropical intraseasonal convection anomalies. *Journal of the Atmospheric Sciences, Boston, MA.*, Vol. 47, No. 3; 357 – 379.

Ruttlant, J., 1983: Coastal lows in Central Chile. First international conference on Southern Hemisphere Meteorology. *In Proceedings*; 344 - 346.

Schumann, E. H., 1983: Long-period coastal trapped waves off the southeast coast of southern Africa. Continental Shelf Research, 2; 97 – 107.

Schumann, Cohen and Jury 1995: Coastal sea surface temperature variability along the south coast of South Africa and the relationship to regional and global climate. *Journal of Marine Research,* 53, 231 - 248.

Shillington, F. A., 1984: Propagation speeds of micro-pressure oscillations in the atmosphere along the south coast. *Abstracts and Summary of the*

Coastal Low Workshop, Institute of Maritime Technology, Simonstown, 16.

Smith, R. K., R. N. Ridley, M. A. Page, J. T. Steiner, and A. P. Sturman, 1991: Southerly changes on the east coast of New Zealand. *Mon. Wea. Rev.*, 119; 1259 – 1282.

Taljaard, J.J., 1972: Synoptic Meteorology of the Southern Hemisphere. Ch.8 in *Meteor. Monogr.*, 13 No. 35, Amer. Meteor. Soc., Boston.

Torrance, J. D., 1995: Some aspects of the South African coastal low and its rogue waves. *Weather Magazine*, Vol. 50, No. 5; 163 – 170.

Webster, P. J. and Stephens, G. L., 1980: Tropical upper tropospheric extended clouds: inferences from Winter MONEX. *J. Atmos. Sci.*, 37; 1521 – 1541.

Appendix A: List of all 642 coastal lows 1987 – 1996 (Number, Year, Month, Day, and Hour).

1	87	1	5	2		46	87	10	22	11		91	88	7	6	12		136	89	3	12	19
2	87	1	11	1		47	87	10	27	22		92	88	7	8	22		137	89	3	17	3
3	87	1	17	14		48	87	10	30	22		93	88	7	14	22		138	89	3	22	0
4	87	1	27	11		49	87	11	3	1		94	88	7	20	7		139	89	3	27	1
5	87	2	1	12		50	87	11	8	17		95	88	7	22	12		140	89	3	29	2
6	87	2	3	7		51	87	11	17	19		96	88	7	28	11		141	89	4	7	6
7	87	2	5	12		52	87	11	22	18		97	88	8	5	14		142	89	4	10	14
8	87	2	8	15		53	87	11	29	12		98	88	8	11	12		143	89	4	13	15
9	87	2	13	8		54	87	12	4	15		99	88	8	26	2		144	89	4	19	14
10	87	2	19	8		55	87	12	17	21		100	88	9	5	9		145	89	4	25	13
11	87	2	21	20		56	87	12	22	8		101	88	9	7	22		146	89	4	27	9
12	87	3	5	21		57	87	12	26	18		102	88	9	9	15		147	89	5	3	19
13	87	3	18	22		58	87	12	29	23		103	88	9	19	21		148	89	5	9	2
14	87	3	24	4		59	88	1	1	14		104	88	9	21	12		149	89	5	18	5
15	87	3	28	2		60	88	1	5	10		105	88	9	24	12		150	89	5	21	2
16	87	4	2	20		61	88	1	12	1		106	88	10	3	12		151	89	5	24	6
17	87	4	5	12		62	88	1	17	18		107	88	10	15	22		152	89	6	7	6
18	87	4	9	9		63	88	1	20	19		108	88	10	21	10		153	89	6	13	13
19	87	4	12	13		64	88	1	23	21		109	88	10	24	11		154	89	6	21	7
20	87	4	19	1		65	88	1	26	6		110	88	10	31	7		155	89	6	23	1
21	87	4	22	9		66	88	2	3	5		111	88	11	2	11		156	89	6	28	13
22	87	4	27	3		67	88	2	5	0		112	88	11	13	23		157	89	7	4	14
23	87	5	1	8		68	88	2	11	20		113	88	11	18	19		158	89	7	8	19
24	87	5	4	15		69	88	2	14	5		114	88	11	23	8		159	89	7	10	11
25	87	5	10	10		70	88	2	18	3		115	88	11	27	16		160	89	7	16	15
26	87	5	23	10		71	88	2	23	4		116	88	12	10	6		161	89	7	25	3
27	87	6	9	13		72	88	2	26	20		117	88	12	19	10		162	89	8	6	11
28	87	6	13	12		73	88	3	4	23		118	88	12	24	11		163	89	8	9	8
29	87	7	1	5		74	88	3	12	1		119	88	12	29	4		164	89	8	11	18
30	87	7	10	8		75	88	3	18	2		120	89	1	5	11		165	89	8	18	19
31	87	7	19	9		76	88	3	22	4		121	89	1	10	7		166	89	8	26	18
32	87	7	25	22		77	88	3	28	7		122	89	1	14	5		167	89	8	29	5
33	87	7	31	12		78	88	4	10	8		123	89	1	19	16		168	89	9	1	10
34	87	8	10	4		79	88	4	14	10		124	89	1	22	4		169	89	9	15	16
35	87	8	14	22		80	88	4	18	8		125	89	1	27	7		170	89	9	24	2
36	87	8	18	13		81	88	4	23	19		126	89	1	30	23		171	89	9	27	5
37	87	8	21	6		82	88	4	30	13		127	89	2	5	3		172	89	9	29	5
38	87	8	27	13		83	88	5	3	11		128	89	2	8	11		173	89	10	14	11
39	87	8	29	20		84	88	5	8	15		129	89	2	12	2		174	89	10	17	20
40	87	9	19	19		85	88	5	15	23		130	89	2	20	13		175	89	10	26	15
41	87	10	5	4		86	88	5	25	20		131	89	2	24	2		176	89	11	13	9
42	87	10	9	4		87	88	6	1	11		132	89	2	26	21		177	89	11	21	2
43	87	10	10	19		88	88	6	20	1		133	89	2	28	23		178	89	11	23	10
44	87	10	14	10		89	88	6	26	12		134	89	3	5	12		179	89	11	25	23
45	87	10	17	9		90	88	7	1	2		135	89	3	9	0		180	89	12	1	9

181	89	12	7	1		226	90	7	29	0		271	91	3	20	21		316	91	12	10	22
182	89	12	10	6		227	90	8	8	14		272	91	3	31	5		317	91	12	13	2
183	89	12	18	2		228	90	8	10	4		273	91	4	4	15		318	91	12	17	14
184	89	12	23	7		229	90	8	15	22		274	91	4	9	15		319	91	12	23	7
185	89	12	26	19		230	90	8	26	2		275	91	4	13	19		320	91	12	24	18
186	89	12	29	3		231	90	9	3	3		276	91	4	19	17		321	91	12	30	21
187	90	1	1	17		232	90	9	5	23		277	91	4	24	8		322	92	1	5	6
188	90	1	5	23		233	90	9	10	22		278	91	4	26	17		323	92	1	7	17
189	90	1	9	8		234	90	9	16	8		279	91	5	1	3		324	92	1	12	14
190	90	1	17	18		235	90	9	22	20		280	91	5	4	10		325	92	1	15	18
191	90	1	22	15		236	90	9	25	13		281	91	5	7	9		326	92	1	23	21
192	90	1	25	23		237	90	9	28	8		282	91	6	12	10		327	92	1	26	9
193	90	1	29	22		238	90	10	2	9		283	91	7	18	14		328	92	1	30	8
194	90	2	2	20		239	90	10	5	15		284	91	7	21	12		329	92	2	3	21
195	90	2	14	17		240	90	10	10	3		285	91	7	25	15		330	92	2	8	22
196	90	2	18	0		241	90	10	21	23		286	91	7	30	7		331	92	2	11	3
197	90	2	28	1		242	90	10	28	17		287	91	8	5	16		332	92	2	15	21
198	90	3	2	13		243	90	11	1	18		288	91	8	9	12		333	92	2	23	19
199	90	3	6	9		244	90	11	10	22		289	91	8	15	8		334	92	3	8	1
200	90	3	9	9		245	90	11	18	8		290	91	8	22	19		335	92	3	9	22
201	90	3	13	22		246	90	11	22	18		291	91	8	24	9		336	92	3	18	18
202	90	3	27	12		247	90	11	28	7		292	91	8	27	13		337	92	3	25	21
203	90	3	31	9		248	90	12	4	12		293	91	9	3	13		338	92	3	28	7
204	90	4	5	18		249	90	12	7	12		294	91	9	7	10		339	92	4	3	11
205	90	4	8	17		250	90	12	11	15		295	91	9	13	5		340	92	4	5	9
206	90	4	11	21		251	90	12	21	12		296	91	9	15	12		341	92	4	9	9
207	90	4	18	3		252	90	12	23	8		297	91	9	18	5		342	92	4	15	13
208	90	4	27	20		253	90	12	28	21		298	91	9	22	23		343	92	4	23	6
209	90	5	7	15		254	91	1	3	3		299	91	9	27	8		344	92	5	1	3
210	90	5	9	18		255	91	1	7	20		300	91	10	1	14		345	92	5	6	20
211	90	5	12	7		256	91	1	11	9		301	91	10	7	9		346	92	5	8	22
212	90	5	17	21		257	91	1	13	20		302	91	10	10	20		347	92	5	14	11
213	90	5	24	13		258	91	1	21	13		303	91	10	14	19		348	92	5	16	20
214	90	5	26	17		259	91	1	29	6		304	91	10	17	13		349	92	5	22	21
215	90	5	29	8		260	91	1	30	22		305	91	10	22	13		350	92	5	30	5
216	90	6	2	18		261	91	2	2	16		306	91	10	26	8		351	92	6	2	11
217	90	6	7	17		262	91	2	5	4		307	91	10	28	8		352	92	6	10	21
218	90	6	15	14		263	91	2	11	9		308	91	11	2	21		353	92	6	17	22
219	90	6	20	18		264	91	2	17	7		309	91	11	9	21		354	92	6	27	14
220	90	7	3	9		265	91	2	19	21		310	91	11	16	1		355	92	7	4	18
221	90	7	8	23		266	91	2	27	2		311	91	11	18	17		356	92	7	10	11
222	90	7	12	3		267	91	3	2	15		312	91	11	24	2		357	92	7	14	19
223	90	7	15	16		268	91	3	7	12		313	91	11	27	17		358	92	7	18	5
224	90	7	17	13		269	91	3	9	21		314	91	12	3	10		359	92	7	21	3
225	90	7	26	8		270	91	3	18	19		315	91	12	6	15		360	92	7	25	13

361	92	8	2	13		406	93	3	26	18		451	93	12	6	8		496	94	8	6	11
362	92	8	6	2		407	93	3	30	4		452	93	12	13	12		497	94	8	11	17
363	92	8	13	11		408	93	4	1	20		453	93	12	21	10		498	94	8	16	15
364	92	8	19	4		409	93	4	8	19		454	93	12	24	10		499	94	8	23	17
365	92	8	28	23		410	93	4	10	18		455	93	12	28	22		500	94	8	26	2
366	92	9	4	12		411	93	4	16	7		456	93	12	31	20		501	94	8	30	10
367	92	9	8	9		412	93	4	23	0		457	94	1	5	22		502	94	9	2	5
368	92	9	11	10		413	93	4	25	16		458	94	1	7	10		503	94	9	4	18
369	92	9	14	14		414	93	5	5	12		459	94	1	12	14		504	94	9	6	17
370	92	9	18	6		415	93	5	11	18		460	94	1	19	0		505	94	9	11	10
371	92	9	23	21		416	93	5	13	12		461	94	1	25	23		506	94	9	16	18
372	92	9	29	13		417	93	5	19	14		462	94	1	27	18		507	94	9	20	7
373	92	10	2	16		418	93	5	25	13		463	94	1	30	14		508	94	9	22	9
374	92	10	6	9		419	93	6	2	18		464	94	2	1	14		509	94	9	25	8
375	92	10	10	19		420	93	6	6	5		465	94	2	6	18		510	94	9	30	8
376	92	10	13	13		421	93	6	9	9		466	94	2	9	12		511	94	10	9	1
377	92	10	19	9		422	93	6	18	15		467	94	2	14	7		512	94	10	12	10
378	92	11	2	6		423	93	7	17	1		468	94	2	18	19		513	94	10	16	21
379	92	11	5	4		424	93	7	19	15		469	94	2	26	20		514	94	10	24	9
380	92	11	9	0		425	93	7	24	13		470	94	2	28	19		515	94	10	29	7
381	92	11	15	1		426	93	7	31	22		471	94	3	6	1		516	94	10	31	22
382	92	11	19	2		427	93	8	10	6		472	94	3	12	18		517	94	11	3	7
383	92	11	28	23		428	93	8	14	13		473	94	3	17	11		518	94	11	8	8
384	92	12	9	20		429	93	8	20	7		474	94	3	21	1		519	94	11	16	23
385	92	12	13	10		430	93	8	25	17		475	94	3	31	14		520	94	12	1	1
386	92	12	22	14		431	93	9	3	3		476	94	4	5	1		521	94	12	4	9
387	92	12	26	23		432	93	9	7	4		477	94	4	8	20		522	94	12	8	9
388	93	1	1	1		433	93	9	10	3		478	94	4	11	22		523	94	12	13	11
389	93	1	5	9		434	93	9	12	23		479	94	4	16	0		524	94	12	16	17
390	93	1	7	11		435	93	9	18	10		480	94	5	1	10		525	94	12	20	2
391	93	1	16	4		436	93	9	20	6		481	94	5	9	2		526	94	12	30	22
392	93	1	23	0		437	93	10	2	13		482	94	5	14	17		527	95	1	5	12
393	93	1	27	13		438	93	10	8	13		483	94	5	17	15		528	95	1	12	11
394	93	1	29	20		439	93	10	12	5		484	94	5	25	19		529	95	1	16	12
395	93	2	2	22		440	93	10	15	7		485	94	6	3	5		530	95	1	22	9
396	93	2	6	23		441	93	10	19	2		486	94	6	11	17		531	95	1	24	15
397	93	2	10	16		442	93	10	20	23		487	94	6	23	15		532	95	1	28	7
398	93	2	12	15		443	93	10	23	8		488	94	7	3	11		533	95	1	31	9
399	93	2	20	12		444	93	10	26	8		489	94	7	7	14		534	95	2	6	19
400	93	2	26	5		445	93	11	8	11		490	94	7	12	13		535	95	2	10	12
401	93	3	1	4		446	93	11	14	21		491	94	7	16	20		536	95	2	13	21
402	93	3	8	20		447	93	11	17	23		492	94	7	18	12		537	95	2	19	3
403	93	3	11	12		448	93	11	21	14		493	94	7	20	14		538	95	2	23	17
404	93	3	18	1		449	93	11	27	19		494	94	7	29	18		539	95	2	26	2
405	93	3	20	19		450	93	11	30	1		495	94	8	1	7		540	95	3	3	22

541	95	3	4	15		586	96	1	4	10		631	96	11	10	21
542	95	3	8	6		587	96	1	14	9		632	96	11	15	12
543	95	3	16	16		588	96	1	15	21		633	96	11	24	12
544	95	3	29	21		589	96	1	18	3		634	96	11	29	0
545	95	4	3	9		590	96	1	22	13		635	96	12	1	10
546	95	4	7	15		591	96	1	29	19		636	96	12	3	6
547	95	4	14	5		592	96	2	2	23		637	96	12	6	1
548	95	4	18	8		593	96	2	6	8		638	96	12	10	20
549	95	4	22	18		594	96	2	8	18		639	96	12	17	10
550	95	5	10	13		595	96	2	12	20		640	96	12	21	0
551	95	5	16	5		596	96	2	17	5		641	96	12	23	10
552	95	5	18	11		597	96	2	19	17		642	96	12	27	6
553	95	5	26	7		598	96	2	28	22						
554	95	6	13	11		599	96	3	1	17						
555	95	6	21	3		600	96	3	6	22						
556	95	6	26	11		601	96	3	10	1						
557	95	6	27	23		602	96	3	18	20						
558	95	7	2	12		603	96	3	25	17						
559	95	7	4	17		604	96	4	6	18						
560	95	7	16	4		605	96	4	14	15						
561	95	7	24	12		606	96	4	18	1						
562	95	7	25	17		607	96	4	24	14						
563	95	8	2	23		608	96	5	1	22						
564	95	8	8	12		609	96	5	4	3						
565	95	8	14	15		610	96	5	7	9						
566	95	8	18	18		611	96	5	9	13						
567	95	8	25	12		612	96	5	12	15						
568	95	8	28	22		613	96	5	21	10						
569	95	9	1	11		614	96	5	30	21						
570	95	9	6	9		615	96	6	6	14						
571	95	9	15	21		616	96	6	11	22						
572	95	9	20	10		617	96	6	14	16						
573	95	9	23	11		618	96	7	3	6						
574	95	9	26	1		619	96	7	12	15						
575	95	10	11	17		620	96	8	9	19						
576	95	11	3	21		621	96	8	12	15						
577	95	11	7	2		622	96	8	23	20						
578	95	11	11	1		623	96	9	1	22						
579	95	11	15	1		624	96	9	16	6						
580	95	11	21	3		625	96	9	20	21						
581	95	12	5	10		626	96	9	28	19						
582	95	12	9	23		627	96	10	6	19						
583	95	12	14	12		628	96	10	26	15						
584	95	12	25	3		629	96	10	30	14						
585	95	12	31	14		630	96	11	3	19						

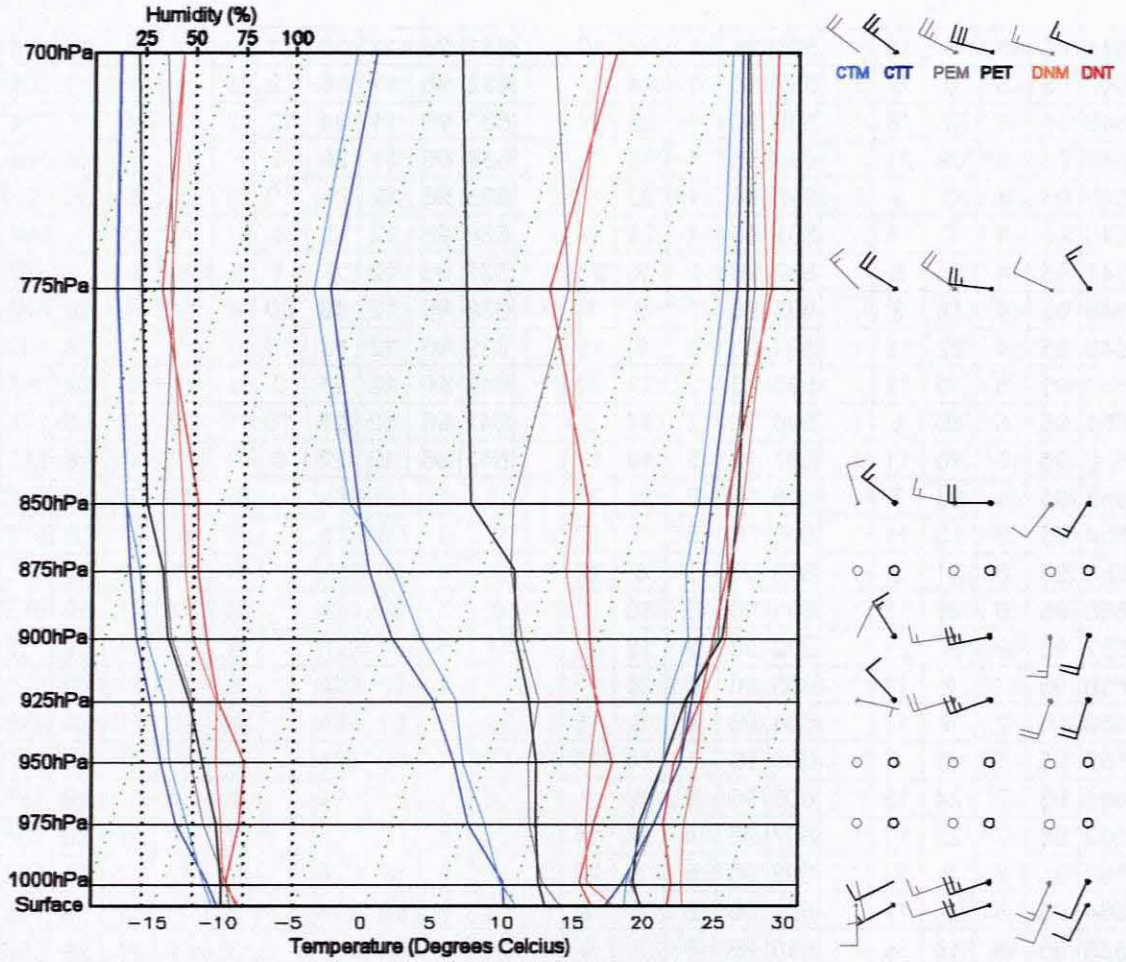

Fig. A1 Aeronautical diagram of the averaged ascents at Cape Town (blue), Port Elizabeth (gray) and Durban (red) with the darker shades showing the top 10% of coastal lows and light the mean 10% of the coastal lows. Temperature, dew point temperature and humidity traces are shown for each averaged ascent trace. Significant level data have been added, however no wind data is available for these levels (zero's plotted). CTM is the mean ascent trace for Cape Town, with CTT the top 10% averaged ascent trace, and similar abbreviations for Port Elizabeth (PEM, PET) and Durban (DNM, DNT). Wind is in knots with each barb equal to 10 knots and half a barb equal to 5 knots.

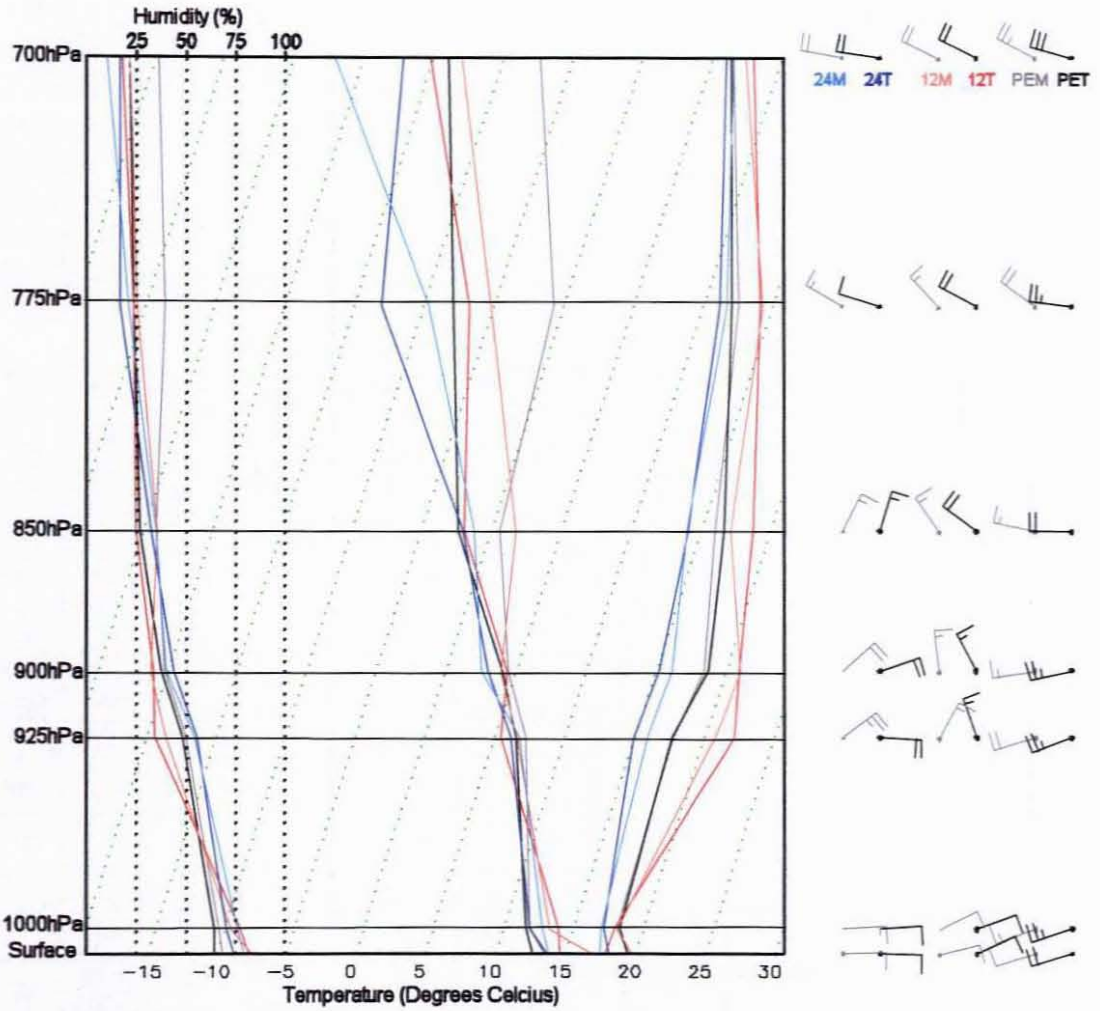

Fig. A.2 Aeronautical diagram of the averaged ascents at 24 hours before coastal low passage at Port Elizabeth (blue), 12 hours before coastal low passage (red) and at coastal low passage (gray) with the darker shades showing the top 10% of coastal lows and light the mean 10% of the coastal lows. Only standard level data were plotted. Temperature, dew point temperature and humidity traces are shown for each averaged ascent trace. 24M is the mean ascent trace for 24-hours before coastal low passage at Port Elizabeth, with 24T the top 10% averaged ascent trace, and similar abbreviations for 12-hours before coastal low passage at Port Elizabeth (12M, 12T) and at coastal low passage at Port Elizabeth (PEM, PET). Wind is in knots with each barb equal to 10 knots and half a barb equal to 5 knots.

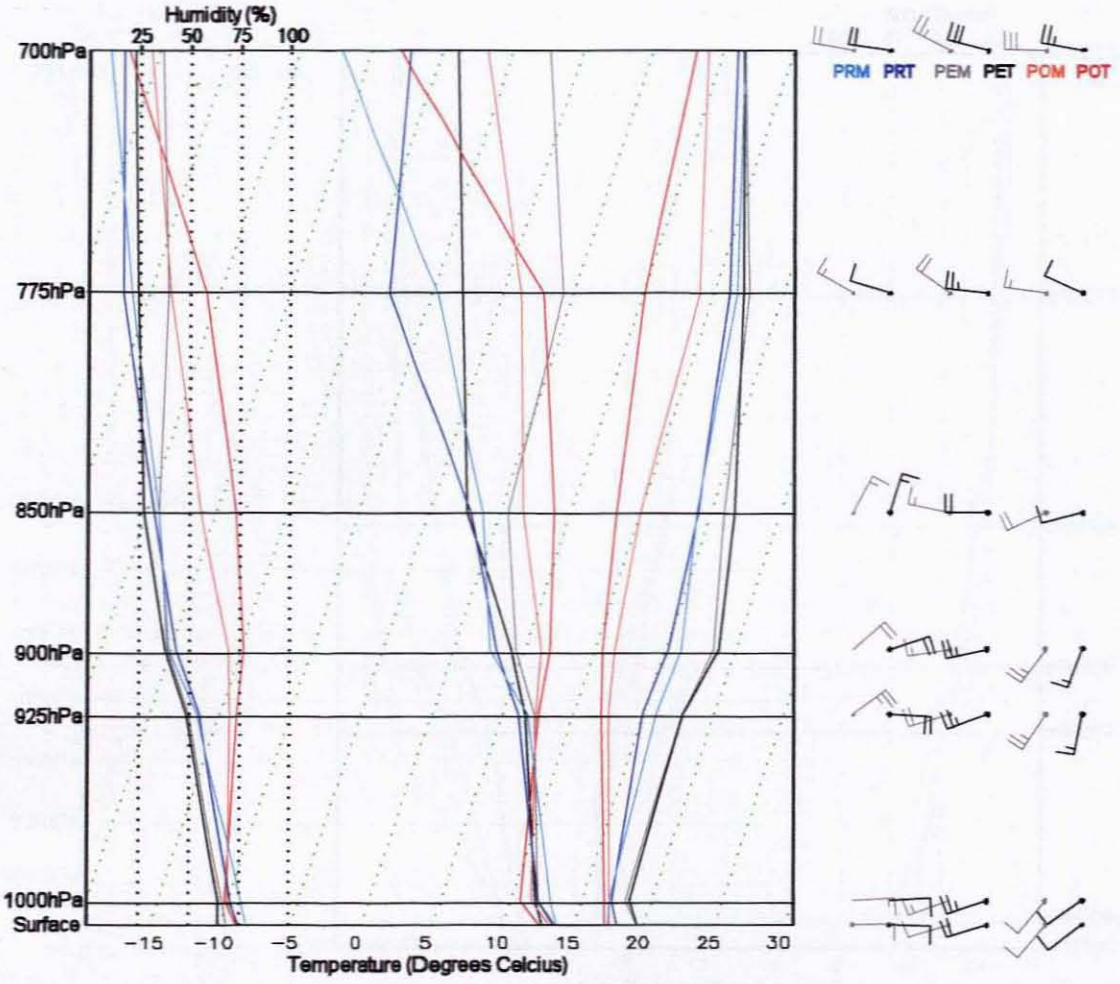

Fig. A.3 Aeronautical diagram of the averaged ascents at 24 hours before coastal low passage at Port Elizabeth (blue), at coastal low passage (gray) and at 24 hours after coastal low passage (red) with the darker shades showing the top 10% of coastal lows and light the mean 10% of the coastal lows. Only standard level data were plotted. Temperature, dew point temperature and humidity traces are shown for each averaged ascent trace. PRM is the mean ascent trace for 24-hours before coastal low passage at Port Elizabeth, with PRT the top 10% averaged ascent trace, and similar abbreviations for the averaged ascents at passage at Port Elizabeth (PEM, PET) and 24-hours after coastal low passage at Port Elizabeth (POM, POT). Wind is in knots with each barb equal to 10 knots and half a barb equal to 5 knots.

Table A1 Top 10% of SON coastal lows tracked from Cape Town (C) to George (G), to Port Elizabeth (P), to East London (E) and on to Durban (D). The time taken in hours is also noted from Cape Town to Port Elizabeth and from Port Elizabeth to Durban, and finally from Cape Town to Durban. At George, the abbreviation PM is used to indicate when the pressure minima were used, rather than the wind shift. Y, M, D and H show the year, month, day and hour of coastal low passage at Port Elizabeth with 'Speed' showing coastal low mean 8-hour wind speed of the coastal low. Average time taken in hours is boxed at the bottom of the table.

C/P	CT	C/G	GG	G/P	Y	M	D	H	Speed	P/E	EL	E/D	DN	P/D	C/D
13	18th 2200	6	PM 20th 0400	7	95	9	20	11	12.6	1	20th 1200	11	20th 2300	12	25
22	17th 0200	7	17th 0900	15	93	11	18	0	12.4	5	18th 0500	16	18th 2100	21	43
14	22nd 1400	12	23rd 1000	2	95	9	23	12	12.4	6	23rd 1800	9	24th 0300	15	29
29	11th 0100	16	11th 1700	13	93	10	12	6	12.1	2	12th 0800	12	12th 2000	14	43
29	23rd 0000	24	PM 24th 0200	5	94	10	24	7	11.8	1	24th 0800	13	24th 2100	14	43
16	17th 1700	13	11th 0600	3	90	11	18	9	11.5	5	18th 1400	9	18th 2300	14	30
19	25th 2100	12	26th 0900	7	96	10	26	16	11.5	6	26th 2200	4	27th 0200	10	29
22	07th 1100	16	PM 08th 0300	6	94	11	8	9	11.1	3	08th 1200	6	08th 1800	9	31
26	02nd 0600	23	03rd 0500	3	94	11	3	8	11.1	6	03rd 1400	11	04th 0100	17	43
11	28th 1900	6	09th 0100	5	89	9	29	6	10.7	3	29th 0900	8	29th 1700	11	22
26	15th 1800	17	16th 1100	9	94	9	16	20	10.3	4	17th 0000	11	17th 1100	15	41
13	14th 2000	9	16th 0500	4	90	9	16	9	10.3	1	16th 1000	11	16th 2100	12	25
28	13th 1800	21	14th 1500	7	93	11	14	22	10.2	5	15th 0300	22	16th 0100	27	55
28	13th 1600	19	14th 1100	9	91	10	14	20	10.1	4	15th 0000	7	15th 0700	11	39
22	29th 1200	17	PM 30th 0500	5	94	9	30	10	9.6	0	30th 1000	11	30th 2100	11	33
32	21st 1100	23	22nd 1000	9	87	11	22	19	9.2	6	23rd 0100	8	23rd 0900	14	46
21.9		15.1		6.8						3.6		10.6		14.2	36.1

Table A2 Mean 10% of SON coastal lows tracked from Cape Town (C) to George (G), to Port Elizabeth (P), to East London (E) and on to Durban (D). The time taken in hours is also noted from Cape Town to Port Elizabeth and from Port Elizabeth to Durban, and finally from Cape Town to Durban. At George, the abbreviation PM is used to indicate when the pressure minima were used, rather than the wind shift. Y, M, D and H show the year, month, day and hour of coastal low passage at Port Elizabeth with 'Speed' showing coastal low mean 8-hour wind speed of the coastal low. Average time taken in hours is boxed at the bottom of the table.

C/P	CT	C/G	GG	G/P	Y	M	D	H	Speed	P/E	EL	E/D	DN	P/D	C/D
32	26th 1100	22	27th 0900	10	91	11	27	19	7.3	4	27th 2300	7	28th 0600	11	43
15	19th 1200	13	21st 0100	2	89	11	21	3	7.3	11	21st 0800	13	21st 2100	24	39
36	25th 0400	30	26th 1000	6	89	10	26	16	7.3	7	26th 2300	22	27th 2100	29	65
30	04th 1800	24	05th 1800	6	90	9	6	0	7.2	6	06th 0600	14	06th 2000	20	50
27	20th 1000	19	PM 21st 0500	8	88	9	21	13	7.2	7	21st 2000	6	22nd 0200	13	40
26	07th 1200	15	08th 0300	11	93	10	8	14	7.2	7	08th 2100	22	09th 2300	29	55
30	19th 0200	26	PM 20th 0400	4	94	9	20	8	7.1	1	20th 0900	12	20th 2100	13	43
24	08th 0200	19	08th 2100	5	87	10	9	2	6.9	4	09th 0600	13	09th 1900	17	41
37	20th 0200	30	21st 0800	7	93	11	21	15	6.8	8	21st 2300	12	22nd 1100	20	57
30	03rd 1300	21	04th 1000	9	94	9	4	19	6.8	7	05th 0200	8	05th 1000	15	45
30	26th 1400	18	27th 0800	12	93	11	27	20	6.8	5	28th 0100	23	29th 0200	28	58
24	30th 1900	16	01st 1100	8	90	11	1	19	6.7	5	02nd 0000	9	02nd 0900	14	38
38	05th 1200	22	06th 1000	16	96	10	6	20	6.7	6	07th 0200	6	07th 0800	12	50
56	27th 0000	40	28th 1600	16	96	11	29	1	6.6	7	29th 0800	11	29th 1900	18	74
43	01st 0200	32	02nd 1000	11	93	10	2	14	6.5	7	02nd 2100	9	03rd 0600	16	59
36	14th 0800	26	15th 1000	10	96	11	15	13	6.5	7	11th 2000	7	16th 0300	14	50
32.1		23.3		8.8						6.2		12.1		18.3	50.4

Table A3 Temperature inversions on the top 10% of SON upper air ascents at Cape Town (CTT), Port Elizabeth (PET) and Durban (DNT) within the 12-hour period preceding coastal low passage at the stations. The average inversion is calculated by only using the first inversion noted. ND denotes nil ascent data.

CTT	Time	1/2 Inv	SFC	PET	Time	1/2 Inv	SFC	DNT	Time	1/2 Inv	SFC
9/19/1995	0105	1016.8	1016.8	9/20/1995	1222	968.9	1000.5	9/21/1995	0302	947.7	1013.7
11/17/1993	0112	1006.7 973.8	1006.7	11/18/1993	0139	979.4	1000.4	11/19/1993	0139	919.9	1015.4
9/22/1995	1342		1010.7	9/23/1995	1240	971.3	1006.3	9/24/1995	1234	990.5 854.4	1016.3
10/11/1993	0120	1011.5	1011.5	10/12/1993	1233	936.9	1007.6	10/13/1993	0140	854	1016.4
10/23/1994	0132	1019.1	1019.1	10/24/1994	1245	979.7 950	1008.8	10/25/1994	0101	937	1014.6
11/18/1990	0136	1012 990.4	1012	11/18/1989	1237		1009.3	11/19/1990	0139	945.5	1012
10/26/1996	0114	1011	1011	10/27/1996	0113	882.5	1011.1	10/27/1996	0140	1013.4 947.7	1013.4
11/7/1994	1238	977.1	1005.1	11/8/1994	1307	972.8	996.9	11/9/1994	0136	982 949.4	1001.6
11/2/1994	1302		1004.1	11/3/1994	1241	940.9	1005.7	11/4/1994	0111	1013 917.1	1013
9/29/1989	0125	930	1007.7	9/29/1989	1232	903.9	1005.3	9/30/1989	0044		1015.5
9/19/1994	0112	1013.3	1013.3	9/17/1994	0135	969.3 928.6	1000.6	9/17/1994	1238	977.4	1005.2
9/15/1990	0130	990.7 941.2	1015.9	ND 16/09/1990				9/17/1990	0131		1013.1
11/14/1993	0116	1001.1	1001.1	11/15/1993	0247	1002 975.1	1002	11/16/1993	0136	964.2	1011.2
10/14/1991	0317	1004.5	1004.5	10/15/1991	0122		1002.5	10/15/1991	1231		1017.2
9/29/1994	1247	888.7	1019.5	9/30/1994	1241		1010.1	10/1/1994	0149	1016.6	1016.6
11/21/1987	1230	970.1	1011.4	11/23/1987	0143	913	1008.8	ND 23/11/1987			
Average inversion		989.5				951.7				963.4	
Meters		887.0				555.0				658.0	
Feet		2910.0				1821.0				2159.0	
Average surface pressure			1010.7				1005.1				1013.0

Table A4 Temperature inversions on the mean 10% of SON upper air ascents at Cape Town (CTM), Port Elizabeth (PEM) and Durban (DNM) within the 12-hour period preceding coastal low passage at the stations. The average inversion is calculated by only using the first inversion noted. ND denotes nil ascent data.

CTM	Time	1/2 Inv	SFC	PEM	Time	1/2 Inv	SFC	DNM	Time	1/2 Inv	SFC
11/26/1991	1231	983.7	1007.8	11/28/1991	0132	1004.3	1004.3	11/28/1991	1237	892.4	1011.5
11/19/1989	1235	924.9	1015.8	11/21/1989	1230	929.3 921.5	1007.4	11/22/1989	0107		1017
10/25/1989	1230	982.8	1012.1	10/27/1989	0137	986.4	1002	10/28/1989	0158	855.3	1014
9/5/1990	0145	1010.8	1010.8	ND 06/09/1990				9/7/1990	0239	875.4	1016.5
9/20/1988	1230		1010.1	9/21/1988	1253	969.7 888.4	1012.5	9/22/1988	0102	1017	1017
10/7/1993	1233		1010.2	10/8/1993	1237		1003.4	10/10/1993	0103	949.9 890.7	1014.9
9/19/1994	0112	1013.7 866.7	1018.2	9/20/1994	1255	946.1	1013.1	9/21/1994	0139	910.7	1020.3
10/8/1987	0133	1008.1	1008.1	10/9/1987	0134	985.8 909.9	1000.8	10/10/1987	0103		1006
11/20/1993	0150	962.9	1008.9	11/22/1993	0200	998.9	998.9	11/22/1993	1230	956.8	1004
9/3/1994	1237	898.5 853	1014.6	9/5/1994	0146	1011	1011	9/5/1994	1235	1012	1017.2
11/26/1993	1244	872.7	1009.2	11/28/1993	0137	976.8	1004.8	11/29/1993	0137	1010.5	1010.5
10/31/1990	0120	988.6 963.7	1016	ND 02/11/1990				11/2/1990	1232	972 916.5	1015.9
10/5/1996	1239	870.1	1012.3	10/7/1996	0108	918.7	1009.6	10/7/1996	1236	880.7	1016.2
11/27/1996	0118	1012.2	1012.2	11/29/1996	0139	997.4	997.4	11/30/1996	0135		1010
10/1/1993	0106	1010	1010	10/2/1993	1239	923	1008.2	10/3/1993	1239	861.6	1018.1
11/14/1996	1239		1011.9	11/15/1996	1251		1004.9	11/16/1996	1241		1010.1
Average inversion		**964.5**				**970.6**				**932.9**	
Meters		**668.0**				**721.0**				**1291.0**	
Feet		**2192.0**				**2366.0**				**4236.0**	
Average surface pressure			**1011.8**				**1005.6**				**1013.7**

Table A5 Legend for Tables A3 and A4, with all ascent data in hPa unless otherwise stated.

Date of ascent	Time of ascent	1st Inversion Surface Pressure 2nd Inversion

Appendix B: Condensed notes on forecasting strong coastal lows along the south eastern coastal belt from Cape St. Francis through to East London for operational forecaster use.

The following findings are from the analysis of coastal lows, which took place during the SON (September, October and November) seasons for the 10-year period from 1987 – 1996. In general these findings should also apply to the rest of the year (taking into consideration the fact that the average position of the IOA moves further south during the summer, and further northwards during winter seasons). Strong coastal lows in the following notes pertain particularly to the strength of the southwesterly wind surge following coastal low passage.

Long term forecast on the global scale forecast operational model.

1. The IOA is approximately 6 hPa stronger during strong coastal low days and its centre is placed around 15° further to the southeast than during average coastal low days (See Figs. 4.1; 4.2 and 4.3).
2. The following frontal trough system is less intense during strong coastal low days, however the centre associated with that trough is placed about 5° further north-eastwards than during average coastal low days (showing that its northwards extent is greater), leading to stronger northwesterly flow at 700 hPa over the southern parts of the country on the day of coastal low passage along the south coast (See Figs. 4.12; 4.13; 5.23 and 5.24).
3. Due to the stronger IOA, the easterly flow along the southeast coast before coastal low passage is stronger during strong case coastal lows (See Fig. 4.21).

4. The pressure minima in the region of the coastal low should be deeper on the global scale models as well during strong coastal low days than on average coastal low days (See Fig. 4.20)
5. Even at two days before coastal low passage on the south coast, a positive departure of 1.2°C is already visible at 850 hPa over Namibia on the eastern side of the interior trough for strong coastal low cases.

Short term forecast on the mesoscale regional scale forecast operational model.

1. The easterly wind at about 18 hours before coastal low passage is approximately 6 knots stronger on the strong coastal low days than during average coastal low cases.
2. The north to northwesterly offshore flow at plateau level over the southern interior, on the eastern side of the interior thermal trough, is about 3 – 4 knots stronger during strong case coastal low days.
3. The surface pressure minimum just before coastal low passage is almost 4 hPa deeper during the strong coastal low cases.
4. The higher temperatures at two days before strong case coastal lows on the south coast, is maintained between surface and 800hPa over the southern interior on the eastern side of the interior thermal trough, but by the day of coastal low passage these temperatures are up to 5°C higher during the strong case days than during the average coastal low ones. While this should also be apparent on the actual observed surface maximum temperatures experienced over the southern interior, these temperatures are dependant on local and diurnal variation. A better and more consistent pointer would be the elevated

temperatures above surface level shown by upper air ascents or by the mesoscale model, particularly when the coastal low passes overnight.

Other considerations:

This research has shown that there is a good chance that one strong coastal low is followed by another within the same month. Strong coastal lows also propagate faster along the coast with period of 4 - 5 days as opposed to 5 – 6 days for the mean cases.